SPARSE LINEAR SENSOR ARRAYS: ANALYSIS OF RECENT COARRAY BASED ARRAYS AND ARRAY DESIGN FOR NONLINEAR PROCESSING

A THESIS SUBMITTED TO
THE GRADUATE SCHOOL OF NATURAL AND APPLIED SCIENCES
OF
MIDDLE EAST TECHNICAL UNIVERSITY

BY

ERDAL EPÇAÇAN

IN PARTIAL FULFILLMENT OF THE REQUIREMENTS
FOR
THE DEGREE OF DOCTOR OF PHILOSOPHY
IN
ELECTRICAL AND ELECTRONICS ENGINEERING

SEPTEMBER 2021

Approval of the thesis:

SPARSE LINEAR SENSOR ARRAYS: ANALYSIS OF RECENT COARRAY BASED ARRAYS AND ARRAY DESIGN FOR NONLINEAR PROCESSING

submitted by **ERDAL EPÇAÇAN** in partial fulfillment of the requirements for the degree of **Doctor of Philosophy in Electrical and Electronics Engineering Department, Middle East Technical University** by,

Prof. Dr. Halil KALIPÇILAR
Dean, Graduate School of **Natural and Applied Sciences** _____

Prof. Dr. İlkay Ulusoy
Head of Department, **Electrical and Electronics Engineering** _____

Prof. Dr. Tolga Çiloğlu
Supervisor, **Electrical and Electronics Engineering, METU** _____

Examining Committee Members:

Prof. Dr. Umut Orguner
Electrical and Electronics Engineering, METU _____

Prof. Dr. Tolga Çiloğlu
Electrical and Electronics Engineering, METU _____

Prof. Dr. Orhan Arıkan
Electrical and Electronics Engineering, Bilkent University _____

Prof. Dr. Çağatay Candan
Electrical and Electronics Engineering, METU _____

Assist. Prof. Dr. Yakup Özkazanç
Electrical and Electronics Engineering, Hacettepe University _____

Date: 09.09.2021

I hereby declare that all information in this document has been obtained and presented in accordance with academic rules and ethical conduct. I also declare that, as required by these rules and conduct, I have fully cited and referenced all material and results that are not original to this work.

Name, Surname: Erdal Epçaçan

Signature :

ABSTRACT

SPARSE LINEAR SENSOR ARRAYS: ANALYSIS OF RECENT COARRAY BASED ARRAYS AND ARRAY DESIGN FOR NONLINEAR PROCESSING

Epçaçan, Erdal
Ph.D., Department of Electrical and Electronics Engineering
Supervisor: Prof. Dr. Tolga Çiloğlu

September 2021, 124 pages

In this thesis, sparse linear sensor arrays have been studied. The study of sparse arrays in this work can be considered under two main headings: Analysis and comparison of recently proposed coarray based arrays, and the adaptation of the nonlinear apodization method for linear arrays and its use in sparse linear array design.

Recently proposed coarray-based sparse arrays are designed with closed form structures without the need for any optimization and have much higher degrees of freedom (DOF) than a uniform linear array with the same number of sensors. DOF gives the number of targets that can be resolved. In this thesis, the analysis and comparison of the most known of these arrays have been made by considering the accuracy in direction of arrival, DOF, resolution in direction of arrival and mutual coupling. The aim is to reveal the advantages, disadvantages, and aspects accompanying the increased DOF. As a result of the simulations, it can be concluded that the increase in the DOF and in the resolution of direction of arrival is mainly provided by the enlarged array aperture. On the other hand, the effective use of the enlarged array aperture and no need of any optimization are superiority of these methods.

Nonlinear apodization has been used to solve the trade off between sidelobe level and mainlobe width. In this method, it is aimed to suppress sidelobe levels without increasing the mainlobe width. In this thesis, a variant of nonlinear apodization has been adapted to the spatial domain and it is used in beamforming. One of the most common problems in the design of sparse arrays is the increase in the sidelobe level and/or the emergence of grating lobes while narrowing the mainlobe width. Considering the success of the nonlinear apodization method in this topic, a sparse linear array design method using nonlinear apodization and the genetic algorithm is proposed.

Keywords: sensor arrays, sparse linear arrays,nonlinear apodization, DOA estimation, beamforming

ÖZ

SEYREK DOĞRUSAL SENSÖR DİZİNLERİ: GÜNCEL "COARRAY" TABANLI DİZİNLERİN ANALİZİ VE DOĞRUSAL OLMAYAN İŞLEME İÇİN DİZİN TASARIMI

Epçaçan, Erdal
Doktora, Elektrik ve Elektronik Mühendisliği Bölümü
Tez Yöneticisi: Prof. Dr. Tolga Çiloğlu

Eylül 2021 , 124 sayfa

Bu tezde seyrek doğrusal sensör dizinleri çalışılmıştır. Tezde seyrek dizinlerle ilgili yapılan çalışmalar iki ana başlık altında ele alınabilir: Yakın zamanda önerilmiş olan "coarray" tabanlı dizinlerin analizi ve karşılaştırması, ve doğrusal olmayan pencereleme yönteminin doğrusal dizinler için uyarlanması ve seyrek doğrusal dizin tasarımında kullanılması.

"Coarray" tabanlı seyrek dizinler herhangi bir optimizasyon gerektirmeden, kapalı form yapıları ile tasarlanmakta ve aynı sayıda sensöre sahip düzgün bir doğrusal dizine göre çok daha yüksek serbestlik derecesine (SD) sahip olmaktadır. SD, ayırt edilebilen hedef sayısını vermektedir. Bu tezde, bu dizinlerin en çok bilinenlerinin analizi ve karşılaştırması, yön kestirim doğruluğu, SD, yön kestirim hassasiyeti ve karşılıklı etkileşim hususları göz önünde bulundurularak yapılmıştır. Amaç, bu dizinlerin üstün ve zayıf yönlerini incelemek ve belirtilen özelliklerinin beraberinde gelen niteliklerini belirlemektir. Benzetimler sonucunda, SD ve yön çözünürlüğündeki artışın esas olarak genişletilmiş dizin açıklığı tarafından sağlandığı sonucuna varılabilir.

Öte yandan, genişletilmiş dizin açıklığının etkin kullanımı ve herhangi bir optimizasyona gerek olmaması bu yöntemlerin üstünlüğüdür.

Doğrusal olmayan pencereleme yöntemi, yan lob seviyesi ve ana lob genişliği dengesini sağlamak amacıyla kullanılmıştır. Bu yöntemde ana lob genişliği artırılmadan yan lob seviyelerinin bastırılması amaçlanmaktadır. Bu tezde doğrusal olmayan pencerelemenin bir türü uzaysal alana uyarlanmış ve hüzmelemede kullanılmıştır. Seyrek dizinlerin tasarımında en sık karşılaşılan problemlerdem biri ana lob genişliği daraltılırken yan lob seviyesinin yükselmesi veya istenmeyen lobların ortaya çıkmasıdır. Doğrusal olmayan pencereleme yönteminin bu konudaki başarısı göz önünde bulundurularak doğrusal olmayan pencereleme ve genetik algoritma yöntemini kullanan bir seyrek doğrusal dizin tasarım yöntemi sunulmuştur.

Anahtar Kelimeler: sensör dizinleri,seyrek doğrusal dizinler, doğrusal olmayan pencereleme, geliş yönü kestirimi, hüzme şekillendirme

to my family

ACKNOWLEDGMENTS

First and foremost, I would like to express my gratitude to my supervisor Prof. Dr. Tolga ÇİLOĞLU for his guidance throughout my thesis studies. I have always admired his deep knowledge, and his inspiring teaching style. This thesis would not be possible without his endless patience and encouragement.

I express my gratitude to thesis monitoring committee members Prof. Dr. Çağatay CANDAN and Assist. Prof. Dr. Yakup ÖZKAZANÇ for their great contribution in conducting my research. This thesis would not have been completed without their pertinent recommendations.

I would like to thank my thesis committee members Umut ORGUNER and Orhan ARIKAN for their patience and recommendations.

Heartfelt thanks should be given to my beloved wife Elif for her endless love, patience, help, and kindness during conducting my PhD thesis. She was always there to ease my burden through all ups and downs of this journey.

TABLE OF CONTENTS

LIST OF TABLES

TABLES

LIST OF FIGURES

FIGURES

LIST OF ABBREVIATIONS

DOA	Direction Of Arrival
ULA	Uniform Linear Array
ML	maximum-likelihood
SML	Stochastic Maximum Likelihood
DML	Deterministic Maximum Likelihood
MUSIC	Multiple Signal Classification
ESPRIT	Estimation of Signal Parameters via Rotation Invariant Techniques
LS-ESPRIT	Least Squares ESPRIT
SAR	Synthetic Aperture Radar
SVA	Spatially Variant Apodization
MSVA	Modified SVA
DTFT	Discrete Time Fourier Transform
DFT	Discrete Fourire Transform
MVSE	Minimum Variance Spectral Estimator
SNR	Signal to Noise Ratio
MRA	Minimum Redundancy Arrays
MRLA	Minimum Redundancy Linear Arrays
MHLA	Minimum Hole Linear Arrays
GA	Genetic Algorithm
OMP	Orthogonal Matching Pursuit
CS	Compressive Sensing
BCS	Bayesian Compressive Sensing
NA	Nested Array

CA	Co-prime Arrays
ANA	Augmented Nested Arrays
SNA	Super Nested Arrays
SRA	Sparse Ruler Array
DOF	Degree Of Freedom
uDOF	uniform DOF
CRLB	Cramer Rao Lower Bound
SS	Spatial Smoothing
DA	Direct Augmentation
AG	Array Group
RMSE	Root Mean Square Error
PSLL	Peak Sidelobe Level
CTR	Current Taper Ratio
BP	Beam Pattern
BWNN	Beam Width Null-to-Null
FNBW	First Null BeamWidth

CHAPTER 1

INTRODUCTION

In this thesis, linear sensor arrays and in particular sparse linear sensor arrays have been studied. A sparse array contains neighboring elements with a spacing larger than the Nyquist spatial limit. Nyquist spatial limit is the counterpart of the Nyquist sampling limit in the time domain. A spacing larger than this limit causes spatial aliasing which yields undesired grating lobes and increased sidelobe levels in the array pattern. On the other hand, the spatial resolution of an array is proportional to its aperture. Increasing the aperture by obeying the Nyquist spatial limit means increasing the number of sensors. Consequently, this means increasing the cost, the complexity and the computational burden of the system. This tradeoff is the first problem that a designer will face and should solve. Therefore, although there are many studies to understand the properties of sparse linear sensor arrays, most of them aim to design/construct new sparse linear sensor arrays fitting to the case-specific purposes. Common purposes in these designs are to reduce the complexity and the cost. A rich variety of methods have been developed in this context. Some use linear or nonlinear optimization methods while some others do not. Optimization parameters in the design process are sensor positions and/or sensor weights. This study has started with a similar motivation. The study can be divided into two main branches.

In the first branch, the analysis and the comparison of "coarray based arrays" have been conducted. The term "coarray based array" has been introduced in this thesis to describe the recently proposed sparse linear arrays which rely on the concept of the difference coarray. The difference or sum coarray of an array is defined as the virtual array located at distinct differences or sums between the locations of the sensors. Broadly speaking, coarray based methods aim to minimize "redundancy" in the

coarray, maximize the length of the "hole" free segment of the coarray, and therefore maximize array aperture and resolution. **Redundancy** indicates the amount of the repeating lags in the coarray except the zero lag. If an array has no repeating lags in its coarray except the zero lag, then it is called as a nonredundant array. On the other hand, **hole** indicates a missing lag. The design of sparse arrays based on coarray concepts has a long history which dates back even before the use of the term coarray. For example, "minimum redundancy arrays" are designed based on coarray concepts [1,2]. The coarray concept regained attention recently. The basic motivating arguments in the recently proposed arrays are the lack of the need for optimization routines for array element placement, i.e., the existence of closed-form expressions for array topology, and that the degrees of freedom (DOF) can be significantly increased compared to that of a uniform linear array of the same amount of elements. DOF of an array is related to the maximum number of sources that it can resolve. Our motivation is also based on these two arguments. A series of simulations have been conducted to fulfill our purpose. In simulations, the performance of coarray based arrays are compared in terms of DOA estimation accuracy, CRLB, degrees of freedom, DOA resolution and mutual coupling. DOA estimation accuracy is the primary concern. For DOA estimation, firstly a modified signal model is obtained from the auto-correlation matrix of the array output through Khatri-Rao product [3]. Then spatial smoothing methods are used to construct a suitable matrix, also called as spatially smoothed matrix. Finally, MUSIC method is applied to the spatially smoothed matrix. The MUSIC method in coarray based processing has been called as coarray-based MUSIC. The simulations have shown that it is the expanded aperture that increases DOF and the resolvability opposing to the second argument.

In the second branch, we study the design of sparse arrays for nonlinear processing, in particular for "nonlinear apodization". Nonlinear apodization as the name implies uses a nonlinear method for windowing/tapering/apodization (Tapering and apodization are terms used for windowing in sensor array and optical signal processing, respectively). Nonlinear apodization has been first presented to increase resolution in synthetic aperture radar images. Similar to sparse array design, there is a tradeoff between sidelobe level and mainlobe width in windowing operation. This tradeoff is the main problem that designers should handle. The aim is to obtain the narrowest

mainlobe and the lowest sidelobe level possible. Conventionally, windowing is used at the expense of widening the mainlobe in order to reduce the sidelobe level. However, in nonlinear apodization, the sidelobe level can be reduced without increasing the mainlobe width. The main idea is to use multiple windows instead of a single window and to select the minimum spectral value for each frequency. Patterns of some of these windows have a good sidelobe level while some of them have good mainlobe width. Nonlinear apodization successfully combines their good spatial regions. This method eases the tradeoff between sidelobe level and mainlobe width to some extent. Nonlinear apodization can reduce the sidelobe level at most down to the noise level. Moreover, using multiple windows naturally increases the complexity and the computational burden. In this study, firstly, nonlinear apodization has been adapted to the spatial domain. Then, because windowing and sparse array design problems have similar tradeoffs, nonlinear apodization has been used for the sparse linear array design together with the Genetic Algorithm (GA). The design contains a special layout which consists of two sub-arrays. One of the sub-arrays is designed by GA, whereas the other one is designed according to results of the aforementioned design. Dual-apodization is applied to the sub-arrays to obtain the output. One of the sub-arrays have a good behavior around the mainlobe regions and the other at sidelobe regions. Obviously, the aim is to have good behaviour in all regions while steering to any particular direction. However, a perfect solution is not possible with only two sub-arrays but a great many. On the other hand, this is practically and computationally very difficult. Instead, a design with a moderate computational load for a limited number of targets is proposed.

The outline of the thesis is as follows: Chapters 2 and 4 give required background knowledge about the topics in this thesis. Chapter 3 gives the study conducted in the first branch of this thesis. While, chapters 4, 5, and 6 construct the second branch, and give the corresponding works.

In Chapter 2, a brief overview of sensor array signal processing and modeling has been provided. The DOA estimation methods used in this thesis and their performances with comparative examples in the case of sparse linear arrays are presented.

In Chapter 3, firstly a history of sparse arrays is provided. Then, detailed analysis

and comparison of coarray based methods have been given. The advantages and disadvantages of these methods with simulation results have been provided. The arguments of these methods have been examined and their justifications have been questioned.

Chapter 4 presents the details of nonlinear apodization methods. One of the nonlinear apodization methods known as Spatially Variant Apodization is shown to be a variant of the minimum variance estimator.

In Chapter 5, Spatially Variant Apodization (SVA) has been adapted to the spatial domain and a beamforming method using SVA has been presented.

Nonlinear Apodization and Genetic Algorithm have been combined and a novel hybrid sparse array design method has been presented in Chapter 6. This novel method has a better sidelobe level and mainlobe resolution compared to some existing solutions.

Chapter 7 concludes up the study and Appendix A give some DOA estimation methods widely used in the literature.

Contributions of this work are included in chapters 3, 5, and 6, and can be summarized as follows,

- An analysis and comparison of coarray based arrays of recent interest have been carried out. Aspects accompanying the ability to detect more sources than sensors have been investigated. The importance of extended aperture as the basis of the increase in DOF has been emphasised. In particular, coarray based arrays have been studied with the two points of view: the layout for a fixed number of sensors, and the number of sensors for a fixed aperture.

- Spatially Variant Apodization (SVA) method has been adapted to beamforming and implementation issues have been investigated.

- A novel sparse array design approach for nonlinear processing has been proposed. Despite its low computational demand, the proposed approach uses a given aperture and array elements efficiently.

The notation used in this thesis is as follows: scalar quantities are shown by italic lowercase letters , vectors by bold lowercase letters , and matrices by bold uppercase letters . The transposition, complex conjugation, and complex conjugate transposition operations are denoted by superscripts T, $*$ and H respectively.

CHAPTER 2

BACKGROUND OF THE PROCESSING METHODS IN THIS WORK

The main objective in array signal processing is to detect and extract information in the wave or signal gathered by an array of sensors. The information may be the content of the signal or it can be the location of the source. Many different methods from other areas have been adapted to the area of sensor array signal processing in order to extract this useful information. Sensor arrays can be found in many areas such as communication, sonar, radar, seismology, bio-medicine, astronomy, and imaging, [4].

A sensor array can be considered as a spatial window which samples the components of the field on that particular location. The rate of spatial sampling is determined by the distance between sensors. The pattern of the this spatial window is determined by the weights and the locations of the sensors. This pattern can change according to steered direction if array aperture and sensor locations are not uniform for all directions. The field is a result of the sources located at different directions. The powers and the directions of the sources relative to the sensor array determine the pattern of the field. For a particular direction, sum of the multiplication of the array pattern and the field pattern gives the output of the sensor array for that particular direction. This operation reminds us the convolution operation. Therefore, assuming array pattern is uniform for all directions, the array output can be obtained by the convolution of the array pattern and the field pattern.

Beamforming and direction of arrival (DOA) estimation are among the most common and important tasks in array signal processing. Various methods have been developed for such purposes. In this chapter, the methods that are used in the thesis will be summarized. Some other important methods worth mentioning are provided in Appendix A.

In practice, there are various array geometries, in this work, linear arrays in which identical elements are placed on a line are considered. In particular, the focus will be on sparse linear arrays.

2.1 Array Signal Model

To have a basic model of the spatial sampling process, some assumptions are made about the signal and the medium. The assumptions are listed below [5]:

- The incoming wave is a narrowband signal, that is the propagation delay across the array is very small compared to the reciprocal of the signal bandwidth.
- The source is in the far-field of the array, therefore the incoming signal is a planar wave.
- The sensor array and the sources are assumed to be on the same plane.
- The sources and the receivers are point elements.
- The propagation medium is homogeneous.

Consider an array of M sensors and K narrowband sources, $M \geq K$. Let the DOA of the signals be $\boldsymbol{\theta}_1 ..., \boldsymbol{\theta}_K$ where $\boldsymbol{\theta}_k = [\theta_k \ \phi_k]$ and θ_k is the azimuth of the k^{th} source measured from positive x axis and ϕ_k is the elevation measured from positive z axis. For simplicity unless otherwise stated the elevation angle is taken as $\pi/2$ in calculations, so DOA will be defined only by the azimuth angle.

Using the assumptions given above, the output vector of the sensor array, $\mathbf{y}(t)$, at time instant t, also called a *snapshot*, is given as [6],

$$\mathbf{y}(t) = \mathbf{A}(\boldsymbol{\theta})\mathbf{s}(t) + \mathbf{v}(t), \tag{2.1}$$

where $\mathbf{s}(t) = [s_1(t)s_2(t)...s_K(t)]^T_{K\times 1}$ are source signals and $\boldsymbol{\theta} = [\theta_1 \ \theta_2 ... \theta_K]^T$ are related DOAs, $\mathbf{v}(t)$ is $M \times 1$ noise vector and $\mathbf{A}(\boldsymbol{\theta}) = [\mathbf{a}(\theta_1), \mathbf{a}(\theta_2)...\mathbf{a}(\theta_K)]$ is $M \times K$

steering matrix. The noise is assumed to be zero mean, spatially and temporarily white, and Gaussian. The steering vector $\mathbf{a}(\theta_k)$ for $k = 1, 2, ..., K$ is given as,

$$\mathbf{a}(\theta_k) = [g_1(\theta_k)e^{-j\omega_c\tau_1(\theta_k)}g_2(\theta_k)e^{-j\omega_c\tau_2(\theta_k)}...g_M(\theta_k)e^{-j\omega_c\tau_M(\theta_k)}]^T, \tag{2.2}$$

where $g_m(\theta_k),\ m = 1, 2, ..., M$ is the sensitivity of the m^{th} sensor at direction θ_k, $\tau_m(\theta_k)$ is the time delay of arrival between the m^{th} sensor and some reference point and ω_c is the center frequency. In this report, it is assumed that all sensors are identical and omni-directional, therefore $g_m(\theta_k) = 1,$ for $m = 1, 2, ..., M$, moreover the reference point is taken as the first sensor of the array and its position is accepted to be the origin of the coordinate system in which sensor array and sources are located.

A plane wave propagating in direction θ_k has the direction vector $\mathbf{g}_k$ given as,

$$\mathbf{g}_k = \begin{bmatrix} \cos\theta_k \sin\phi_k \\ \sin\theta_k \sin\phi_k \\ \cos\phi_k \end{bmatrix} = \begin{bmatrix} \cos\theta_k \\ \sin\theta_k \\ 0 \end{bmatrix}. \tag{2.3}$$

Let the position of the m^{th} sensor be $\mathbf{p}_m$, then the time delay $\tau_m(\theta_k)$ is

$$\tau_m(\theta_k) = \frac{-\mathbf{g}_k^T\mathbf{p}_m}{c}, \tag{2.4}$$

where c is the speed of the wave in the medium. Therefore, (2.2) now can be written as,

$$\mathbf{a}(\theta_k) = [1, e^{\frac{j\omega_c\mathbf{g}_k^T\mathbf{p}_2}{c}}, ..., e^{\frac{j\omega_c\mathbf{g}_k^T\mathbf{p}_M}{c}}]^T. \tag{2.5}$$

The given model can be extended for N snapshots. Then, the model given in (2.1) can be rewritten as follows,

$$\mathbf{Y} = \mathbf{A}(\boldsymbol{\theta})\mathbf{S} + \mathbf{V}, \tag{2.6}$$

where $\mathbf{Y}$ and $\mathbf{V}$ are $M \times N$ matrices and $\mathbf{S}$ is $K \times N$ and they are given as follows,

$$\begin{aligned}\mathbf{Y} &= [\mathbf{y}(t_1), \mathbf{y}(t_2), ..., \mathbf{y}(t_N)] \\ \mathbf{V} &= [\mathbf{v}(t_1), \mathbf{v}(t_2), ..., \mathbf{v}(t_N)] \\ \mathbf{S} &= [\mathbf{s}(t_1), \mathbf{s}(t_2), ..., \mathbf{s}(t_N)].\end{aligned} \tag{2.7}$$

Now let's consider a uniform linear array (ULA) with sensor separation d. In this case, the delay between the m^{th} sensor and the reference point is $\tau_m(\theta_k) = d(m-1)cos(\theta_k)/c$ for $m = 1, 2, ...M$.

Assuming there are K sources in the medium with DOAs $\theta_k,\ k = 1, 2, ..., K$, and noting that $c = \lambda f_c$ where λ is the wavelength of the signal and $\omega_c = 2\pi f_c$, the steering matrix for M sensors is obtained as follows,

$$\mathbf{A}(\boldsymbol{\theta}) = \begin{bmatrix} 1 & 1 & \dots & 1 \\ e^{j2\pi\frac{d}{\lambda}cos(\theta_1)} & e^{j2\pi\frac{d}{\lambda}cos(\theta_2)} & \dots & e^{j2\pi\frac{d}{\lambda}cos(\theta_K)} \\ \vdots & \vdots & \ddots & \vdots \\ e^{j2\pi\frac{d}{\lambda}(M-1)cos(\theta_1)} & e^{j2\pi\frac{d}{\lambda}(M-1)cos(\theta_2)} & \dots & e^{j2\pi\frac{d}{\lambda}(M-1)cos(\theta_K)} \end{bmatrix}. \tag{2.8}$$

Note that in (2.8), in order to have a unique $\mathbf{A}(\boldsymbol{\theta})$ or to have no spatial aliasing it is required that $2\pi\frac{d}{\lambda}cos(\theta_k) \leq \pi$ for $k = 1, 2, ..., K$. Since $|\cos(\theta_k)| \leq 1$, the maximum separation between the sensors is obtained as $d \leq \lambda/2$; this is known as the Nyquist spatial limit.

2.2 DOA Estimation Methods

DOA estimation is one of the most important topics in array signal processing. Many methods have been developed in the literature for DOA estimation [7]. DOA estimation methods can be categorized into two main parts; non-parametric methods and parametric methods. In non-parametric methods, generally a spectrum-like function (spatial spectrum) concerning DOA is obtained and DOAs are determined by an analysis of the peaks of the spectrum. Beamforming and some subspace-based methods

are the most known spectral approaches. Parametric methods fully exploit the underlying data model and better estimation accuracy is obtained at the expense of an increase in the computational burden. In parametric methods, a multidimensional search is conducted over parameters of interest. Moreover, spectral-based methods may be insufficient in the case of highly correlated or coherent signals, but parametric methods have the robustness in these cases. Maximum-likelihood (ML) techniques are the most famous parametric methods. In this chapter, conventional beamforming, Capon beamforming (MVDR), and MUSIC methods are reviewed. For an interested reader, ESPRIT and maximum-likelihood methods are described in Appendix A.

2.2.1 Beamforming

A sensor array performs a spatial sampling similar to the temporal sampling. Spatial sampling helps to discriminate signals having similar time and frequency content but different DOA. Beamforming combines temporal and spatial filtering, spatiotemporal filtering [6], for two main purposes; finding the DOA of the incoming signal and enhancing the signals from the interested direction while attenuating signals from other directions. In this thesis, beamforming is used for the first purpose.

The main idea in beamforming is to "steer" the array to all directions electronically by adjusting the phases. Then, the power is measured for each direction. DOA estimates are obtained by an analysis of the angular spectrum. To achieve steering, the output of the sensor array is weighted by $\mathbf{w}$, yielding $y_f(t) = \mathbf{w}^H \mathbf{y}(t)$. Choices of weighting vector $\mathbf{w}$ determine the type of the beamformer.

2.2.1.1 Conventional Beamforming

Conventional Beamforming (CBF) algorithm is one of the oldest DOA estimation techniques. The weights are chosen such that the power is maximized in a certain direction. Suppose that there is a single source at θ_k, then the optimal weight vector is obtained by solving the following optimization problem [7]:

$$\begin{aligned}\mathbf{w}_{opt} &= \arg\max_{\mathbf{w}} \; E\{y_f(t)y_f(t)^H\} \\ &= \arg\max_{\mathbf{w}} \; E\{\mathbf{w}^H\mathbf{y}(t)\mathbf{y}^H(t)\mathbf{w}\} \\ &= \arg\max_{\mathbf{w}} \; \mathbf{w}^H E\{\mathbf{y}(t)\mathbf{y}^H(t)\}\mathbf{w}, \qquad \text{subject to } \mathbf{w}^H\mathbf{w} = 1 \end{aligned} \tag{2.9}$$

Remembering the signal model given in (2.1), (2.9) becomes as follows,

$$\begin{aligned}\mathbf{w}_{opt} &= \arg\max_{\mathbf{w}} \; \sigma_s^2\mathbf{w}^H\mathbf{a}(\theta_k)\mathbf{a}^H(\theta_k)\mathbf{w} + \sigma_v^2\mathbf{w}^H\mathbf{w}, \qquad \text{subject to } \mathbf{w}^H\mathbf{w} = 1 \\ &= \arg\max_{\mathbf{w}} \; \sigma_s^2|\mathbf{w}^H\mathbf{a}(\theta_k)|^2 + \sigma_v^2|\mathbf{w}|^2, \qquad \text{subject to } |\mathbf{w}| = 1, \end{aligned} \tag{2.10}$$

where σ_s^2 is the signal power and σ_v^2 is the noise power. Then, the optimum weights are obtained as [7],

$$\mathbf{w}_{CBF} = \frac{\mathbf{a}(\theta_k)}{\sqrt{\mathbf{a}^H(\theta_k)\mathbf{a}(\theta_k)}}. \tag{2.11}$$

DOA estimate is taken as the angle of the largest peak of the spatial spectrum, $|\mathbf{w}_{CBF}^H\mathbf{y}(t)|^2$. Using (2.11), the spatial spectrum is obtained as follows [5],

$$P_{CBF}(\theta) = \frac{|\mathbf{a}^H(\theta)\mathbf{y}(t)|^2}{\mathbf{a}^H(\theta)\mathbf{a}(\theta)}. \tag{2.12}$$

When there are K sources in the medium, the location of K largest peaks of (2.12) are taken as DOA estimates. The main problem in conventional beamforming is the resolution performance. Independent of the quality or amount of the available data, the resolution of the conventional beamformer is limited [7]. The resolution here is the ability to separate two sources close to each other in terms of angle of arrival.

Algorithmic steps for conventional beamforming in the existence of K sources are as follows:

1. Collect output data samples **y**(t)

2. Calculate weights $\mathbf{w}(\theta)$ using 2.11

3. Evaluate (2.12) for all θ directions

4. Locations of K largest peaks are DOAs

2.2.1.2 Capon Beamforming

In order to improve the resolution performance of the conventional beamformer, a new method has been proposed by Capon [8]. The optimization problem for a single source is now given as follows:

$$\mathbf{w}_{opt} = \arg\min_{\mathbf{w}} \ \mathbf{w}^H \mathbf{R}_y \mathbf{w} \qquad \text{subject to } \mathbf{w}^H \mathbf{a}(\theta_k) = 1 \tag{2.13}$$

where $\mathbf{R}_y = E\{\mathbf{y}(t)\mathbf{y}^H(t)\}$ is the output covariance matrix. In this formulation, as it is seen from (2.13), the aim is to minimize the output power while keeping the power in steering direction θ_k constant, therefore the method is also known as Minimum Variance Distortionless Response (MVDR). In this way, while noise and interference from directions other than the steering direction are attenuated, the power of the signal coming from steering direction is kept constant. The optimum weights for Capon beamformer (CPN) are obtained as [5],

$$\mathbf{w}_{CPN} = \frac{\mathbf{R}_y^{-1}\mathbf{a}(\theta_k)}{\mathbf{a}^H(\theta_k)\mathbf{R}_y^{-1}\mathbf{a}(\theta_k)}. \tag{2.14}$$

The spatial spectrum using (2.14) is,

$$P_{CPN}(\theta) = \frac{1}{\mathbf{a}^H(\theta)\mathbf{R}_y^{-1}\mathbf{a}(\theta)}. \tag{2.15}$$

The location of the largest peak in spatial spectrum (2.15) is the DOA estimate. In case of K sources the locations of K largest peaks of (2.15) are DOA estimates.

Although Capon beamforming has a better resolution compared to conventional beamforming, its resolution limit also depends on the number of sensors and SNR [5].

Moreover, computing $\mathbf{R}_y^{-1}$ becomes computationally prohibitive as the number of sensors increase and it may fail in case of coherent signals since $\mathbf{R}_y$ becomes ill-conditioned [9]. Robust variants of Capon beamforming have been proposed to overcome this problem [10, 11].

In practice, output covariance matrix $\mathbf{R}_y$ is not available, therefore an estimate, sample covariance matrix, computed from output data samples is found as,

$$\hat{\mathbf{R}}_y = \frac{1}{N}\sum_{t=1}^{N}\mathbf{y}(t)\mathbf{y}^H(t). \tag{2.16}$$

Fundamental steps of Capon beamforming algorithm for K sources are as follows:

1. Collect output data samples, also known as snapshots, **y**(1), **y**(2), ..., **y**(N)
2. Evaluate the estimate of the covariance matrix from (2.16)
3. Evaluate (2.15) for all θ directions
4. Locations of K highest peaks are DOAs

2.2.2 Subspace Based Methods

The main idea in subspace based methods is to partition the covariance matrix $\mathbf{R}_y$, of the array output $\mathbf{y}(t)$, into signal and noise subspaces. These two subspaces are orthogonal and obtained by eigenvector decomposition. It is assumed that there are K sources which are incoherent, wide sense stationary processes [5]. Subspace methods are sub-optimal, high-resolution methods, and they are widely used in practice. Moreover, the estimates are statistically better in comparison to beamforming techniques [7]. However, they require much more computation, and in low SNR cases "subspace swap" may cause serious problems.

Consider the signal model given by (2.1). Assuming the noise in sensors are spatially and temporarily white, Gaussian, and uncorrelated with the sources, the auto-

correlation matrix of the array output is determined as,

$$\mathbf{R}_y = \mathbf{A}\mathbf{R}_s\mathbf{A}^H + \sigma_v^2\mathbf{I}, \tag{2.17}$$

where $\mathbf{R}_s$ is $K \times K$ covariance matrix of the sources. Since the sources are incoherent, $\mathbf{R}_s$ is full rank. $\boldsymbol{\theta}$ has been dropped in (2.17) for simplicity. σ_v^2 is the power of the noise signals which are both temporarily and spatially independent from each other, and are white Gaussian processes with zero mean, and $\mathbf{I}$ is identity matrix.

Let $\mathbf{U} = [\mathbf{u}_1\mathbf{u}_2...\mathbf{u}_M]$ and $\mathbf{V} = diag(\lambda_1, \lambda_2, ..., \lambda_M)$ where $\mathbf{u}_m$ and λ_m are the m^{th} eigenvector and corresponding eigenvalue of $\mathbf{R}_y$, respectively. $\mathbf{A}$ is full rank (K), however $\mathbf{A}\mathbf{R}_s\mathbf{A}^H$ is M dimensional therefore $M - K$ eigenvalues of $\mathbf{A}\mathbf{R}_s\mathbf{A}^H$ are zero. Thus, $M - K$ smallest eigenvalues of $\mathbf{R}_y$ are σ_v^2. Let $\lambda_1 \geq \lambda_2 \geq ... \geq \lambda_{K+1} = \lambda_{K+2}... = \lambda_M = \sigma_v^2$ with corresponding eigenvectors $\mathbf{u}_1, \mathbf{u}_2, ..., \mathbf{u}_M$. The eigenvectors spanning signal subspace are the first K eigenvectors, $\mathbf{U}_s = [\mathbf{u}_1\mathbf{u}_2...\mathbf{u}_K]$, and the ones which span noise subspace are the remaining $M - K$ eigenvectors, $\mathbf{U}_n = [\mathbf{u}_{K+1}\mathbf{u}_{K+2}...\mathbf{u}_M]$ [7]. Here, $\mathbf{U}_s \perp \mathbf{U}_n$ and $\mathbf{A} \perp \mathbf{U}_n$. Moreover, $\mathbf{A}$ and $\mathbf{U}_s$ span the same column space [5, 7, 9].

2.2.2.1 MUSIC

MUSIC (MUltiple SIgnal Classification) is one of the oldest and most commonly used noise subspace methods for DOA estimation [9]. There are variations of MUSIC such as Root-MUSIC, Weighted MUSIC, Spectral MUSIC. Here *Spectral-MUSIC* method will be described.

Noting that all eigenvectors in $\mathbf{U}_n$ correspond to the same eigenvalue σ_v^2 we have, $\mathbf{R}_y\mathbf{U}_n = \sigma_v^2\mathbf{U}_n$. Inserting (2.17) into this expression we get

$$(\mathbf{A}\mathbf{R}_s\mathbf{A}^H + \sigma_v^2\mathbf{I})\mathbf{U}_n = \sigma_v^2\mathbf{U}_n \rightarrow \mathbf{A}\mathbf{R}_s\mathbf{A}^H\mathbf{U}_n = \mathbf{0} \tag{2.18}$$

It is known that $\mathbf{A}$ is full rank and $\mathbf{R}_s$ is nonsingular [9], this implies that $\mathbf{A}^H\mathbf{U}_n = \mathbf{0}$, as indicated previously, $\mathbf{A} \perp \mathbf{U}_n$. Remember that $\mathbf{A} = \mathbf{A}(\boldsymbol{\theta}) = [\mathbf{a}(\theta_1), \mathbf{a}(\theta_2), ..., \mathbf{a}(\theta_K)]$

therefore, all steering vectors with true DOA will satisfy $\mathbf{a}^H(\theta_\mathrm{k})\mathbf{U}_n\mathbf{U}_n^H\mathbf{a}(\theta_\mathrm{k}) = 0$, for $k = 1, 2, ..., K$. Thus, the MUSIC spatial spectrum is defined as [9],

$$P_{MUSIC}(\theta) = \frac{1}{\mathbf{a}^H(\theta)\mathbf{U}_n\mathbf{U}_n^H\mathbf{a}(\theta)}. \tag{2.19}$$

The DOA estimates can be found as locations of K largest peaks of the spectrum obtained by (2.19).

Fundamental steps of MUSIC in case of K sources are as follows:

1. Collect output data samples **y**(1), **y**(2), ..., **y**(N).
2. Evaluate the estimate of the covariance matrix from (2.16).
3. Find the eigenvalues and the eigenvectors of $\hat{\mathbf{R}}_y$ and determine noise subspace $\mathbf{U}_n$. Note that the number of sources can be found by extracting the number of repeating smallest eigenvalues from the number of sensors.
4. Evaluate (2.19) for all θ.
5. Locations of K highest peaks are DOAs.

2.2.3 Comparison of DOA Methods

In this section a comparison of the DOA methods given above will be presented using a sparse linear array. For comparison, a Minimum Redundancy Array (MRA) with 8 sensors will be used [1]. MRAs achieve maximum resolution by minimizing the redundant spacings present in the array. There is no closed form expression for the topology of these arrays, they are obtained by optimization algorithms [1,2]. The lay-out of the array is given in Figure 2.1. In DOA estimation and resolution simulations, the result for each SNR is an average of 1000 Monte Carlo runs.

2.2.3.1 Spatial Spectrum

The spatial spectra obtained by conventional beamforming (CBF), Capon and MUSIC methods are given in figures 2.2, 2.3 and 2.4. In Figure 2.2, there is a single target

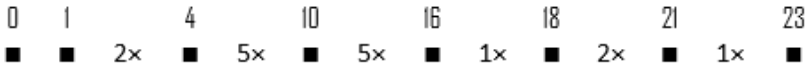

Figure 2.1: MRA layout. Solid Rectangles stand for sensors and crosses represent number of empty spaces or holes. Elements are located at multiples of $d = \lambda/2$ (half-wavelength).

at broadside ($\theta = 90$) of the array, and there are 4 SNR values. The number of snapshots for Capon and MUSIC is 50. The spatial spectra for a line array is symmetric with respect to end-fire of the array, therefore, results for $[0\ 180]^\circ$ interval have been provided.

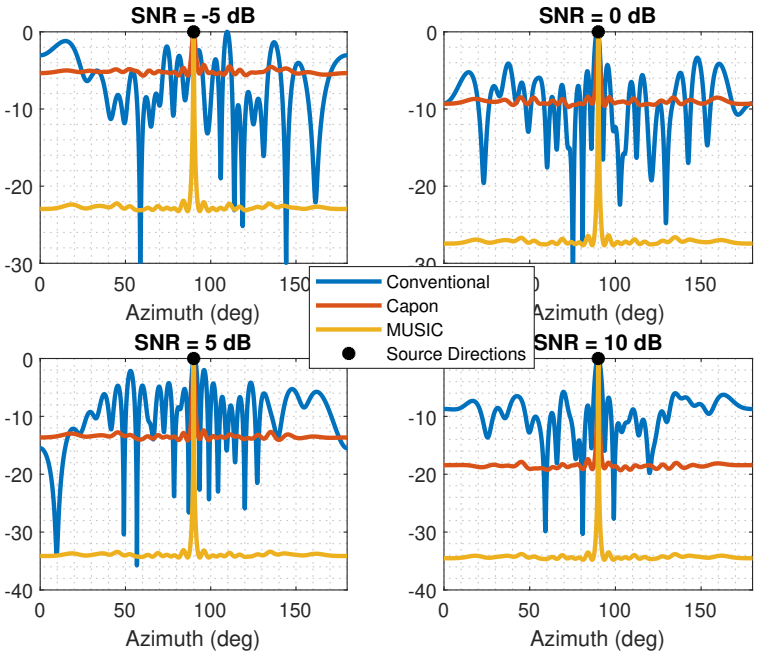

Figure 2.2: Comparison of spatial spectra for different SNR values, single target.

Figure 2.2 tells us that CBF performs very poorly due to missing sensors even at high SNR, however, Capon and MUSIC are not affected much since they collect the information provided by the missing sensors from the auto-correlation function of the array. Moreover, these methods are more appropriate for a coarray based design. In Capon and MUSIC, the sidelobes are suppressed more as SNR increases.

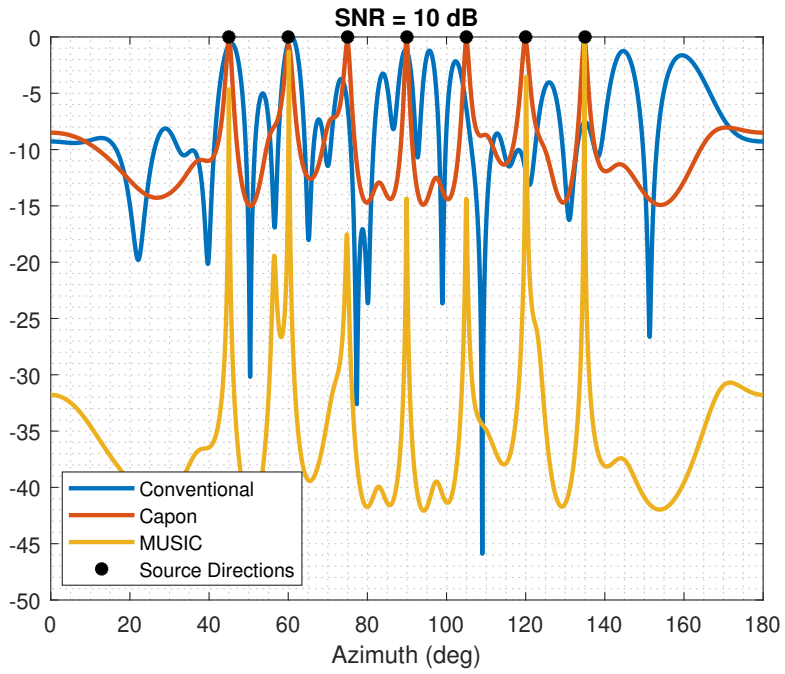

Figure 2.3: Comparison of spatial spectra for 7 targets.

In figures 2.3 and 2.4 there are 7 and 9 targets, respectively. Due to restriction in number of sources in MUSIC, at most 7 sources can be resolved by this method, therefore in Figure 2.4 MUSIC is not given. However, there is no restriction for CBF or Capon. CBF performs poorly due to missing sensors as expected. On the other hand, Capon successfully detects all sources in the given examples. Moreover, notice that the spurious peaks observed in both MUSIC and Capon spatial spectra gets higher and increases in number. Specifically, in MUSIC spatial spectrum, the spurious peak at around 50° is very high. Moreover, although all sources have the same SNR, the level of some of the targets in MUSIC spectrum is lower due to sparsity. Therefore, although Capon and MUSIC may have satisfactory results for a single target and high SNR, as the number of targets increases their performances degrades for the given sparse array.

2.2.3.2 DOA Estimation

RMSE of DOA estimation for a single target with respect to SNR is given in Figure 2.5. DOA has been randomly selected in each run between $[45,\ 135]^\circ$. For smaller

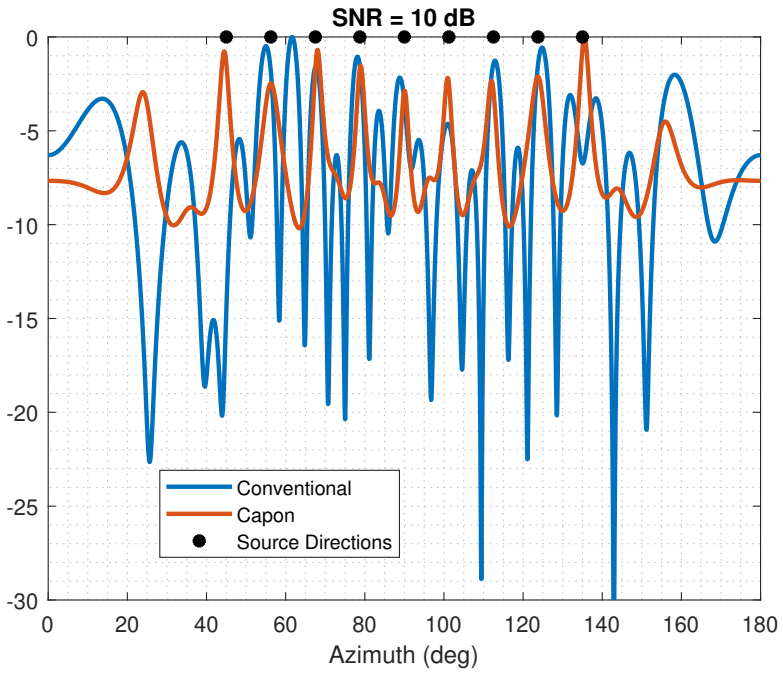

Figure 2.4: Comparison of spatial spectra for 9 targets.

SNR values the performances of Capon and MUSIC also degrade due to missing sensors. Capon and MUSIC performs very similarly, except that MUSIC makes the sharp decrease before the Capon.

2.2.3.3 DOA Resolution

The resolution here is defined as the ability of discriminating two close targets, and results are provided in Figure 2.6. In resolution simulations, two closely located sources are considered. The sources are located at $90 \pm \Delta\theta$ degrees. If two peaks are observed around 90 degrees with separation bigger than $\Delta\theta$, then it is assumed that the sources are resolved otherwise they are not resolved. The superiority of MUSIC in resolution is observed in Figure 2.6. CBF cannot succeed to resolve the targets even at 10 degrees separation.

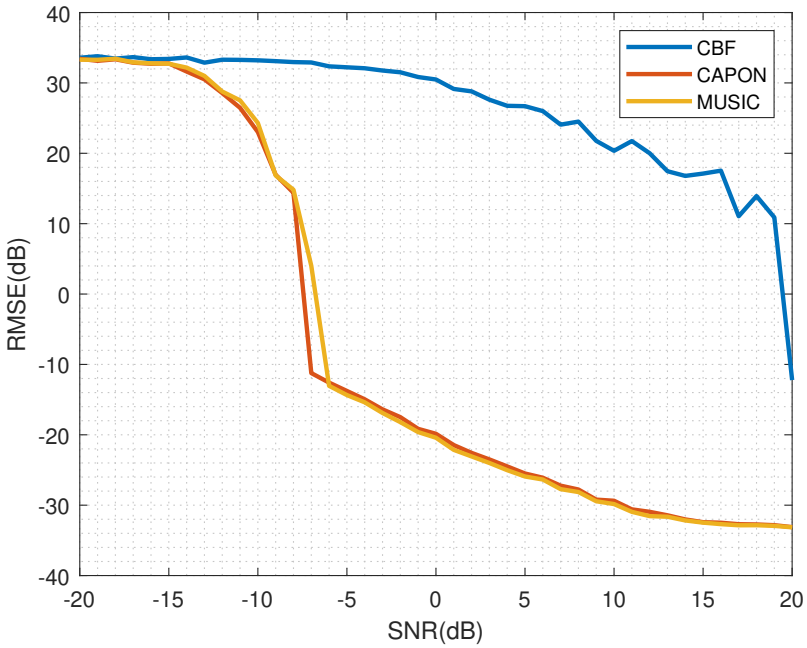

Figure 2.5: RMSE results of methods for a single target for different SNR values

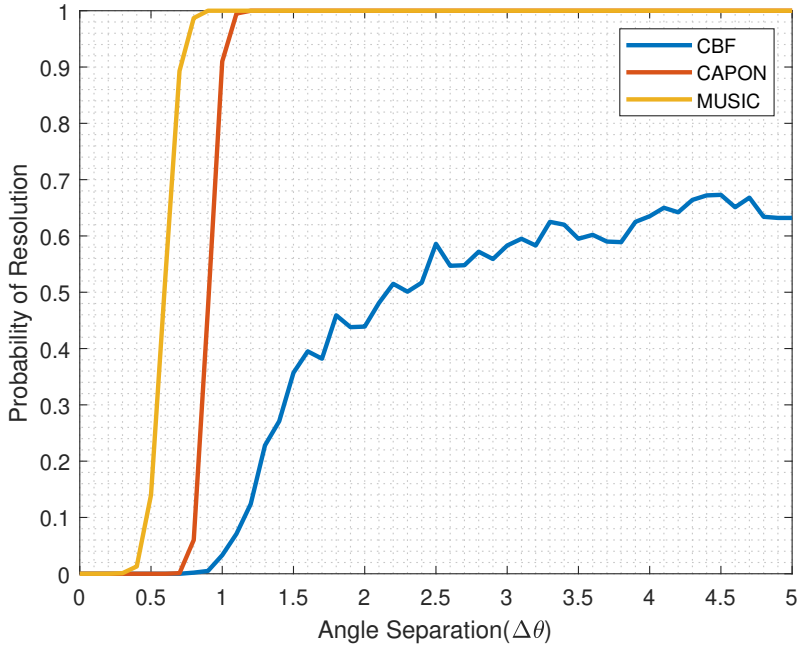

Figure 2.6: Resolution results of methods for SNR = 10 dB

2.3 Conclusion

In this chapter, DOA estimation methods used in the following chapters are presented. MUSIC is used in Chapter 3, and CBF is used in Chapters 5 and 6. On the other hand, Capon has also been included because of its similarity to SVA presented in Chapter 4.

The focus of this thesis is on sparse linear arrays, therefore in the last section of this chapter, a sparse linear array has been used to compare the performance of CBF, Capon, and MUSIC. The conclusion of simulations can be stated as; CBF performs poorly in DOA estimation with the sparse array presented in Figure 2.1. Capon and MUSIC, on the other hand, have given sufficient and acceptable results for a single target. Moreover, it can be concluded these methods can be used with an appropriate choice of a sparse array. MUSIC is restricted by the number of sensors but has better resolution and RMSE performance compared to Capon.

CHAPTER 3

ANALYSIS AND COMPARISON OF COARRAY BASED SPARSE ARRAYS

The study of sparse linear arrays has started in the 1960's and remains a hot topic. Since then, the problem has been approached in a variety of ways, and many different optimization algorithms have been used to design sparse arrays. In the early years of sparse array research, in addition to other methods that involve array pattern related measures, the problem had been handled in terms of the coarray structure. Such methods do not directly involve pattern-based objectives, and in some cases, they have closed-form structures; we call these methods as coarray based methods. Nowadays, coarray based methods are attracting considerable attention again. In this chapter, the analysis and comparison of the most commonly known ones of those arrays are conducted. Moreover, the necessity and the success of those arrays are discussed by chasing answers to two questions with simulation results. First, while keeping the number of sensors fixed what is the optimum layout? Secondly, while keeping the aperture fixed what is the optimum number of sensors to be used?

3.1 A History of Sparse Arrays

The work on sparse linear array design dates back to the 1960's (in some cases, "nonuniform" instead of "sparse" may be more appropriate for these early studies) [1, 12–21]. One motivation behind these early studies is to realize a tapered field distribution over the antenna aperture by properly adjusting the spacing between the elements of a discrete element antenna instead of varying element excitations. This approach has been called "space tapering". Space tapering was considered as an alternative to amplitude tapering in reducing sidelobes. By that time, sidelobe reduction

by tapering a continuous source distribution had already been studied [22–24].

In [12], a sparse array design has been made by varying the spaces between the array elements using the continuous field distribution of a reference pattern. The aperture is kept fixed and the number of sensors is reduced compared to a ULA with the same aperture. In [13] for the first time, as of our knowledge, an optimization technique, dynamic programming, has been used for "thinned" array design. It is basically a trial-and-error computational technique which systematically eliminates most of the possible configurations in searching for an optimum configuration to achieve a desired pattern. As the authors report, their designs were better than the reported methods at that time at the expense of significantly more computations. The effects of the design parameters are studied but the optimality of the results has not been verified in the paper. The authors in [14] make use of Poisson's sum formula and a "Source Position Function", and derive a transformation between an equivalent continuous source distribution and a given unequally-spaced array. Then, according to the number of elements, desired side lobe and grating lobe suppression levels, the continuous source distribution is found. The element locations of the unequally-spaced array can be obtained by the transformation. The method has been especially successful in suppressing the sidelobes near the mainlobe, however, its performance degrades at distant sidelobes. This is mainly because the underlying assumptions are not sufficiently supported in those regions. The method in [14] has been extended in [15] and an analytical array design method has been presented. The problem of having high sidelobes in regions far from the mainlobe has been solved. In addition to that, the design has been modified such that the beam-pattern does not have any high sidelobes in the bandwidth determined by the design parameters. A statistical analysis was made in [16] to reveal the interaction between the physical antenna properties (number of elements, element placement, aperture size) and performance indicators (sidelobe level, resolution, gain, beamwidth). The study has led to promising conclusions about nonuniform placement of the array elements. In [17], finding the optimum values of element excitations and locations was formulated as a constrained nonlinear optimization problem. The problem is transformed into a series of unconstrained nonlinear problems and solved by the Fletcher-Powell method. In [21], space tapered 2-D arrays were designed by adjusting the element spacing according to a reference

amplitude tapering. Specific locations of antenna elements were determined by a probabilistic method. In [19], space tapered arrays were designed by using analog and digital computers together. In each round, a sequence of antenna patterns are computed for varied positions of a single element, and the best position is determined for that element. In [20], the results of the studies conducted up to that time have been examined, and it has been concluded that the results obtained by trial-and-error methods and by non-global optimization methods are not very different and that the design with the lowest sidelobe can only be found by using truly global optimization methods.

After the work of Arsac, [25], towards the end of the 1960's, Moffet, [1], introduced the terms "Redundancy" and "Minimum Redundancy Linear Array" (MRLA) in the context of sparse array design. In [1], the objective in finding the element locations of an array for a given number of total elements is the maximization of the resolution. To achieve this, the target is set as the maximization of the support of the complete part (without zeros) of the spatial/spectral sensitivity function stated as "the minimization of the number of redundant spacings present in the array". In doing this, elements locations form a subset of multiples of half wavelength. Such an objective also serves to obtain a complete set of autocorrelation values up to a maximized lag, a point of attention after the introduction of high resolution array processing methods. Spatial/spectral sensitivity function and difference coarray have overlapping meanings. The term coarray was first used in [26], [27]. Obtaining a complete spatial/spectral sensitivity function was an important requirement to observe completely the spectrum of the intensity variation on the sun's surface [28], [29], [30]. No design criteria other than elimination of zeros of the spatial/spectral sentivity function while maximizing array aperture has been mentioned. This contrasts the array pattern referenced design trend which dominates in this field. A particular geometry presented under the name of "Compound Grating Interferometer" [1] is important since later this geometry has been presented as 'Nested Arrays' in 2010 [31]. A very similar configuration for a large number of arrays has been presented in [32].

The studies on nonuniform/sparse linear antenna design show a slowdown by the number of published papers in the 1970's. Besides the variation of choices of the optimization (free) variables, proposed methods aim to achieve predefined array pat-

terns. In [33], a shaped-beam is synthesized by using simple array pattern formulas without a rigorous optimality concern. However, after inserting the parameters of the desired shaped-beam into array pattern formula, the locations and related amplitudes are selected manually. Reference [34] extended the application of optimal pattern design in the minimax sense to nonuniform symmetric linear arrays and has demonstrated that by just using an unequal spacing instead of equal spacing, the sidelobe levels can be decreased. The method finds the excitations of the elements for a given set of element positions. On the other hand, a very basic result has been shown in [34]; for a given aperture size, as sidelobe level decreases, the beamwidth increases. Reference [35] is one of the initial works to include element positions into the optimization process. A perturbation technique has been applied in [35] to design an array pattern employing L_2 or L_∞ norms. In the perturbation, either the positions and currents of antenna or only the antenna currents have been varied. The method starts with initial values for positions and currents and stops when the error between the desired array factor and designed array factor does not decrease anymore by any perturbation. The designed array factors seem to reach desired ones, however, the complexity is high since too many iterations have to be implemented. Moreover, the iterations may not converge depending on the initial values. The authors of [35] have used the perturbation method in another work [36], but this time perturbing only positions or only phases of antenna elements. Divergence problem was also reported in [36]. In [37] another iterative method for symmetric nonuniform array design has been used. Element excitations are kept the same and fixed during the design process. In each iteration, the element positions are perturbed by a small value and using the array pattern function of unperturbed and perturbed array, the new positions of array elements are determined. The element positions to perturb are taken from the previous iteration. As the search is performed in a heuristic manner, the array pattern after a perturbation may not be satisfactory, in that case, another perturbation is made. The solution for a desired array pattern may not be unique.

MRLA for a large number of sensors has been presented in [2]. The problem statement to obtain an MRLA has been given and different methods have been proposed for the solution. Two of the proposed methods use a systematic approach using a combination and recursion of smaller MRLAs to design MRLAs with many elements. In

addition to those systematic approaches, 3 ad-hoc methods that use the power of digital computation have also been used. While the systematic approaches can only be used for a specific number of antennas, ad-hoc methods do not have considerable superiority over existing MRLAs, on the other hand, they require too much computation.

It seems that the research activity on sparse linear arrays has a lower profile in 1980's also, and again mostly follows array pattern-based approach. In [38], MRLAs and "Minimum Hole Linear Arrays" (MHLA) have been studied considering the concept of coarray. A method to design a recursive MHLA has been provided. The optimum array structures depending on the algorithm used have been stated for source detection and bearing resolvability. In [39] a detailed comparison between sparse and uniform arrays on the basis of array patterns with supporting examples has been provided. A design procedure in which the elements are only located on the multiples of the half wavelength has been presented. The procedure is applicable to only symmetric arrays. A uniform array is thinned by removing a symmetric pair of sensors which results in minimum side lobe level for the newly formed array, this procedure is repeated until the desired number of sensors is obtained. After determining sensor locations, best weights are searched with linear programming.

In the 1990's and 2000's, a remarkable increase in the number of published works related to sparse linear arrays, is observed. The focus of research is at achieving predefined array patterns with emphasis on sidelobe characteristics. In general, both element locations and weights are included as optimization variables. Starting from early 1990s till the end of 2010s, the genetic algorithm (GA) and the simulated annealing seem to be the mostly applied methods for sparse array design due to the combinatorial nature of the problem, [40–50]. As of our knowledge, the genetic algorithm has been used for array synthesizing in [40] for the first time. The steps of the GA are well described and adapted for the array design. The advantages of the GA are being more efficient for a large number of sensors and in contrast to the existing methods in that time, the ability to overcome the local minima due to the mutation step [40]. On the other hand, the problems of GA are that the convergence can be very slow to have a good design and that it is not applicable to real-time optimization procedures. Moreover, there is no single way to implement the steps of GA which

are crossover, selection and mutation. This results in having different outcomes for different implementation ways. In [49], GA has been simplified by using the array excitation weights as chromosomes and avoiding encoding/decoding. Although, the design proposed in [49] seems to be successful in terms of sidelobe suppression, the design only includes weight optimization. In other words, the layout optimization of the array is not done in [49]. Moreover, when the array is steered to a different direction than the broadside, the sidelobe level increases.

Simulated Annealing (SA) was first proposed to "simulate the behavior of the molecules of a pure substance during the slow cooling that results in the formation of a perfect crystal (minimum-energy state)" [42, 51]. Later, it has been used for different optimization problems in which the variables that minimizes the cost function have similar states to that of the molecules. Non-optimal solution and slow convergence disadvantages seen in GA are also observed in SA. In [42], as authors state, Simulated Annealing (SA) has been applied to array design type problems for the first time. SA has been adapted such that the positions and the weights of the sensors are optimized to have minimum sidelobe level. The results seem to be better than the existing solutions at that time. However, due to nature of SA, the obtained solution may not be optimal and even in some cases may be worse than the existing solutions.

Compressive Sensing (CS) is one of the most recently applied methods in linear sparse array design. [52–59]. Under suitable conditions, CS indicates that it is possible to reconstruct necessary information from an incomplete data set [60]. Reference [58] uses a famous greedy algorithm known as Orthogonal Matching Pursuit together with spherical wave expansion for the problem. In the design process of that study, both element field patterns and mutual coupling between elements are considered. In [57], the extension of CS to wideband arrays has been provided. Inspiring the idea used in robust beamforming methods, a robust CS method has been presented in [54] by adding an extra constraint. Extension of Bayesian Compressive Sensing to sparse arrays has been successfully used in [55] and [52].

Recently, coarray based methods regained attention, [31, 61–64]. Design of sparse arrays based on coarray concepts is not new (even before the use of the term "coarray") [1, 26–30, 65]. Coarray based methods aim to minimize redundancy in the coar-

ray, maximize the length of hole free segment of the coarray, and therefore maximize array aperture and resolution. Coarray based designs were applied in radio astronomy, and for DOA estimation combined with MUSIC type processing. Recently, following the study on “Nested Arrays", [31], other methods have been proposed; “Co-prime Arrays" (CA) [61], “Augmented Nested Arrays" (ANA) [63], “Super Nested Arrays" (SNA) [64] and “Sparse Ruler Array" (SRA) [62]. The basic motivating arguments are the lack of the need for optimization routines for array element placement, i.e., existence of closed form expressions for array topology (except SRA), and that the degree of freedom (DOF) can be significantly increased compared to that of a uniform linear array of the same amount of elements. DOF of an array is related to the maximum number of sources that it can resolve. On the processing side, spatial smoothing methods are used to have a full rank correlation matrix and the MUSIC method is applied for DOA estimation. In particular, the MUSIC method in coarray based processing has been called as coarray-based MUSIC.

In this chapter, the analysis and the comparison of coarray based sparse arrays are presented. The comparison criteria are Cramér-Rao Lower Bound (CRLB), DOA estimation accuracy, degrees of freedom, DOA resolution and mutual coupling. However, the main purpose is to answer two fundamental questions based on the results of simulations made for analysis and comparison. Firstly, we look for the array layout which yields the best results while keeping the number of sensors fixed. Secondly, assuming the cost and complexity issues are neglected, we look for the array which shows the best performance in a fixed physical aperture scenario.

In Section 3.2, the signal model used in coarray domain and the signal model under mutual coupling are presented. Moreover, candidate arrays used for comparison and their design details are explained. Section 3.3 gives the Coarray-MUSIC and spatial smoothing methods used in Coarray-MUSIC. The CRLB for DOA estimation in under-determined signal model is also provided in Section 3.3. The simulations and analyses are presented in Section 3.4. Section 3.5 concludes up the chapter.

3.2 Coarray Based Signal Models and Coarray Based Arrays

The difference coarray of an array is the collection of differences between the locations of its sensors. Specifically, if the sensor locations (at some multiples of $\lambda/2$) are $\mathbb{S} = \{d_1, d_2, ..., d_M\}$, the corray is $\mathbb{D} = \{d_i - d_j\},\ i, j = 1, 2, ..., M$. An array without "holes" in its coarray is preferable.

In [3], a new model for aperture extension by vectorizing array covariance matrix has been introduced. Consider an M element sparse linear array with sensor locations $\mathbb{S}$, and K uncorrelated, far field sources with directions $\boldsymbol{\theta} = [\theta_1, \theta_2, ...\theta_K]^T$, the array output at t^{th} snapshot is given as,

$$\mathbf{y}(t) = \mathbf{A}(\boldsymbol{\theta})\mathbf{s}(t) + \mathbf{v}(t), \tag{3.1}$$

where $\mathbf{s}(t) = [s_1(t), s_2(t), ..., s_K(t)]^T$ are the incoming signals, $\mathbf{v}(t)$ is the $M \times 1$ noise vector, and $\mathbf{A}(\boldsymbol{\theta}) = [\mathbf{a}(\theta_1), \mathbf{a}(\theta_2), ..., \mathbf{a}(\theta_K)]$ is the $M \times K$ manifold matrix. The noise is assumed to be zero mean, spatially and temporarily white. The array steering vector is,

$$\begin{aligned} \mathbf{a}(\theta_k) =& [e^{j\frac{2\pi}{\lambda}d_1 \cos\theta_k} \ \ e^{j\frac{2\pi}{\lambda}d_2 \cos\theta_k} \ ... \ e^{j\frac{2\pi}{\lambda}d_M \cos\theta_k}]^T, \\ & k = 1, 2, ..., K. \end{aligned} \tag{3.2}$$

When the elements of the noise vector are spatially and temporarily white, and uncorrelated with sources, the auto-correlation matrix of array output, $\mathbf{R}_y$, becomes

$$\mathbf{R}_y = \mathbf{A}\mathbf{R}_s\mathbf{A}^H + \sigma_v^2\mathbf{I}, \tag{3.3}$$

where $\mathbf{I}$ is the identity matrix and $\mathbf{R}_s$ is the auto-correlation matrix of the sources, and σ_v^2 is the noise power. Assuming sources are uncorrelated, $\mathbf{R}_s$ becomes diagonal, $\mathbf{R}_s = diag(\sigma_1^2, \sigma_2^2, ..., \sigma_K^2)$ where σ_k^2 is the power of the k^{th} source. Vectorizing $\mathbf{R}_y$, stacking its columns on each other, the following model is obtained,

$$\mathbf{z} = vec(\mathbf{R}_y) = (\mathbf{A}^* \odot \mathbf{A})\mathbf{p} + \sigma_v^2\mathbf{1}_v = \mathbf{A}_d\mathbf{p} + \sigma_v^2\mathbf{1}_v, \tag{3.4}$$

where $(\mathbf{A}^* \odot \mathbf{A})_{M^2 \times K} = [\mathbf{a}(\theta_1)^* \otimes \mathbf{a}(\theta_1)\ \mathbf{a}(\theta_2)^* \otimes \mathbf{a}(\theta_2)\ ...\ \mathbf{a}(\theta_K)^* \otimes \mathbf{a}(\theta_K)]$, $\mathbf{p} = [\sigma_1^2,\ \sigma_2^2,\ ...\ , \sigma_K^2]^T$, and $\mathbf{1}_v = [\mathbf{e}_1^T\ \mathbf{e}_2^T\ ...\ \mathbf{e}_M^T]^T$. $\mathbf{e}_m^T$ is a column vector of all zeros except

a 1 at location m, $\odot$ is Khatri-Rao product, and $\otimes$ is Kronecker product. Note that the entries of $[\mathbf{a}(\theta_k)^* \otimes \mathbf{a}(\theta_k)]$ are as $e^{j(2\pi/\lambda)(d_i-d_j)\cos(\theta_k)}$ for $i,j = 1,2,...,M$. $\mathbf{z}$ in (3.4) will be referred to as "**coarray vector**".

Comparing (3.1) and (3.4), it can be concluded that (3.4) is a different version of classical array model with a longer array consisting of virtual sensors located at $(d_i - d_j)$, $i,j = 1,2,...,M$ with sources $\mathbf{p} = [\sigma_1^2, \sigma_2^2, ..., \sigma_K^2]^T$ and noise $\sigma_v^2\mathbf{1}_v$, note that the noise is deterministic in this model. Moreover, the locations of sensors of this new model is the coarray of the actual array. Therefore, coarray based signal model, i.e. coarray vector, can be used for DOA estimation. In the matrix $\mathbf{A}_d = (\mathbf{A}^* \odot \mathbf{A})$, there are repeated rows, in order to use the coarray vector for DOA estimation, either repeated rows are removed after the first occurrence or their mean is used. Let $\mathbf{A}_1$ be the new matrix constructed from $(\mathbf{A}^* \odot \mathbf{A})$ by removing repeated rows, and sorting the rows such that the sensor locations in coarray are in the increasing order, the new model is obtained as

$$\mathbf{z}_1 = \mathbf{A}_1\mathbf{p} + \sigma_v^2\mathbf{e}, \tag{3.5}$$

where $\mathbf{e}$ is a vector of all zeros except a 1 in the center position, location corresponding to 0 in coarray. $\mathbf{z}_1$ can be used for DOA estimation in the coarray domain.

3.2.1 Mutual Coupling

In obtaining the array model in (3.1), it is assumed that there is no mutual coupling between the sensors. As this is not a realistic assumption, mutual coupling is modeled by inserting a coupling matrix $\mathbf{C}$ into (3.1),

$$\mathbf{y}(t) = \mathbf{C}\mathbf{A}(\boldsymbol{\theta})\mathbf{s}(t) + \mathbf{v}(t). \tag{3.6}$$

The coupling matrix $\mathbf{C}$ has many variants depending on the type of sensors, their separation, working mode, operating frequency, impedance, etc. Therefore, there are

different forms of **C**, in this work the B-banded mode, [63, 64, 66, 67], is used,

$$\mathbf{C}_{i,j} = \begin{cases} c_{|d_i - d_j|} & \text{if } |d_i - d_j|/d \leq B, \\ 0 & \text{otherwise.} \end{cases} \tag{3.7}$$

The magnitudes of the elements of the **C** matrix are inversely proportional to sensor separation such that $1 = |c_0| > |c_1| > ... > |c_B| > |c_{B+1}| = 0$. Note that, the off-diagonal entries of **C** characterizes the mutual coupling, hence a diagonal **C** indicates no mutual coupling. Therefore, a coupling leakage, L, has been defined in [64] for the total mutual coupling,

$$L = \frac{||\mathbf{C} - \tilde{\mathbf{C}}||_F}{||\mathbf{C}||_F}, \tilde{\mathbf{C}}_{i,j} = \begin{cases} \mathbf{C}_{i-j} & \text{if } i = j \\ 0 & \text{otherwise.} \end{cases}$$

where $||.||_F$ is the Frobenius norm. Smaller L indicates smaller mutual coupling.

3.2.2 Some Useful Definitions

Before presenting the coarray based arrays, some useful definitions will be given.

Degrees Of Freedom (DOF) : The difference coarray $\mathbb{D}$, may have repetitions. The cardinality of the distinct elements of $\mathbb{D}$, is defined as the degrees of freedom.

Central ULA : The central part of the coarray with no holes.

Uniform DOF (uDOF) : The number of virtual sensors in the central ULA of the coarray is defined as uniform DOF. Actually, this can also be called as **effective DOF**, since this number determines the number of sources that can be resolved or identified by coarray MUSIC and coarray based methods. For a coarray with a uDOF $2M_v - 1$, the number of sources resolvable is $M_v - 1$.

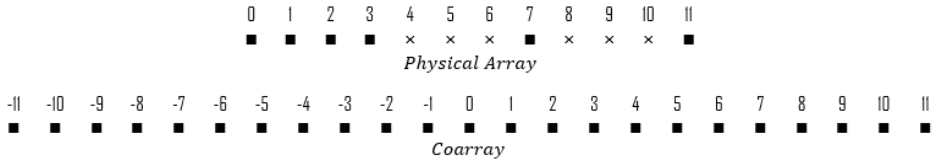

Figure 3.1: A 2-level Nested Array with 3 sensors in each level (top), and its coarray (bottom).

3.2.3 Nested Arrays

In [31], a sparse array structure, "Nested Array" (NA), has been introduced which has a closed form array geometry and provides $O(M^2)$ DOF for $O(M)$ sensors. An NA is a concatenation of uniform linear sub-arrays with different sensor separations. The sensor positions of a K-level NA are given as $S_{Klevel} = \cup_{i=1}^{K} S_i$, where

$$S_i = \left\{ nd \prod_{j=1}^{i-1} (N_j + 1), \quad n = 1, 2, ..., N_i \right\}, \tag{3.8}$$
$$i = 2, 3, ..., K; \quad S_1 = nd, \; n = 1, 2, ..., N_1.$$

$d = \lambda/2$ is the minimum sensor separation, N_i's are the numbers of sensors in each level. A 2-level NA with 3 sensors in each level, and its coarray is shown in Figure 3.1. In figures 3.1 to 3.6 solid rectangles stand for sensors and crosses for holes. The disadvantage of an NA, as the authors claim, is the mutual coupling between the close sensors in the first level. However, the proposed array structure may have holes in its coarray if the level of nesting is greater than two. Moreover, a 2-level NA may have less DOF compared to the Minimum Redundancy Arrays (MRA) for the same number of sensors, since MRAs are optimized to have the longest coarray with no hole. The proposed spatial smoothing method in [31] can be applied to hole free segment of the coarray, which means a loss in DOF when the level order is greater than 2. To reduce mutual coupling, a different array structure, "Coprime Array" is proposed in [61] by the same authors.

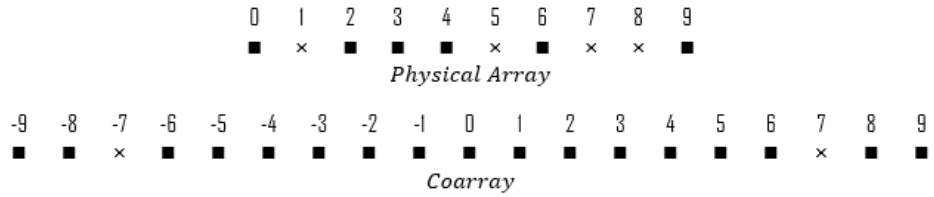

Figure 3.2: A Coprime Array, M = 2, N = 3 (top), and its coarray (bottom).

3.2.4 Coprime Arrays

A Coprime Array (CA) involves two linear sub-arrays. One of the sub-arrays has M sensors with Nd spacing and the other one has N sensors with Md spacing. They share the same sensor as the first element, therefore there are a total of $M + N - 1$ physical sensors. M and N are coprime integers. In some works, the structure is given as M sensors with Nd spacing and $2N - 1$ sensors with Md spacing. Here, we use the structure with the larger physical aperture for the same number of sensors. A CA with $M = 3$ and $N = 2$, and its coarray is seen in Figure 3.2. Notice that, there are holes in the coarray of a CA. This is a disadvantage of CAs and results in a smaller uDOF compared to NAs. Although the main purpose of proposing the CAs is to reduce the mutual coupling, as also observed in the provided example a significant amount of unit spacings may exist.

3.2.5 Super Nested Arrays

"Super Nested Arrays" (SNA) have been introduced in [64] as an improvement reducing the mutual coupling in NA and holes in CA. An SNA is obtained by a systematic approach in which the sensors in the dense subarray of a parent NA are distributed into the sparse subarray. The number of relocated sensors determines the order of SNA. 2nd and 3rd order SNAs are given in [64], whereas higher-order SNAs are given in a companion paper [68]. As the sensors are relocated within the sparse subarray, the physical aperture and coarray of the parent NA and SNA remains unchanged. The only difference is in the redudancy in spatial sampling. SNA usually has smaller sampling counts (spatial sensitivity) for the smaller spatial frequency components. An SNA, parented by the NA given in Figure 3.1, is given in Figure 3.3. The effec-

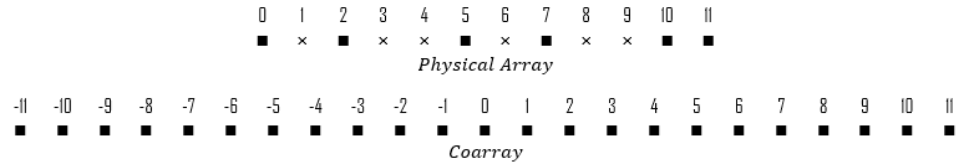

Figure 3.3: A Super Nested Array, parented by the Nested Array in Figure 3.1 (top), and its coarray (bottom).

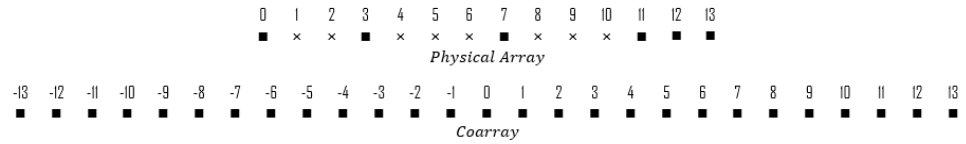

Figure 3.4: An Augmented Nested Array, parented by the NA in Figure 3.1 (top), and its coarray (bottom).

tiveness of the SNA structure becomes more obvious with higher number of sensors and orders.

3.2.6 Augmented Nested Arrays

In [63], NAs have been reorganized to get the structure named “Augmented Nested Array" (ANA). Compared to an NA with the same number of sensors, ANA has a higher DOF and lower mutual coupling. This is achieved by distributing the sensors of a dense subarray of the NA either into two parts (2-level ANA) or into four parts (4-level ANA) by two different methods. Therefore, four different closed-form configurations have been provided which have no holes in their coarrays. A 2-level, type-1 ANA, parented by the NA shown in Figure 3.1, is given in Figure 3.4. Figure 3.4 shows that the mutual coupling has been decreased and DOF has been increased as claimed, however, notice that the physical aperture has been also increased. This is pointed out as the main reason for the simultaneous improvements in mutual coupling and DOF by the authors of [63] as compared to SNAs. As a matter of fact, it should also be noted that the claimed results are applicable for arrays with more than 10 sensors.

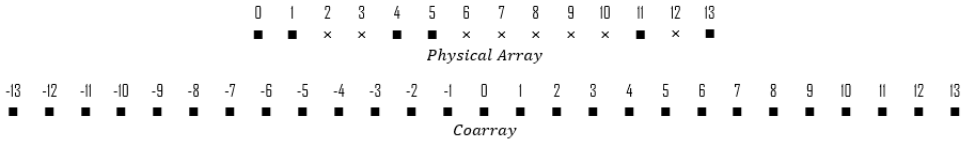

Figure 3.5: A Sparse Ruler Array, (top) and its coarray (bottom).

3.2.7 Sparse Ruler Arrays

"Sparse Ruler Arrays" (SRA) are based on a sparse ruler concept. A sparse ruler can measure all integer distances between 0 and $N-1$ with only M marks, where $M < N$. The sparse ruler with minimum M is the "minimal sparse ruler". Although the adaptation of sparse ruler to sensor arrays was proposed in [62], the problem of the sparse ruler and its solution was first presented in [69]. SRAs have somewhat different structures than those presented above; they do not have closed-form structure, a search is required to find a new structure for a given N. A list of SRAs is given in [69], an example for $M = 6$ and $N = 13$ is given in Figure 3.5.

3.3 DOA Estimation Methods and CRLB

The coarray based signal model, $\mathbf{z}_1$, in (3.5) can be used for DOA estimation in the coarray domain. $\mathbf{z}_1$ can be seen as a single snapshot in conventional sense, however, its correlation matrix $\mathbf{R}_z = \mathbf{z}_1 * \mathbf{z}_1^H$ is a rank-1 matrix. Therefore, subspace based methods cannot be applied directly, further action is required. Assume that the support of the central ULA of the coarray is $-M_v+1,\ -M_v+2,\ \ldots -1\ , 0\ , 1,\ \ldots, M_v-2,\ M_v-1$. The coarray can be partitioned into M_v overlapping subarrays of M_v elements, denoted by $\mathbf{z}_{1\_1}, \ldots, \mathbf{z}_{1\_M_v}$. A partitioning for $M_v = 12$ is shown in Figure 3.6.

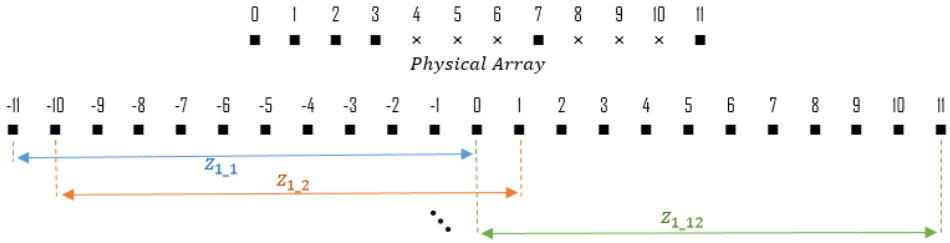

Figure 3.6: Subarray partitioning of a coarray.

3.3.1 Spatially Smoothed (SS)-MUSIC and Direct Augmentation (DA)-MUSIC

In [31], a "Spatial Smoothing" (SS) method has been used to be able to apply the MUSIC method. In spatial smoothing, the auto-correlation matrix is obtained as,

$$\mathbf{R}_{z1} = \frac{1}{M_v} \sum_{i=1}^{M_v} \mathbf{z}_{1\_i} \mathbf{z}_{1\_i}^H. \tag{3.9}$$

$\mathbf{R}_{z1}$ is full-rank, and the method is called SS-MUSIC.

Another method to obtain a full-rank auto-correlation matrix is given in [70] as,

$$\mathbf{R}_{z2} = [\mathbf{z}_{1\_M_v} \;\; \mathbf{z}_{1\_M_v-1} \; ... \; \mathbf{z}_{1\_1}] = \sum_{i=1}^{M_v} \mathbf{z}_{1\_(M_v-i+1)} e_i^T. \tag{3.10}$$

MUSIC with $\mathbf{R}_{z2}$ is called “DA-MUSIC". Actually, $\mathbf{R}_{z1}$ and $\mathbf{R}_{z2}$ are related as $\mathbf{R}_{z1} = \mathbf{R}_{z2}^2/M_v$, [71].

3.3.2 Cramér-Rao Lower Bound (CRLB)

CRLB in DOA estimation for linear arrays has been investigated in [72, 73]. This bound is valid when sensors are more than sources, i.e. it is valid for the over-determined case. CRLB for more sources than sensors, i.e. the under-determined case, has been independently studied in [71, 74, 75]. The common outcome is that the CRLB exists for the stochastic signal model and is strictly nonzero. The CRLB of coarray based DOA estimation for under-determined case, see (3.1), (3.3) and (3.4), has been found as [71, 74, 75],

$$CRLB(\theta) = \frac{1}{T_s} (\mathbf{M}_\theta^H \mathbf{\Pi}_{\mathbf{M}_s}^{\perp} \mathbf{M}_\theta)^{-1}. \tag{3.11}$$

where T_s is the number of snapshots, $\mathbf{M}_\theta = \left(\mathbf{R}_y^T \otimes \mathbf{R}_y\right)^{-1/2}\dot{\mathbf{A}}_d\mathbf{P}$, and $\mathbf{M}_s = \left(\mathbf{R}_y^T \otimes \mathbf{R}_y\right)^{-1/2}[\mathbf{A}_d\mathbf{1}_v]$. $\mathbf{\Pi}^{\perp}_{\mathbf{M}_s}$ is the projection operator onto the null space of $\mathbf{M}_s^H$ and is defined as $\mathbf{\Pi}^{\perp}_{\mathbf{M}_s} = \mathbf{I} - \mathbf{M}_s(\mathbf{M}_s^H\mathbf{M}_s)^{-1}\mathbf{M}_s^H$. $\dot{\mathbf{A}}_d$ is the derivative of $\mathbf{A}_d$ and is defined as $\dot{\mathbf{A}}_d = (\dot{\mathbf{A}}^* \odot \mathbf{A} + \mathbf{A}^* \odot \dot{\mathbf{A}})$ where

$$\dot{\mathbf{A}} = \left[\frac{\partial \mathbf{a}(\theta_1)}{\partial \theta_1}\ \frac{\partial \mathbf{a}(\theta_2)}{\partial \theta_2}\ \ldots\ \frac{\partial \mathbf{a}(\theta_K)}{\partial \theta_K}\right]. \tag{3.12}$$

3.4 Simulation Results

The focus of the simulations is DOA estimation. DOA estimation performances of candidate arrays are compared for two cases, with and without mutual coupling. Additionally, target resolution simulations are also conducted. For a fair comparison, the natural choice is to use the same number of sensors for the same aperture size. However, as will be clear shortly, it is not possible to find such a match for all array types used in the comparison. As a trade-off, the number of sensors is fixed and two individuals from all NA, CA, SNA, ANA and SRA are selected; one with 6, and the other with 10 sensors. The reason of this choice is their wide usage in the literature. We call the 6-element group as Array Group 1 (AG1) and the 10-element group as Array Group 2 (AG2). The sensor positions of the arrays are given in Figure 3.7. By keeping the number of sensors fixed, the success of arrays in spanning the physical aperture will also be compared.

Extra two ULAs have also been included in the simulations. These two arrays serve as references for comparison. The classical MUSIC method has been used for the reference arrays. One ULA (ULA1) has the same number of sensors with the comparison group while the other one (ULA2) has an aperture equal to the biggest one in the comparison group. Remember that, maximum number of resolvable targets with classical MUSIC is $M - 1$, where M is the number of the physical sensors.

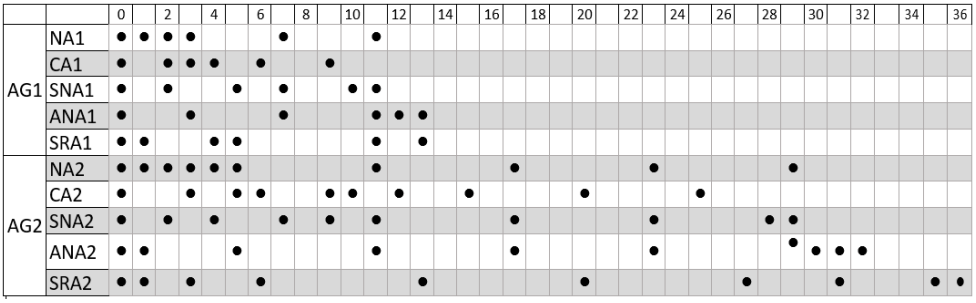

Figure 3.7: Sensor positions of the arrays.

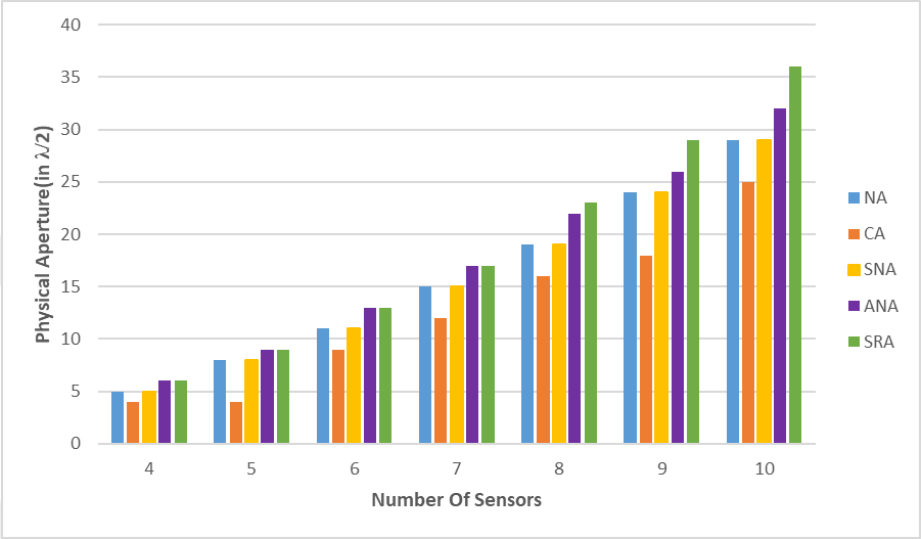

Figure 3.8: The physical apertures spanned by the arrays.

3.4.1 Apertures and uDOFs

The physical apertures, and (uDOF-1)/2 of NA, CA, SNA, ANA, and SRA in terms of the number of sensors are given in figures 3.8 and 3.9. Inspection of Figure 3.8 reveals the reason of different physical apertures in the simulations.

The implications of figures 3.8 and 3.9 are as follows:

- SRA has the maximum aperture, given the number of sensors, or it has the minimum number of elements, given the aperture.
- All arrays have hole-free coarrays except CA. This justifies the minimal uDOF of CA.

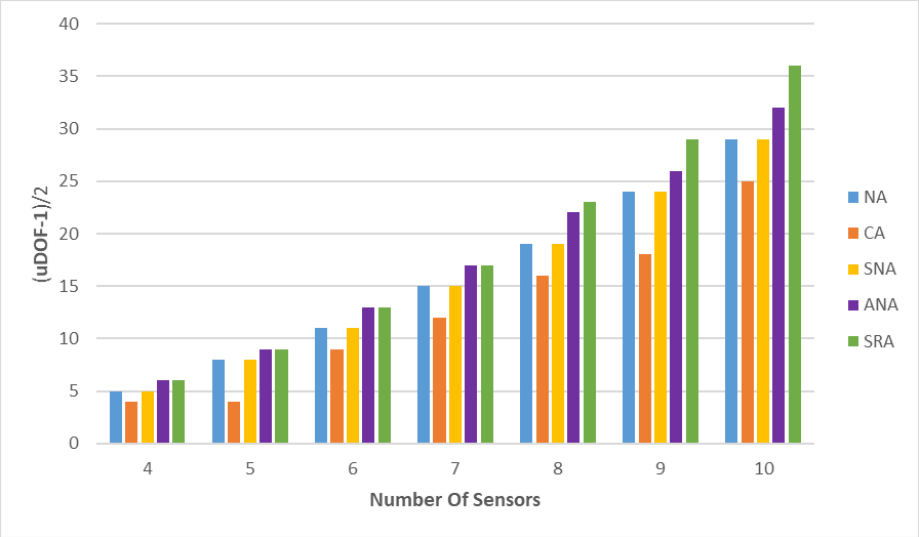

Figure 3.9: uDOF (# of resolvable targets) obtained by the arrays.

- SRA outperforms the others in spanning the physical aperture, in particular as the number of sensors increases.

Remember that the number of resolvable sources is $(uDOF-1)/2$ and notice that the number of resolvable sources is never larger than the physical aperture size in terms of the half-wavelength. This seems to be a critical fact and it points to an aspect of coarray based structures and processing that is not sufficiently emphasized in [31, 61–64]. The main factor that enables detection of more targets from sensors is the enlargement of the aperture for a given number of sensors.

3.4.2 DOA Estimation

It was shown in [70, 71] that SS-MUSIC and DA-MUSIC have the same asymptotic second-order statistics in DOA estimation. In this work SS-MUSIC is used with the models in (3.1) and (3.5). Performance measure in DOA estimation for the candidate arrays is taken as the mean square error of estimation,

$$MSE(\theta) = \frac{1}{RK} \sum_{r=1}^{R} \sum_{k=1}^{K} \left(\hat{\theta}_k^{(r)} - \theta_k^{(r)} \right)^2 \tag{3.13}$$

where $\hat{\theta}_k^{(r)}$ is the estimate of k^{th} source's DOA, θ_k, at the r^{th} Monte-Carlo run, R is the number of total runs which is 1000 in all simulations, and K is the number of sources. The sources are uniformly distributed between [30-150] degrees, and randomly selected in each Monte-Carlo run. 90 degrees is the broadside of the arrays.

Average efficiency is used to measure the statistical efficiency of arrays in DOA estimation. The average efficiency is defined as,

$$\kappa = \frac{mean\ of\ diagonals\ of\ CRLB(\theta)}{MSE(\theta)}. \tag{3.14}$$

Average efficiency is expected to be, $0 \leq \kappa \leq 1$, and for an efficient estimator $\kappa = 1$.

CRLB Analysis:

The CRLBs of AG1, AG2 and the reference arrays with respect to SNR, number of snapshots, $\#_{sn}$, and number of sources, $\#_{so}$, are provided in figures 3.10 and 3.11. These are the traces of the corresponding CRLB matrices in (3.11). CRLBs with respect to SNR have been given for two cases. In the first case, the number of sources is smaller than the number of sensors (over-determined), on the other hand, in the second case the number of sources is bigger than the number of sources (under-determined). Analyzing figures 3.10 and 3.11, the following observations can be made:

- The best and the worst performances in the comparison group are seen in ANA/SRA and CA, respectively.
- Although mostly, ANA and SRA show similar performances, SRA's curve in AG1 shows an odd pattern when SNR increases, and its performance becomes the worst.
- In AG2, ANA and SNA have similar odd patterns.
- Arrays with the same aperture have similar CRLB curves.
- Including the reference arrays, it can be stated that the aperture size seems to be the most dominant parameter in the performance of an array. On the other

hand, having the same aperture ULA2 has a better CRLB curve than ANA and SRA.

- Even though NA and SNA have the same aperture and the coarray, their CRLB values are different particularly for different numbers of snapshots.
- In under-determined cases, CRLB curves converge to a positive constant instead of zero when SNR goes to infinity.

Let us review CRLB results in terms of the questions we are interested in. In the case of a fixed aperture, the best results are obtained for a filled array. Therefore, for a system where complexity and cost issues can be handled, optimization based designs would be recommended. On the other hand, for a fixed number of sensors, the layout is critical. In that case, the configuration which maximizes the aperture and has no holes in the coarray is preferable. The advantage and superiority of coarray based arrays become clear here. This result also supports our argument in the last paragraph of Section 3.4.1.

MSE Analysis:

MSE and average efficiency curves for AG1 and AG2 are given in figures 3.12, 3.13, 3.14 and 3.14 respectively. The observations are as follows:

- The MSE curves wrt. SNR of coarray based arrays cease to decrease, and tend to settle at a level as SNR increases and eventually results in an overcome of ULA1. Accordingly, even though the coarray based arrays have larger physical apertures, with less sources than sensors, ULA1 has better performance at higher SNRs. Therefore, in over-determined case using coarray based arrays and coarray based MUSIC is not advantageous. The same results is observed in average efficiency curves and agrees with the previous results [71, 76].
- The inferior performance of CA becomes more noticeable compared to CRLB profiles. The gap observed in CA's coarrray degrades its performance seriously.
- ULA2 with classical MUSIC yields much better results. Therefore, even though ANA and SRA have the same aperture with ULA2, the number of sensors or the DOA method makes a considerable difference.

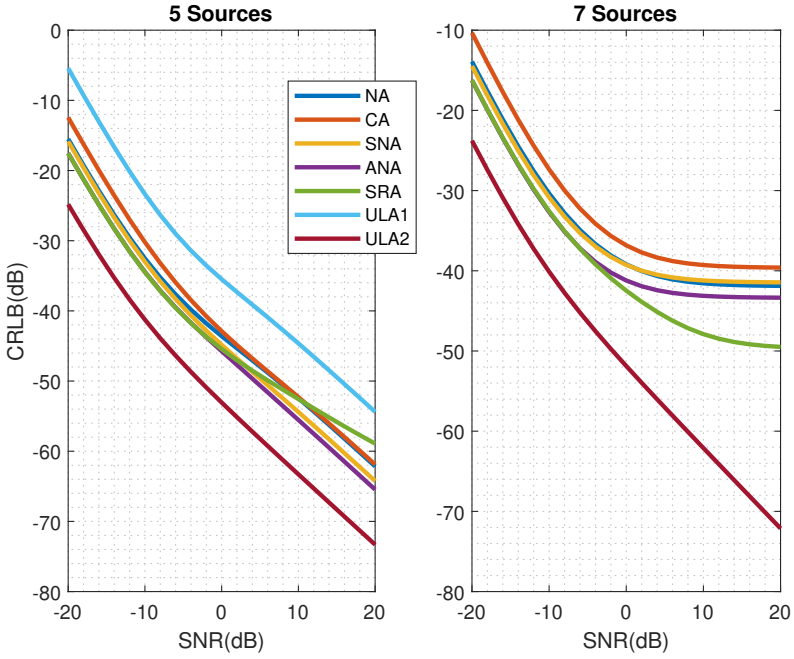

(a)

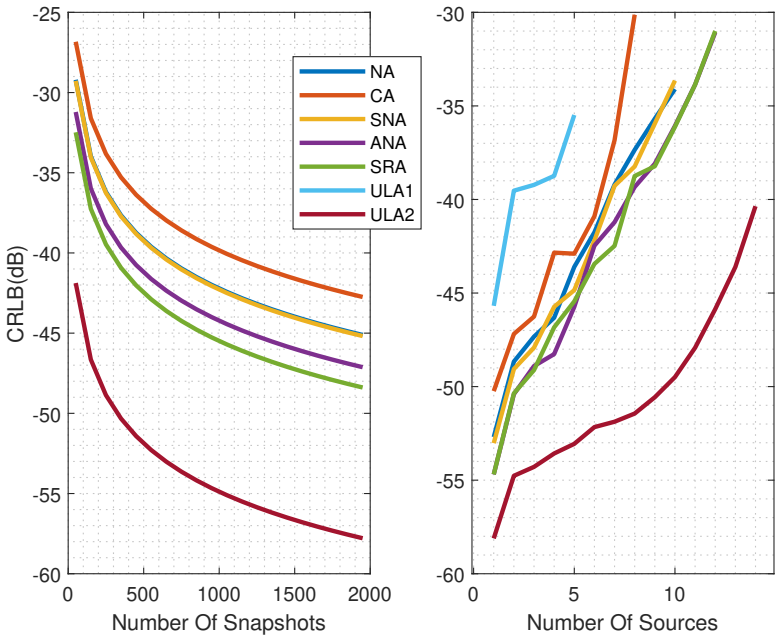

(b)

Figure 3.10: Trace of CRLB(θ) for AG1. **a**: #$_{sn}$= 500, **b-left**: SNR = 0 dB, #$_{so}$= 7, **b-right**: #$_{sn}$= 500, SNR = 0 dB.

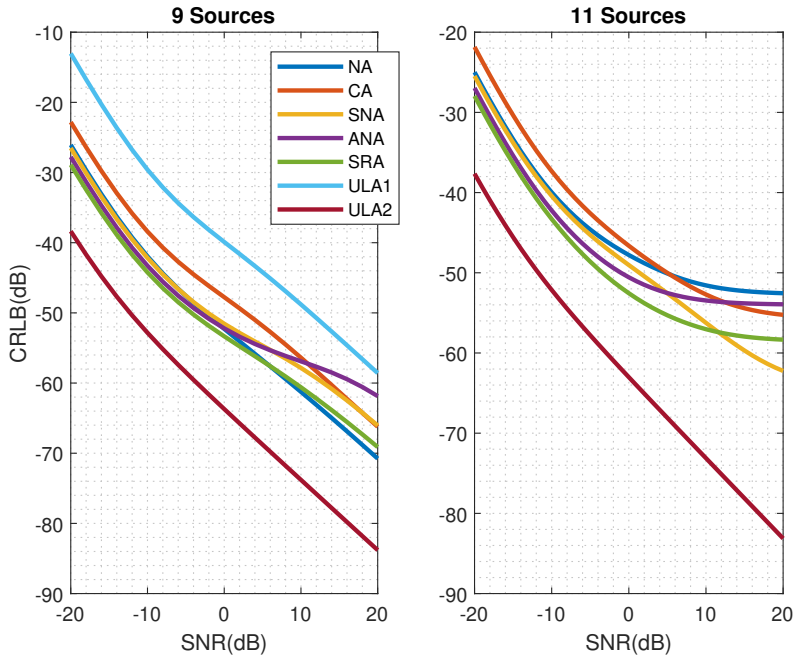

(a)

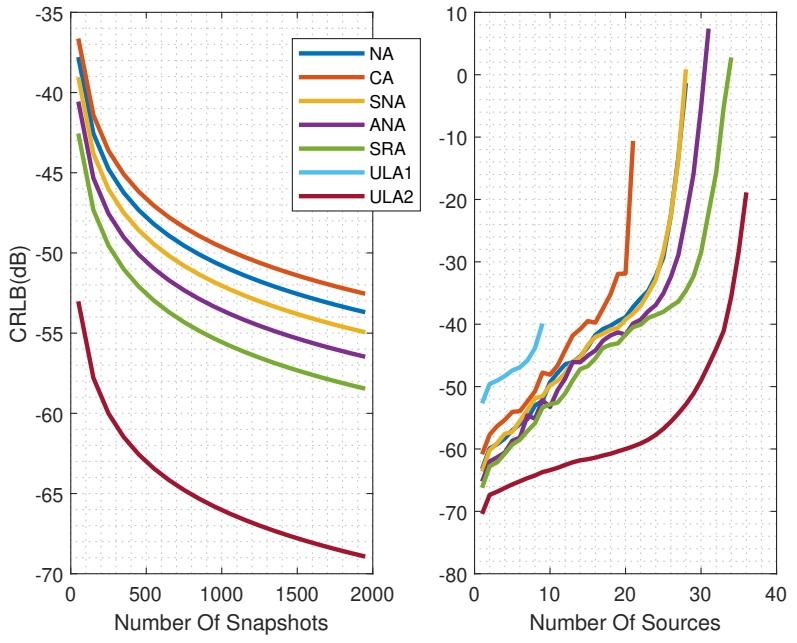

(b)

Figure 3.11: Trace of CRLB(θ) for AG2. **a**: #$_{sn}$= 500, **b-left**: SNR = 0 dB, #$_{so}$= 11, **b-right**: #$_{sn}$= 500, SNR = 0 dB.

- Nonmonotonicities of MSE curves wrt. $\#_{so}$ are observed, especially with ULAs.

- The performance ordering is similar to that observed with the CRLB curves. The aperture size dominates.

- In over-determined case, the average efficiency decreases to zero as SNR increases. On the other hand, in under-determined case average efficiency converges to a positive value. This result is referred as "saturation" behavior of coarray based MUSIC in high SNR regions in the literature [71, 74, 76]. Therefore, higher DOF is obtained at the cost of the reduced statistical efficiency.

- In terms of our questions of interest, the outcomes are parallel to that of the CRLB analysis. Additionally, the superiority of coarray based arrays is lost at at higher SNRs and over-determined signal model.

The estimates for the MSE curves in figures 3.12 and 3.13 are obtained via the local peaks of the spatial MUSIC spectrum. In some cases, the number of peaks was less than the number of sources. In that case, this is assumed a failure, and not included in the MSE calculation. The probabilities of estimating the true number of sources are given in figures 3.16 and 3.17 for AG1 and AG2, respectively. The superiority of having a filled array in a fixed aperture is more obvious in these simulations, particularly in Figure 3.17. The bigger difference in Figure 3.17 is because of a higher sparsity ratio in the comparison group of Figure 3.17.

Resolution Simulations:

The resolution performances of AG1 and AG2 are provided in figures 3.18 and 3.19, respectively. In resolution simulations, two closely located sources are considered. The sources are located at $90 \pm \Delta\theta$ degrees. If two peaks are observed around 90 degrees with separation bigger than $\Delta\theta$ then it is assumed that the sources are resolved. The resolution is closely related to aperture size, therefore the arrays with the same aperture have similar results with minor differences. Within AG1, CA shows the worst performance in resolution. ULA2's performance has a delayed increase at the smallest angles, except against CA, but its sharper slope makes it the earliest to reach 1. The behaviors are similar among AG1 and AG2.

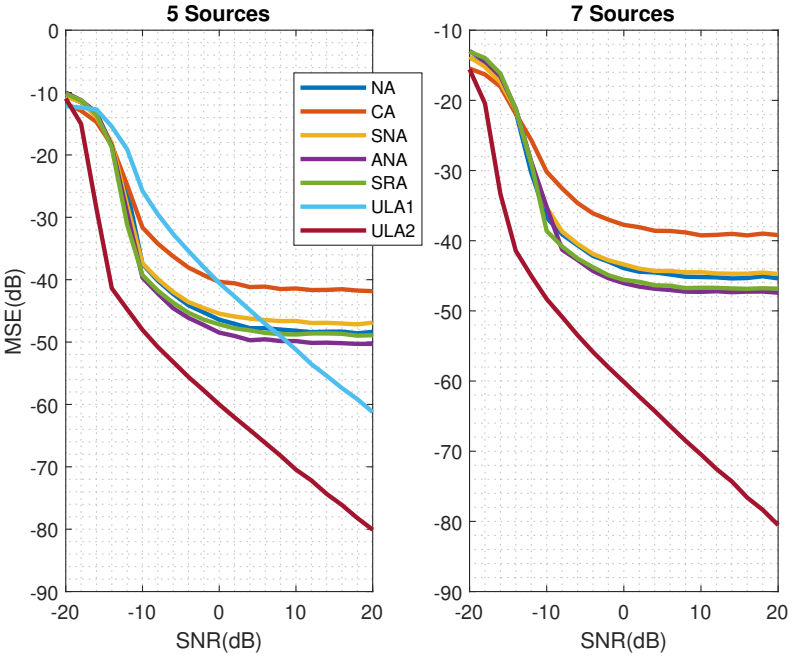

(a)

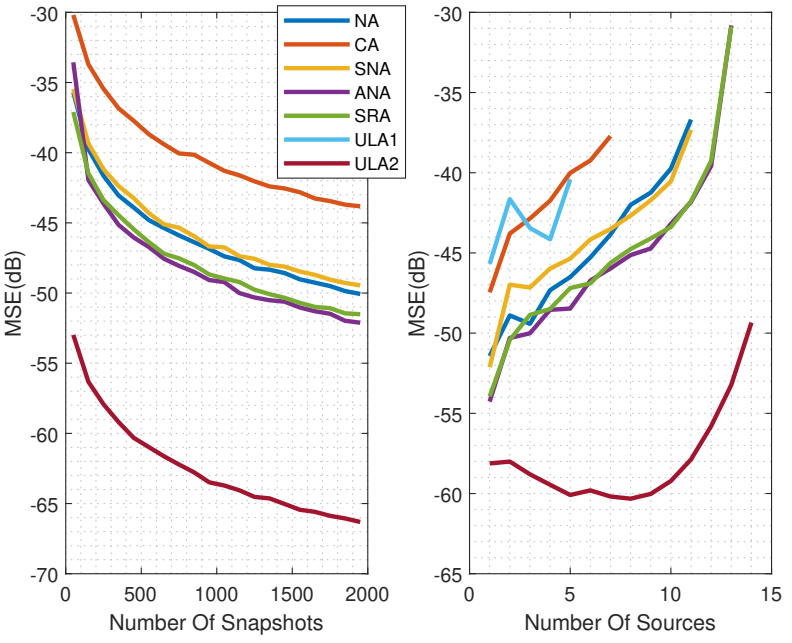

(b)

Figure 3.12: MSE results for AG1. **a**: $\#_{sn}$= 500, **b-left**: SNR = 0 dB, $\#_{so}$= 7, **b-right**: $\#_{sn}$= 500, SNR = 0 dB.

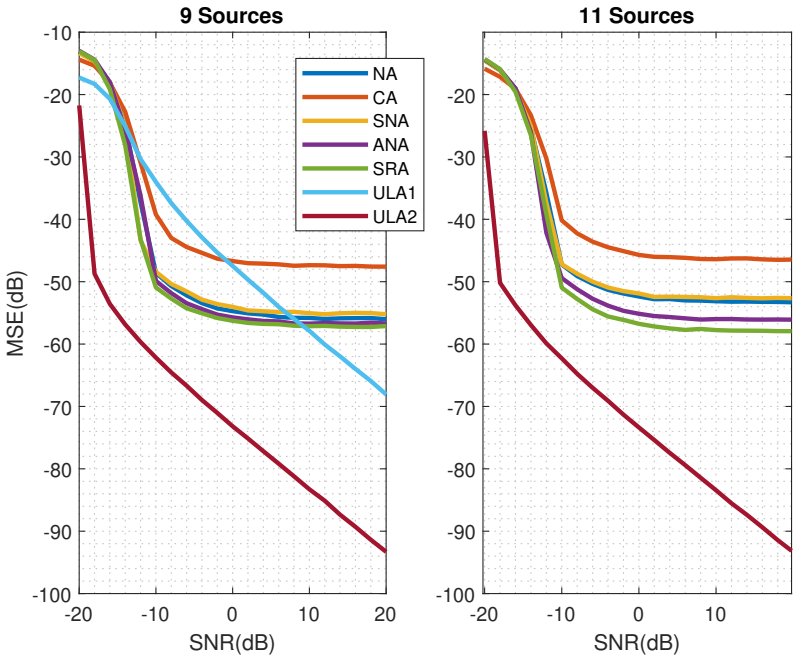

(a)

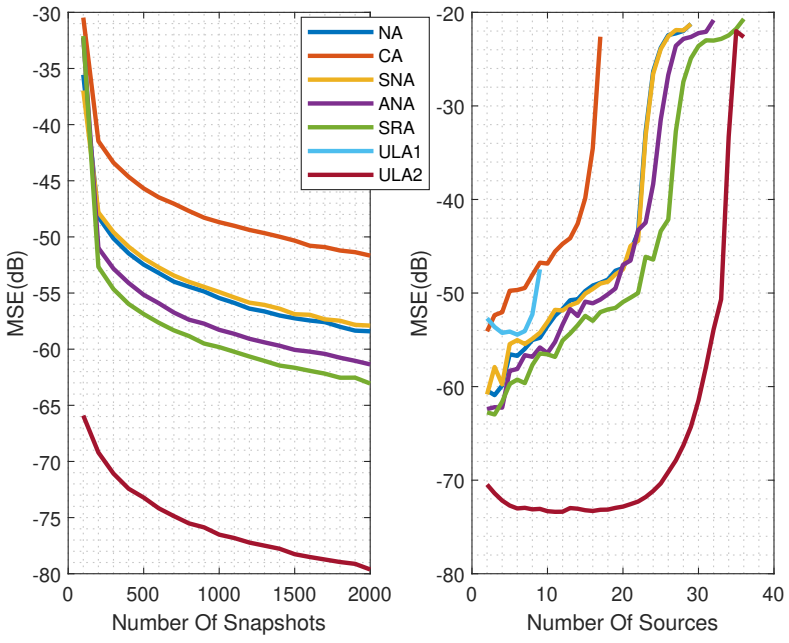

(b)

Figure 3.13: MSE results for AG2. **a**: $\#_{sn}$= 500, **b-left**: SNR = 0 dB, $\#_{so}$= 11, **b-right**: $\#_{sn}$= 500, SNR = 0 dB.

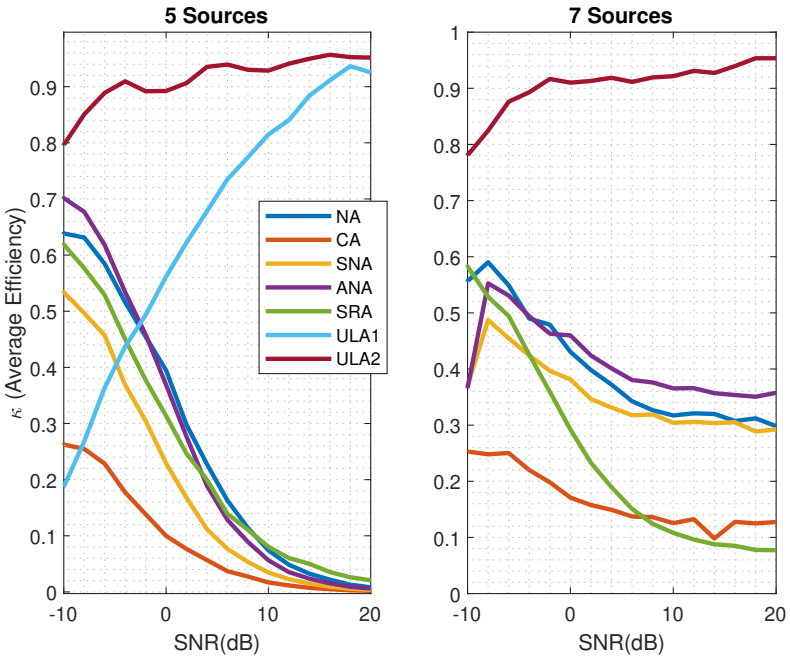

Figure 3.14: Average efficiency results for AG1, $\#_{sn} = 500$

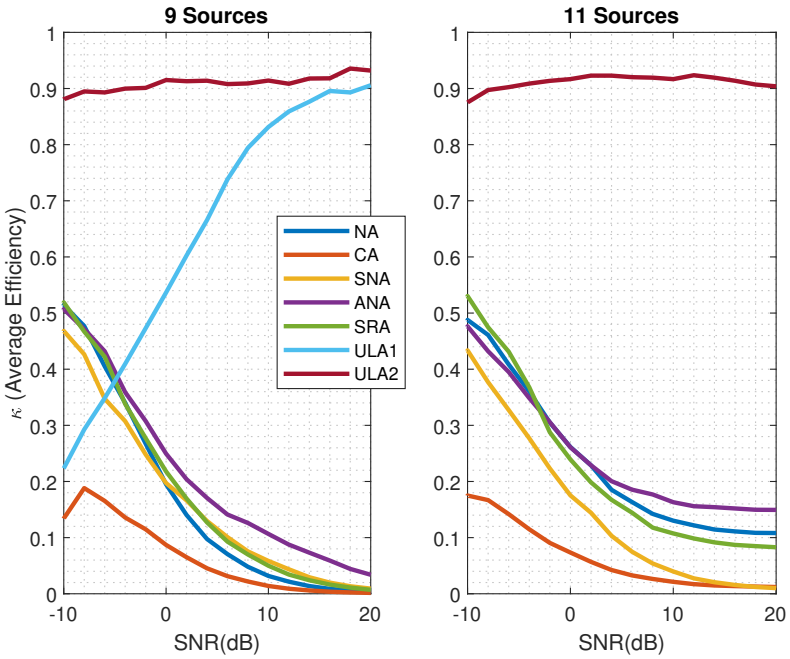

Figure 3.15: Average efficiency results for AG2, $\#_{sn} = 500$

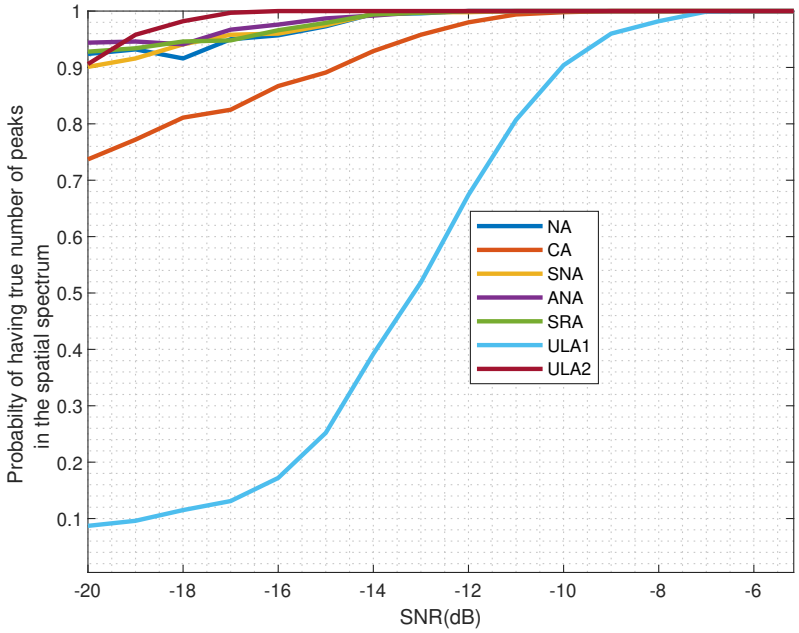

Figure 3.16: Probability of having true number of peaks in the spatial spectra of AG1, $\#_{sn} = 500$ and $\#_{so} = 5$.

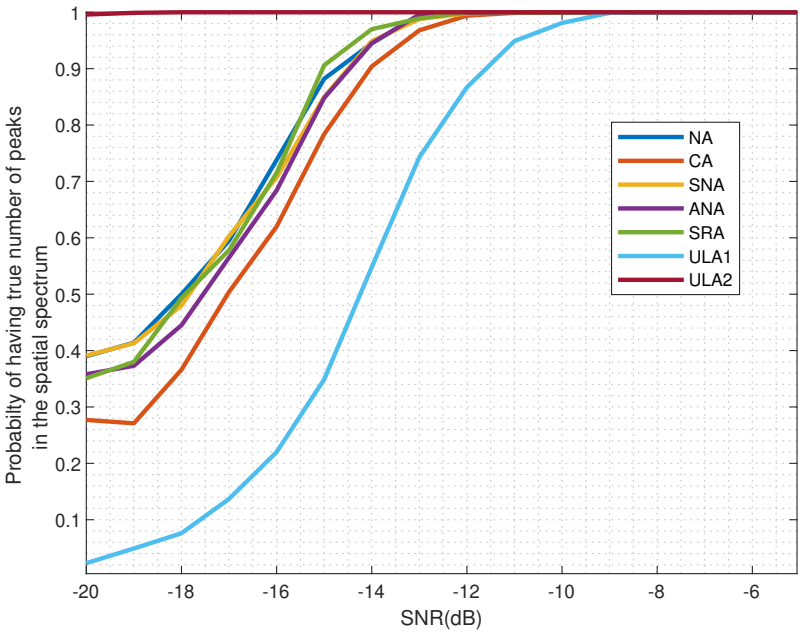

Figure 3.17: Probability of having true number of peaks in the spatial spectra of AG2, $\#_{sn} = 500$ and $\#_{so} = 9$.

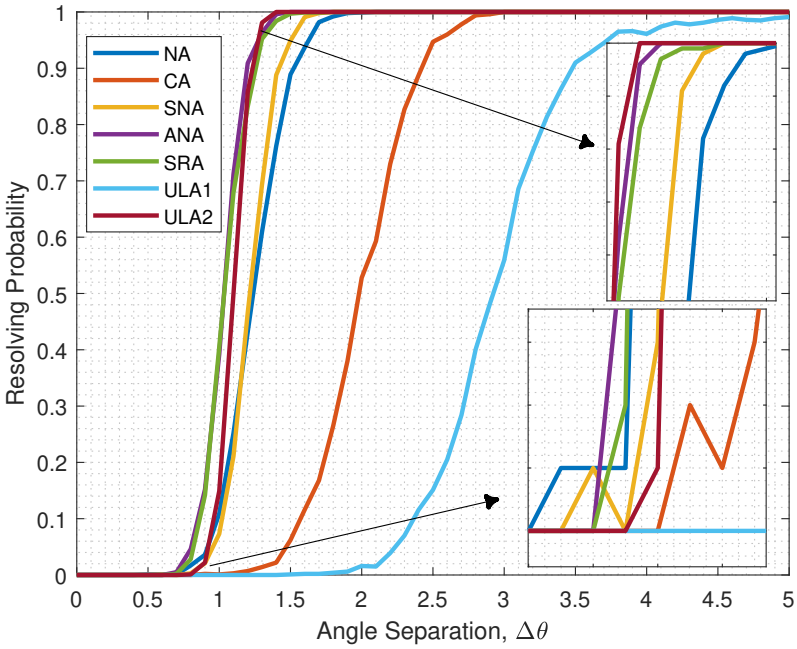

Figure 3.18: Resolution results for AG1. $\#_{sn} = 500$, $SNR = 0$ dB.

3.4.3 Mutual Coupling

MSE simulations have been repeated with mutual coupling. The mutual coupling has been modeled by the B-Banded model in (3.7), with $B = 100$. The entries of C matrix are set as, [63, 64],

$$c_1 = c_s e^{j\pi/3},\ c_l = c_1 e^{-j\pi(l-1)/8}/l,\ \ 2 \leq l \leq B \tag{3.15}$$

where c_s determines the strength of the mutual coupling. The coupling leakage defined in (3.8) for the arrays in AG1 and AG2 for different c_s values are given in tables 3.1 and 3.2. Even though SRA and ANA have higher DOF and larger physical aperture, SNA has the lowest coupling leakage values.

The MSE results of AG1 and AG2 under mutual coupling are provided in figures 3.20 and 3.21. Although ULA2 has the biggest coupling leakage it has the best performance. The reason is that the increase in the number of sensors has suppressed the effect of mutual coupling. When figures 3.12, 3.13, and figures 3.20, 3.21 are

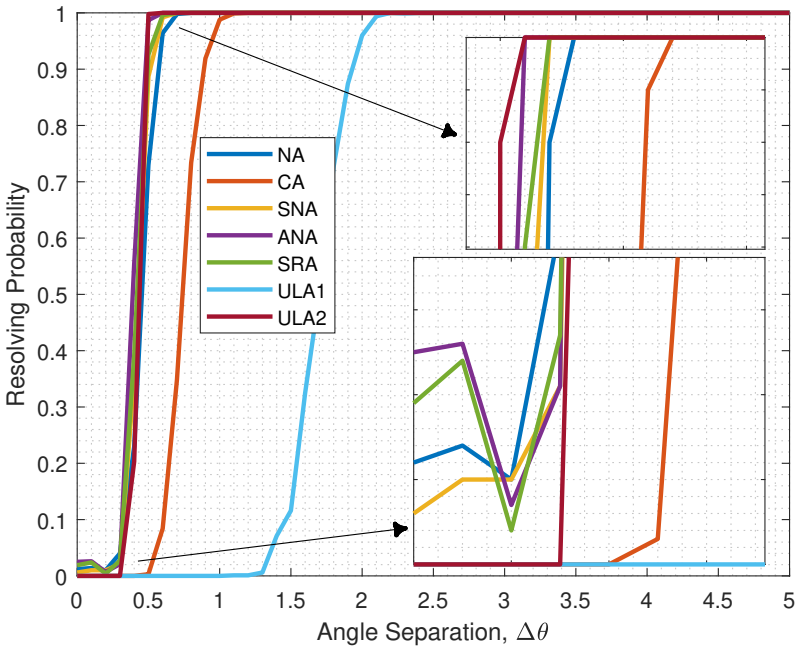

Figure 3.19: Resolution results for AG2. $\#_{sn} = 500$, $SNR = 0$ dB.

Table 3.1: The Coupling Leakage for AG1

c_s	NA	CA	SNA	ANA	SRA	ULA1	ULA2
0.1	0.1129	0.1049	0.0814	0.0933	0.0933	0.1456	0.1627
0.3	0.3225	0.3016	0.2379	0.2706	0.2706	0.4039	0.4434
0.5	0.4938	0.4664	0.3779	0.4242	0.4242	0.5927	0.6361

Table 3.2: The Coupling Leakage for AG2

c_s	NA	CA	SNA	ANA	SRA	ULA1	ULA2
0.1	0.1154	0.0856	0.0724	0.0992	0.0757	0.1566	0.1709
0.3	0.3291	0.2496	0.2128	0.2865	0.2220	0.4295	0.4617
0.5	0.6309	0.5154	0.4531	0.5722	0.4691	0.7429	0.7719

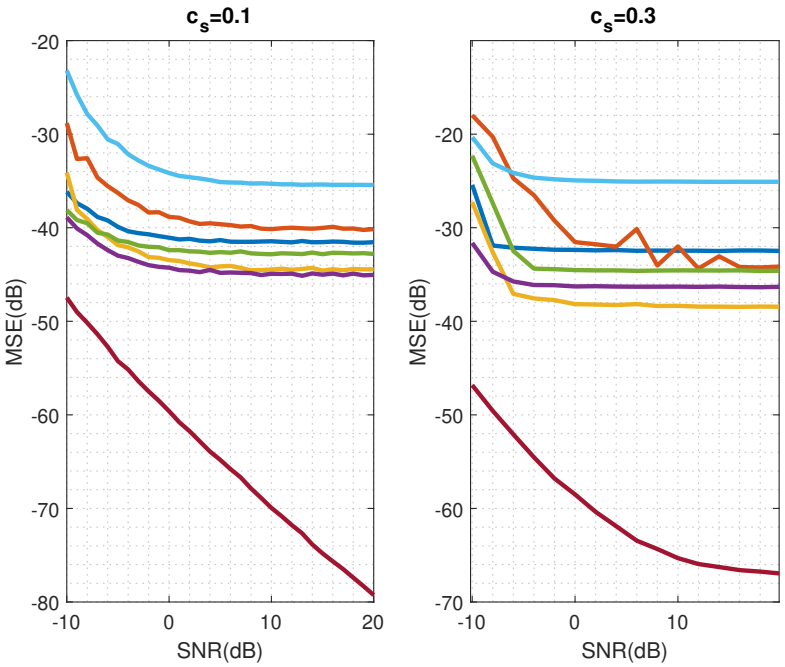

Figure 3.20: MSE results for AG1 under mutual coupling. $c_s = 0.1$ and $c_s = 0.3$, $\#_{sn} = 500$ and $\#_{so} = 5$.

compared, it is seen that all arrays have higher MSE values when mutual coupling is included. The sharp decrease in MSE of ULA1 is lost when mutual coupling exists. Compared to other arrays, SNA has an improvement in MSE results: SNA shows the worst results in figures 3.12, 3.13, except CA, and this has changed in figures 3.20 and 3.21. Therefore, it can be concluded that SNA seems to have the best mutual coupling performance. This result can also be observed in tables 3.1 and 3.2.

3.5 Conclusion

In this chapter, a historical progress of sparse linear arrays, and analysis and comparison of the recently proposed sparse linear arrays have been presented. One of the most recent and popular methods in designing sparse arrays is the "coarray based" method. In this method, no optimization for the placement of array elements is required. A closed-form structure is used, and the aim is to maximize the size of the hole-free segment of the difference coarray. The most known five of these methods have been studied and their performances in terms of DOA estimation accuracy, de-

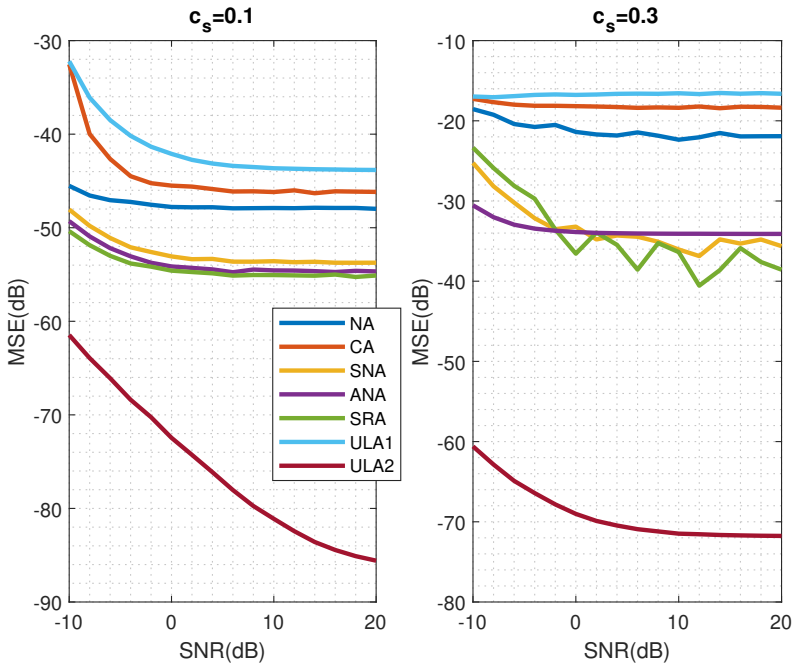

Figure 3.21: MSE results for AG2 under mutual coupling. $c_s = 0.1$ and $c_s = 0.3$, $\#_{sn} = 500$ and $\#_{so} = 9$.

grees of freedom, DOA resolution, and mutual coupling have been compared. The aim is to determine their advantages, disadvantages, necessities, and success in case of fixed aperture and a fixed number of sensors scenarios. The arrays used in the comparison are Nested Array (NA), Co-prime Array (CA), Super Nested Array (SNA), Augmented Nested Array (ANA), and Sparse Ruler Array (SRA), which are called the comparison group. The outcomes of the analysis and comparison can be summarized as follows: In the case of the fixed aperture, using a filled array seems to be the best option in terms of performance. Coarray based arrays are not advantageous in this case. On the other hand, when the number of sensors is fixed, as long as the real world allows, the array which has the largest aperture always has a higher degree of freedom (DOF) and resolvability. In simulations, this one comes out to be SRA. Therefore, contrary to the authors of the comparison group, it needs to be underlined that it is the aperture size that determines DOF and resolvability. However, using the aperture efficiently is the success of the coarray based methods. On the other hand, even if they have the same aperture, their performances may differ depending on their coarray topologies, distribution of redundancies.

CHAPTER 4

NONLINEAR APODIZATION

Sidelobes are common problems in many signal processing applications. The main objective is to obtain the narrowest mainlobe and the lowest sidelobe level possible. In conventional operations, weighting/windowing/apodization is applied to the data to be processed to reduce the sidelobe at the expense of widening the mainlobe [77]. However, in [78], it has been shown that by applying a nonlinear operation, the sidelobe level can be reduced without degrading the mainlobe resolution. The main idea is to use multiple windows instead of a single window and to select the minimum spectral value for each frequency. Using multiple windows naturally increases the complexity and the computational burden. On the other hand, nonlinear apodization can reduce the sidelobe level at most down to the noise level. Three different approaches have been provided in [78] for sidelobe reduction in synthetic aperture radar image formation; dual-apodization, multi-apodization, and spatially variant apodization. In this chapter, these methods are applied for spectrum estimation of time domain data.

4.1 Apodization/Windowing

In real applications, a finite extent of data set is used for processing. Most of the time, the data set does not contain an integer multiple of periods of the signal. That causes discontinuities in the signal and results in spectral leakage in the frequency domain. Moreover, there may be multiple components in the spectrum of the signal. These components may interfere with each other due to spectral leakage. Windowing is used to overcome the discontinuities and to suppress the mutual interference. Windowing also referred to as apodization in the optical signal processing can be considered as

the multiplication of the signal with a sequence whose amplitude varies smoothly and gradually goes to zero at the edges. For a signal $x[n]$ of length N and a window $w[n]$, it can be mathematically expressed as,

$$y[n] = w[n]x[n]. \tag{4.1}$$

It is known that windowing or multiplication in discrete-time domain means periodic convolution in the frequency domain i.e.,

$$\begin{aligned}
Y(e^{j\omega}) &= \sum_{n=-\infty}^{\infty} y[n]e^{-j\omega n} && (4.2)\\
&= \sum_{n=-\infty}^{\infty} x[n]w[n]e^{-j\omega n} && (4.3)\\
&= \sum_{n=-\infty}^{\infty} \left(\frac{1}{2\pi}\int_{-\pi}^{\pi} X(e^{j\theta})e^{j\theta n}d\theta\right) w[n]e^{-j\omega n} && (4.4)\\
&= \frac{1}{2\pi}\int_{-\pi}^{\pi} X(e^{j\theta})\left[\sum_{n=-\infty}^{\infty} w[n]e^{j\theta n}e^{-j\omega n}\right] d\theta && (4.5)\\
&= \frac{1}{2\pi}\int_{-\pi}^{\pi} X(e^{j\theta})W(e^{j(\omega-\theta)}d\theta. && (4.6)
\end{aligned}$$

Equation 4.6 tells us that the value of the $Y(e^{j\omega})$ at a particular frequency, say $\omega = \omega_0$, has contributions from each spectral component of $X(e^{j\omega})$ weighted by the shifted window $W(e^{j(\omega_0-\omega)})$. This can be more easily visualized with the help of an example. Lets assume that $X(e^{j\omega})$ consists of two pure spikes located at ω_a and ω_b with weights X_a and X_b, respectively. Let $W_a(e^{j\omega}) = W(e^{j(\omega_a-\omega)})$ and $W_b(e^{j\omega}) = W(e^{j(\omega_b-\omega)})$, then the spectral components of the output signal at ω_a and ω_b are obtained as,

$$\begin{aligned}
Y(e^{j\omega_a}) &= X_a W_a(\omega_a) + X_b W_a(\omega_b) && (4.7)\\
Y(e^{j\omega_b}) &= X_a W_b(\omega_a) + X_b W_b(\omega_b). && (4.8)
\end{aligned}$$

As it is seen, the spectral leakage causes a bias in the amplitude of the spectral components. Similarly, increasing the number of spikes in the signal, the example can

be extended. Moreover, depending on the mainlobe width and sidelobe level of the window, and the positions and the weights of spikes in the signal, the spectral leakage may cause a bias both in the amplitude and the position of the spectral components.

4.2 Dual-Apodization

Dual apodization is the simplest one and uses two different windows (e.g., rectangular and Hanning) to obtain two different outputs. Then, at each spectral location the minimum absolute value from the two normalized spectra is selected. In this way, the narrow mainlobe of the rectangular window and the low sidelobes of the Hanning window are obtained. Consider an input signal $x[n]$ of length N and two windows $w_1[n]$ and $w_2[n]$, the outputs for these windows are,

$$\begin{aligned} y_1[n] &= w_1[n]x[n] \\ y_2[n] &= w_2[n]x[n] \end{aligned} \tag{4.9}$$

Normalized magnitudes of DTFTs of the windowed data will be obtained as,

$$\begin{aligned} Y_l(e^{j\omega}) &= \left| \sum_{n=0}^{N-1} y_l[n]e^{-j\omega n} \right| = \left| \sum_{n=0}^{N-1} x[n](w_l[n]e^{-j\omega n}) \right|,\ l = 1, 2, \\ Y_l^n(e^{j\omega}) &= Y_l(e^{j\omega}) / \max\left(Y_l(e^{j\omega})\right),\ l = 1, 2. \end{aligned} \tag{4.10}$$

The output of the dual-apodization is found by selecting the minimum spectral value at each frequency bin,

$$Y_{\min}(e^{j\omega}) = \min_{\omega \in [-\pi,\ \pi]} \left(Y_1^n(e^{j\omega}), Y_2^n(e^{j\omega})\right). \tag{4.11}$$

An example of a dual apodization is shown in Figure 4.1. The figure shows that dual-apodization inherits good main-lobe behavior of rectangular window and good side-lobe behavior of Hanning window.

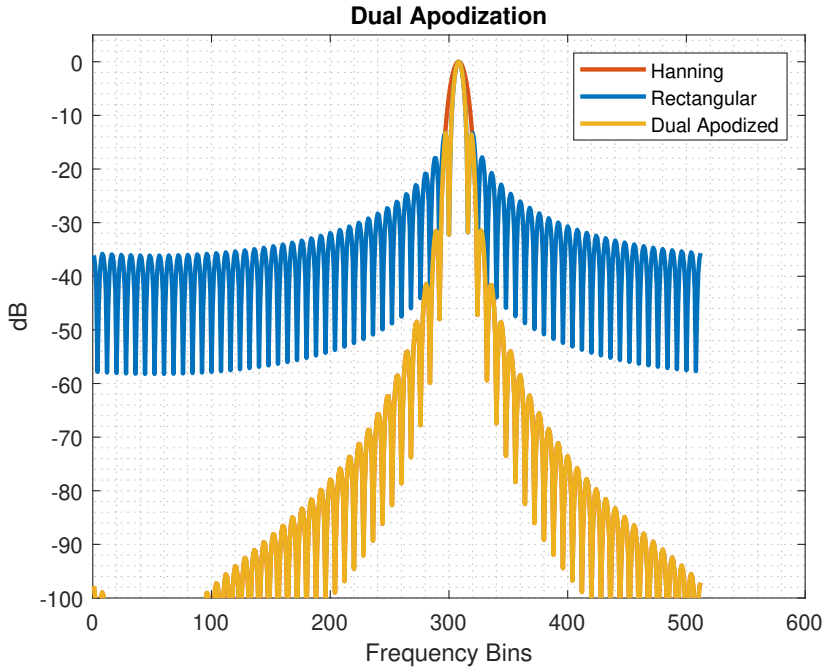

Figure 4.1: Dual Apodization

4.3 Multi-Apodization

As its name implies, multi-apodization is an extension of dual-apodization in which more than two windows are used. The performance gets better compared to dual-apodization however the computational load is increased.

Consider a set of windows $w_l(n), l \in \mathcal{L} = \{1, 2, ...L\}$ and a modeling as given in equation (4.9).The multi-apodization output can be found by selecting the minimum at each spectral location of the normalized magnitude of DTFTs

$$Y_{min}(e^{j\omega}) = \min_{l \in \mathcal{L}} Y_l^n(e^{j\omega}). \tag{4.12}$$

An example of a multi-apodization is shown in Figure 4.2. As it is seen from Figure 4.2 the improvement increases in multi-apodization as the number of windows increases with an expense of an increase in computational load. The key point of the success of the multi-apodization is that each window has a different mainlobe width and different notch points. Therefore, if a sufficient number of windows are used at

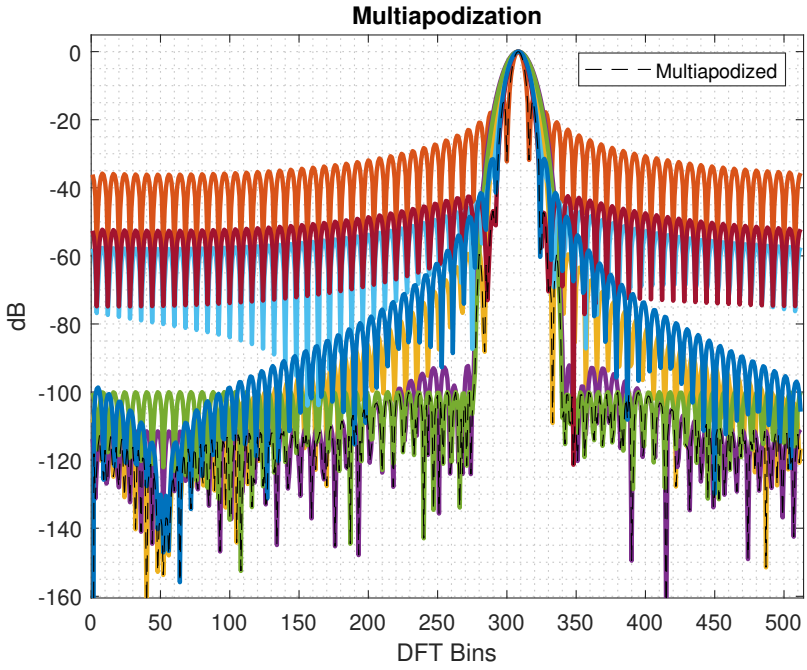

Figure 4.2: Multi-apodization

least one notch will coincide with each of the interfering sources and eliminate their effects. Actually, in the optimum case, the number and the type of the windows should be chosen such that when focusing on a particular spectral location there should be a notch at all interfering spectral locations for a specific window. Although this requires high computational demand and it is practically very difficult, it resembles the idea of Capon. In Capon, when designing weights for a spectral location, notches were inserted to the locations with high interference.

4.4 Spatially Variant Apodization (SVA)

To overcome computational problem of multi-apodization, Spatially Variant Apodization (SVA) approach is introduced in [78]. This approach is also a multi-apodization method but with an infinite set of windows and much better computational efficiency. The requirement is that all windows should be in the form of a raised-cosine function.

The family of raised-cosine window functions are given by

$$w(n;\alpha) = 1 - 2\alpha cos(2\pi n/N), n = 0, 1, \ldots, N-1 \tag{4.13}$$

where N is the window length and

$$0 \leq \alpha \leq 1/2. \tag{4.14}$$

The extreme values $\alpha = 0$ and $\alpha = 1/2$ yield rectangular and Hanning windows, respectively. The DTFT of the raised-cosine function given in (4.13) is

$$W(e^{j\omega}) = 2\pi(-\alpha\delta(e^{j(\omega-2\pi/N)}) + \delta(e^{j\omega}) - \alpha\delta(e^{j(\omega+2\pi/N)})). \tag{4.15}$$

Note that DTFT functions given in this study are for one period only, $-\pi \leq \omega \leq \pi$. As the DTFT of the window function (4.15) contains only three impulses (Dirac delta functions), windowing can be performed easily in frequency domain. Let $X(e^{j\omega})$ be the DTFT of the observation, then the DTFT of the windowed observation is

$$\begin{aligned} Y(e^{j\omega}) = &-\alpha X(e^{j(\omega-2\pi/N)}) + X(e^{j\omega}) \\ &- \alpha X(e^{j(\omega+2\pi/N)}). \end{aligned} \tag{4.16}$$

For each frequency, SVA finds the value of α which minimizes $|Y(e^{j\omega})|^2$ subject to the constraint $0 \leq \alpha \leq 1/2$. The problem is solved by setting the partial derivative of $|Y(e^{j\omega})|^2$ with respect to α to zero and solving for α. The optimal value is [78]

$$\alpha_0(\omega) = Re\left\{\frac{X(e^{j\omega})}{X(e^{j(\omega-2\pi/N)}) + X(e^{j(\omega+2\pi/N)}}\right\}. \tag{4.17}$$

Therefore, the final SVA output with the constraint in (4.14) becomes:

$$Y_f(e^{j\omega}) = \begin{cases} X(e^{j\omega}) & \alpha_0(\omega) < 0, \\ X(e^{j\omega}) - \alpha_0(\omega)S(e^{j\omega}) & 0 \leq \alpha_0(\omega) \leq 1/2, \\ X(e^{j\omega}) - 1/2S(e^{j\omega}) & \alpha_0(\omega) > 1/2 \end{cases} \tag{4.18}$$

where $S(e^{j\omega}) = (X(e^{j(\omega-2\pi/N)}) + X(e^{j(\omega+2\pi/N)}))$. The result in (4.18) is obtained by processing the real (I, in-phase) and imaginary (Q, quadrature) parts of $X(e^{j\omega})$ jointly and is called "I-Q jointly SVA". In [78], a different approach that processes the real and the imaginary parts separately is also given and is called "I-Q separately SVA". The output for "I-Q separately SVA" is given as

$$Y_f(e^{j\omega}) = \begin{cases} X(e^{j\omega}) & \alpha_0(\omega) < 0, \\ 0 & 0 \leq \alpha_0(\omega) \leq 1/2, \\ X(e^{j\omega}) - 1/2S(e^{j\omega}) & \alpha_0(\omega) > 1/2. \end{cases} \tag{4.19}$$

This operation is applied to both in-phase and quadrature components of the complex data.

In practice DTFT will be implemented by DFT, the expressions for "I-Q jointly SVA" and "I-Q separately SVA", respectively, in terms of N-point DFT are

$$Y_f[k] = \begin{cases} X[k] & \alpha_0[k] < 0, \\ X[k] - \alpha_0[k](S[k]) & 0 \leq \alpha_0[k] \leq 1/2, \\ X[k] - 1/2S[k] & \alpha_0[k] > 1/2 \end{cases} \tag{4.20}$$

$$Y_f[k] = \begin{cases} X[k] & \alpha_0[k] < 0, \\ 0 & 0 \leq \alpha_0[k] \leq 1/2, \\ X[k] - 1/2S[k] & \alpha_0[k] > 1/2 \end{cases} \tag{4.21}$$

where $X[k] = X(e^{j\omega})|_{\omega=k2\pi/N}$, $S[k] = X[k-K] + X[k+K]$, $k = 0, 1, ..., N-1$, K is zero padding factor and $\alpha_0[k]$ is given as:

$$\alpha_0[k] = Re\left\{ \frac{X[k]}{X[k-K] + X[k+K]} \right\}. \tag{4.22}$$

Examples for "I-Q jointly SVA" and "I-Q separately SVA" are provided in Figure 4.3. It is seen that, SVA suppresses sidelobes while preserving the mainlobe resolution.

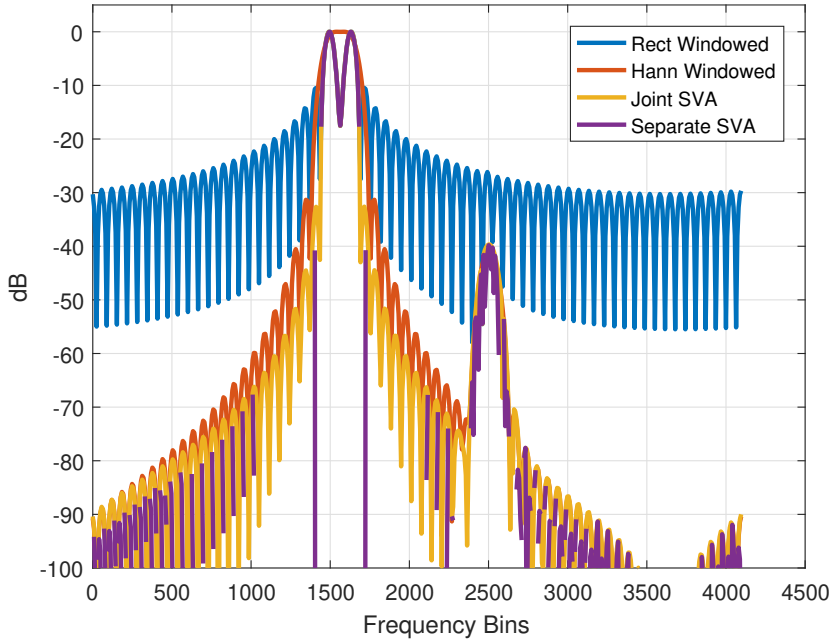

Figure 4.3: SVA for two close, equal power (0 dB) and one distant low power (-40 dB) sources

A disadvantage of the nonlinear methods given above is that they have no effect on the noise, they can reduce the sidelobe level down to the noise level. In Figure 4.3, the SNR has been taken as infinite. When a noise with an SNR of 20 dB is included, the results for SVA methods are given in figures 4.4, 4.5 and 4.6. The low-powered target is observed when its power together with DFT gain overcomes the noise level.

Multi-apodization (or SVA) can be formulated as a power spectral estimator. It has been shown that it is a special version of minimum variance spectral estimator (MVDR or Capon) [79, 80].

Let $\mathbf{w}_l = [w_l(0)\ w_l(1)e^{-j\omega}\ ...\ w_l(N-1)e^{-j(N-1)\omega}]^T$, then the periodogram power spectral density estimate of the signal with window $\mathbf{w}_l$ is

$$P_x(e^{j\omega}) = \frac{1}{N}|\mathbf{w}_l^H \mathbf{x}\mathbf{x}^H \mathbf{w}_l| \tag{4.23}$$

using multiapodization and neglecting $\frac{1}{N}$ term the power spectral density estimate can

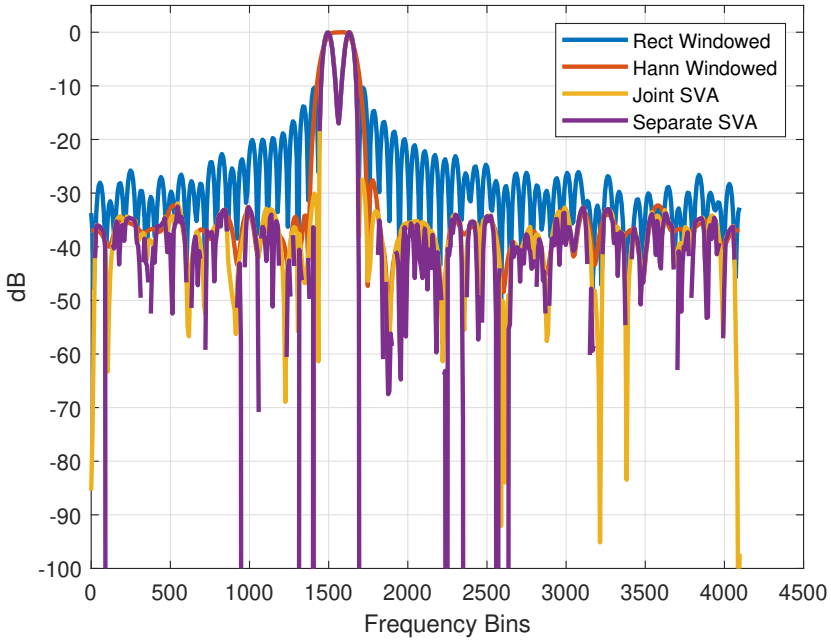

Figure 4.4: SVA for two close, equal power (SNR 20 dB) and one distant low power (SNR -20 dB) sources and noise

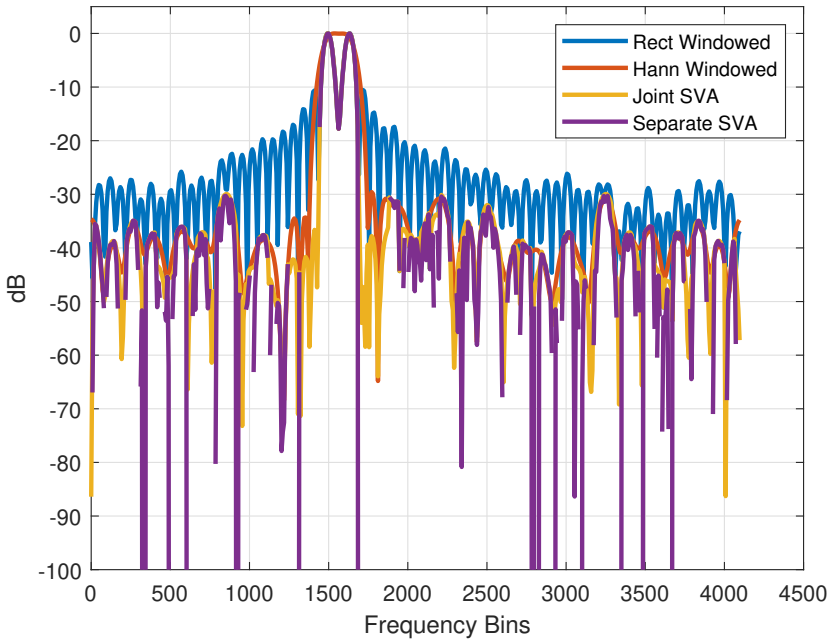

Figure 4.5: SVA for two close, equal power (SNR 20 dB) and one distant low power (SNR -10 dB) sources and noise

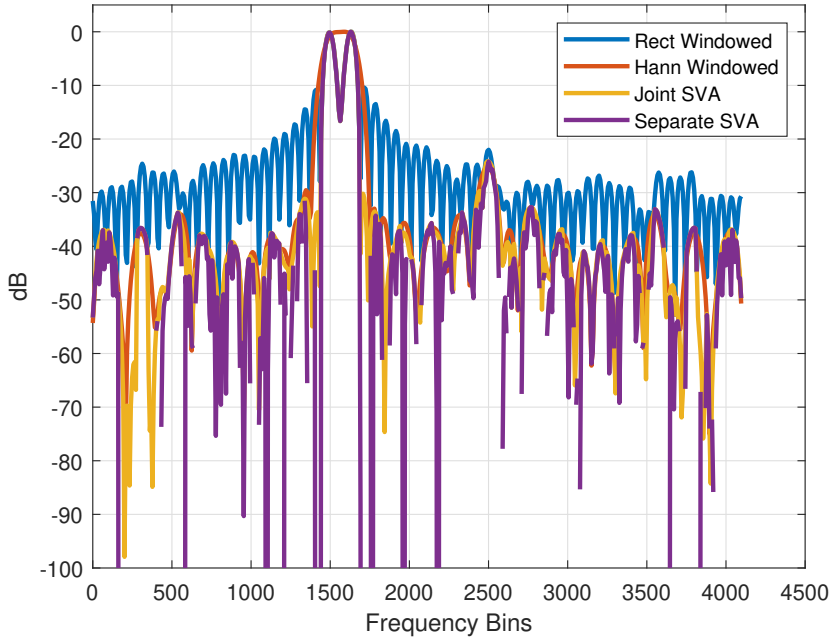

Figure 4.6: SVA for two close, equal power (SNR 20 dB) and one distant low power (SNR -5 dB) sources and noise

be given by

$$\tilde{P}_x(e^{j\omega}) = \min_{l \in \mathcal{L}} \frac{|\mathbf{w}_l^H \mathbf{x}\mathbf{x}^H \mathbf{w}_l|}{\max(|\mathbf{w}_l^H \mathbf{x}\mathbf{x}^H \mathbf{w}_l|)} \tag{4.24}$$

with unity gain constraint $\mathbf{w}_l^H \mathbf{e} = 1$ where $\mathbf{e} = [1\ e^{j\omega}\ ...\ e^{j(N-1)\omega}]$, the minimization problem with multiapodization approach can be stated as follows

$$\begin{aligned} &\tilde{P}_x(e^{j\omega}) = \min_{l \in \mathcal{L}} \frac{|\mathbf{w}_l^H \mathbf{x}\mathbf{x}^H \mathbf{w}_l|}{\max(|\mathbf{w}_l^H \mathbf{x}\mathbf{x}^H \mathbf{w}_l|)} \\ &subject\ to\ \mathbf{w}_l^H \mathbf{e} = 1. \end{aligned} \tag{4.25}$$

The formulation given in equation 4.25 is very similar to formulation in equation 2.13 given for Capon(MVDR), except that input correlation function is replaced by $R_x = xx^H$. In other words, in MVDR multiple snapshots are used to evaluate correlation function, whereas in multiapodization a single snapshot is used for correlation function. Moreover, in MVDR there is no restriction on the number of windows,

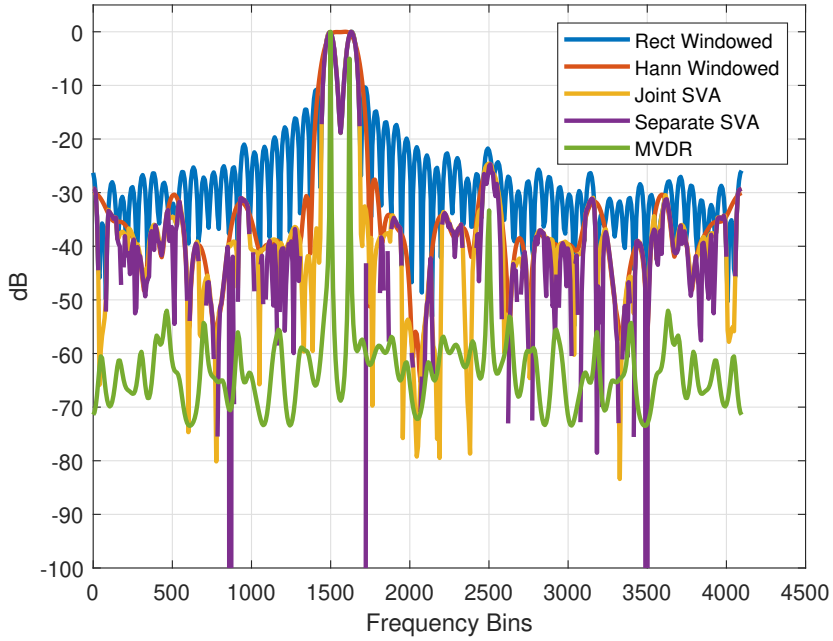

Figure 4.7: SVA and MVDR for two close, equal power (SNR 20 dB) and one distant low power (SNR -5 dB) sources and noise

however in multiapodization the window set is restricted with $\mathcal{L}$. For the conditions given in Figure 4.6 the MVDR and SVA results are given in Figure 4.7. Number of snapshots used for MVDR is 100. MVDR, as expected, has better results since it uses much more information compared to SVA.

4.5 Conclusion

In this chapter, types of nonlinear apodization have been studied. These methods are used to improve the tradeoff between sidelobe level versus mainlobe width. The main idea is to use two or more windows and select the minimum from windowed outputs at each spectral location. The performance improves as the number of windows increases. However, the computational complexity also increases with the number of windows. SVA has been proposed to overcome this problem. In SVA, an infinite number of windows with the form of a raised-cosine function are used. Moreover, the multiapodization or SVA method has been shown to be a version of MVDR. These methods have been adapted to array signal processing. SVA method will be used and

a beamforming method based on SVA will be presented in Chapter 5. On the other hand, dual-apodization will be used in Chapter 6 together with GA to design sparse linear arrays.

CHAPTER 5

SVA BASED BEAMFORMING

A frequency domain method is proposed to reduce the sidelobe level of a uniformly weighted uniform linear array in direction-of-arrival estimation. The development is based on the nonlinear method of "spatially variant apodization" originally proposed for spectral analysis and synthetic aperture radar imagery [78].

5.1 Introduction

Short-time Fourier transform is a basic tool in spectral analysis. In short-time Fourier transform, "short" data/signal segments are generally multiplied by a weighting function (window) prior to the Fourier transform computation. This operation is known as windowing or apodization, the latter term being more widely used in optics. A short-time Fourier spectrum involves the convolution of the Fourier transforms of the signal and the window. Broadly speaking, the effect of the Fourier transform of the window (on the resulting short-time spectrum) is generally quantified in terms of its main lobe width and side lobe level. Main lobe width is related to the accuracy in localizing spectral peaks and side lobe level to the interference among the spectral components. Inherent tradeoff between main lobe width and side lobe level has led to a substantial amount of study on the design of window functions [77, 81, 82] (and references therein). On the other hand in [78], it has been shown that by applying a nonlinear operation, the sidelobe level can be reduced without degrading the mainlobe resolution. The idea is to first compute multiple STFTs each with its own window function and then, for each frequency, keep the value of the one having the minimum magnitude. The detail of this method is given in Chapter 4

This approach has been utilized in [78] for sidelobe reduction in SAR (synthetic aperture radar) imagery. The use of two (dual apodization) or more (multi-apodizaton) windows has been studied. Although, it would be preferred to include as many different types of windows as possible in multi-apodization, this may not be practical because of the accompanying computational demand. In [78], another method, a special case of multi-apodization, called as Spatially Variant Apodization (SVA) has been proposed to incorporate infinitely many windows provided that windows are of raised-cosine type. In [79, 80], SVA has been formulated as a spectral estimator and its relationship to minimum variance spectral estimator (MVSE) has been emphasized. Although SVA is data dependent, it effectively suppresses the sidelobe level without explicit use of a priori information. Moreover, it has much less computational demand compared to MVSE and free from its finite numerical problems since it does not require the inversion of the covariance matrix of the input.

Although it has been stated, [78], that nonlinear apodization techniques have very broad range of applications where the data can be represented as the Fourier transform of a finite-aperture signal and there are some other studies on SVA [83–85], any study adapting SVA to beamforming has not been encountered. As in other signal processing operations, narrow main lobe and low side lobe level in spatial power spectrum estimation is very important for beamforming and direction of arrival (DOA) estimation. In this chapter, an SVA approach will be developed for spatial domain processing of the element outputs of a sensor array. To achieve the goal, we use the similarity of Fourier transform and beamforming operations. In this development beamforming is performed in frequency domain.

In Section 5.2 the relationship between DTFT and beamforming is recalled. SVA based beamforming is presented in Section 5.3. Section 5.4 provides some simulation results. Some of the practical issues are discussed in Section 5.5. Conclusions are given in Section 5.6.

5.2 Relationship between DTFT and Uniform Linear Array Beamformer

The conventional beamformer output of a uniform linear array (ULA) of M sensors (with equal weighting, i.e., rectangular windowing) for a complex plane wave of frequency ω_0 and DOA θ is, [6],

$$X_{BF}(\theta) = \sum_{m=1}^{M} X_m e^{-j\omega_0 \tau_m(\theta)} \tag{5.1}$$

where θ is defined with respect to positive x-axis and sensors are located on x-axis, X_m is the spectral component of the m^{th} sensor output at frequency ω_0, and $\tau_m(\theta)$ is the time delay at the m^{th} sensor with respect to the reference point. Assuming the reference point as the first sensor of the array, $\tau_m(\theta)$ is defined as

$$\tau_m(\theta) = \frac{(m-1)d\cos\theta}{c} \tag{5.2}$$

where d is the separation between the sensors and c is the propagation speed of the wave. Letting $d = d_\lambda \lambda_0,\ d_\lambda > 0$ where $\lambda_0 = 2\pi c/\omega_0$ and a change of variable $n = m - 1$, (5.1) can be written as

$$X_{BF}(\theta) = \sum_{m=0}^{M-1} X_m e^{-jm2\pi d_\lambda \cos(\theta)}. \tag{5.3}$$

On the other hand, DTFT of a length-M signal $x[m]$ is

$$X(e^{j\omega}) = \sum_{m=0}^{M-1} x[m] e^{-j\omega m}. \tag{5.4}$$

Comparing equations (5.3) and (5.4), when $x[m] = X_m$, $X_{BF}(\theta)$ and $X(e^{j\omega})$ are related as

$$X_{BF}(\theta) = X(e^{j\omega_0 \frac{d}{c}\cos(\theta)}) = X(e^{j2\pi d_\lambda \cos(\theta)}),$$
$$X(e^{j\omega}) = X_{BF}\left(\cos^{-1}\left(\frac{\omega c}{\omega_0 d}\right)\right) \tag{5.5}$$
$$= X_{BF}\left(\cos^{-1}\left(\frac{\omega}{2\pi d_\lambda}\right)\right).$$

(5.6)

Therefore the beamformer output of ULA at direction θ can be found by evaluating the Fourier transform of the sensors' spectral components at frequency $\omega = (\omega_0 d\cos(\theta))/c$. In other words, given $X(e^{j\omega})$ we can obtain $X_{BF}(\theta)$ by a nonlinear mapping.

In terms of the DFT values, the results in (5.6) can be approximated as:

$$X_{BF}(\theta) \approx X[int(N\cos(\theta)d_\lambda)],$$
$$X[k] \approx X_{BF}\left(\cos^{-1}\left(\frac{k}{d_\lambda N}\right)\right) \tag{5.7}$$

where $X[k]$ is the $N-$point DFT of the sensors' spectral components. In (5.7), $int(.)$ stands for rounding operation, i.e. the integer closest to the argument.

The simulation results of beamforming (BF) by direct computation and DFT based computation are shown in Figure 5.1. The patterns in Figure 5.1 are obtained for two sources and an array of 32 sensors separated by half wavelength at the operation frequency. 1024 point DFT is used by zero padding.

5.3 SVA Based Beamforming Algorithm

Beamforming by a ULA and DTFT operations are similar. Using this similarity and the fact that SVA is based on the DTFT of the observation, SVA can be applied to beamforming.

Let the output of the m^{th} sensor in a ULA with M sensors be $\tilde{x}_m[n], m = 0, 1, ...M-1$

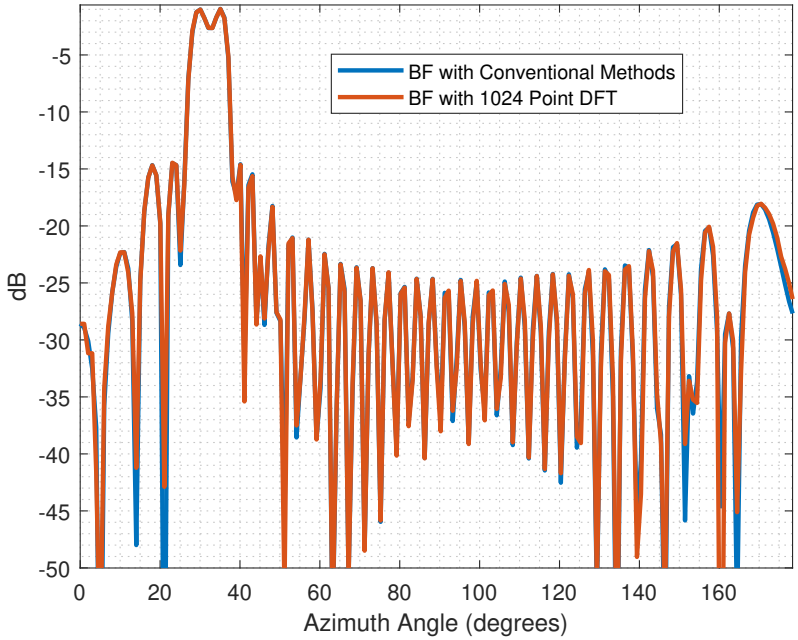

Figure 5.1: Conventional and DFT based beamforming

and its DTFT be $\tilde{X}_m(e^{j\omega})$. Also let the value of the DTFT at frequency ω_0 be $X_m = \tilde{X}_m(e^{j\omega_0})$ and DTFT of $\mathbf{X} = [X_0\ X_1\ ...\ X_{M-1}]$ be $X_s(e^{j\omega})$ ("s" stands for spatial),

$$X_s(e^{j\omega}) = \sum_{m=0}^{M-1} X_m e^{-j\omega m} \tag{5.8}$$

Recall that "I-Q jointly SVA" output for a given DTFT, $X(e^{j\omega})$, is given by (4.16) with $\alpha_0(\omega)$ given by (4.17)

Accordingly, using the relationship in (5.6), SVA beamforming output can be found as

$$Y_{BF}(\theta) = Y(e^{j2\pi d_\lambda \cos(\theta)}) \tag{5.9}$$

Using (4.16) and (5.9):

$$Y_{BF}(\theta) = -\alpha_0(\theta)X_s(e^{j(2\pi d_\lambda \cos(\theta)-2\pi/M)})$$
$$+X_s(e^{j2\pi d_\lambda \cos(\theta)}) - \alpha_0(\theta)X_s(e^{j(2\pi d_\lambda \cos(\theta)+2\pi/M)}) \tag{5.10}$$

Now, using the second line of (5.6), SVA-beamforming output becomes

$$\begin{aligned} Y_{BF}(\theta) = &-\alpha_0(\theta)X_{BF}\left(\cos^{-1}\left(\cos(\theta) - \frac{1}{Md_\lambda}\right)\right) \\ &+ X_{BF}(\theta) \\ &- \alpha_0(\theta)X_{BF}\left(\cos^{-1}\left(\cos(\theta) + \frac{1}{Md_\lambda}\right)\right) \end{aligned} \tag{5.11}$$

$\alpha_0(\theta)$ is given by

$$\alpha_0(\theta) = Re\left\{\frac{X_{BF}(\theta)}{S_{BF}(\theta)}\right\},$$
$$0 \leq \alpha_0(\theta) \leq 0.5 \tag{5.12}$$

where $S_{BF}(\theta) = X_{BF}\left(\cos^{-1}\left(\cos(\theta) - \frac{1}{Md_\lambda}\right)\right) + X_{BF}\left(\cos^{-1}\left(\cos(\theta) + \frac{1}{Md_\lambda}\right)\right)$

In terms of DFT, SVA beamforming output is given by

$$Y_{BF}(\theta) \approx Y[int(N\cos(\theta)d_\lambda)] \tag{5.13}$$

where $Y[k]$ is obtained by applying SVA to $X_s[k]$, (equations (4.20)-(4.22)), and $X_s[k]$ is the N-point DFT of $\mathbf{X} = [X_0\ X_1\ ...\ X_{M-1}]$. Here zero padding factor is $K = N/M$ since $X_m = 0$ for $m \geq M$.

The flowchart for the proposed algorithm is given in Figure 5.2. Firstly, the data at each sensor output is buffered to transform to frequency domain via DFT operation. The aim of the first set of DFT operations is to obtain the magnitudes and the phases of sensor outputs at the frequency of interest. Then, based on the similarity of beamforming and DFT (See Eqs. 5.1 and 5.4), N point DFT ($N \geq M$) is applied to those

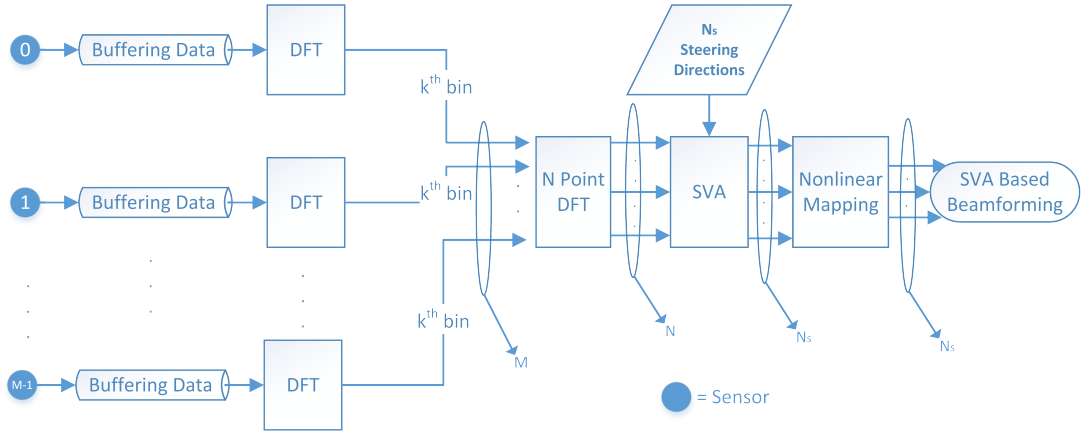

Figure 5.2: Flowchart for the proposed algorithm. The numbers of paths at the outputs of the blocks are indicated by the arrows.

components by padding $N - M$ zeros to the end of the data, and therefore, we get the result of beamforming corresponding to a rectangular window. Following the DFT operation, SVA is applied. For lower computational complexity, SVA is computed only for desired steering directions (N_s is the number of desired steering directions, $N \geq N_s$). Finally, by the nonlinear mapping (See Eq. 5.7) SVA applied beamforming is obtained for the specific N_s steering directions. In Figure 5.2, the size of data at the output of each block is shown by arrows.

5.4 Results

Mainlobe widths (resolution) and sidelobe levels, obtained by SVA based beamforming and by alternative methods will be compared. Figure 5.3 shows an example with 3 targets in the environment. The target at azimuth angle of $75°$ has $50\ dB$ lower power compared to the other two targets. In this example ULA has 64 sensors with $d_\lambda = 1/2$. SNR is infinite and 1024-point DFT is used. It is seen that beamforming with Hanning shading cannot resolve two close targets and beamforming with rectangular shading cannot find the low power target whereas SVA beamforming can resolve two close sources and find the low power target. In the example above, "I-Q jointly SVA" has been applied.

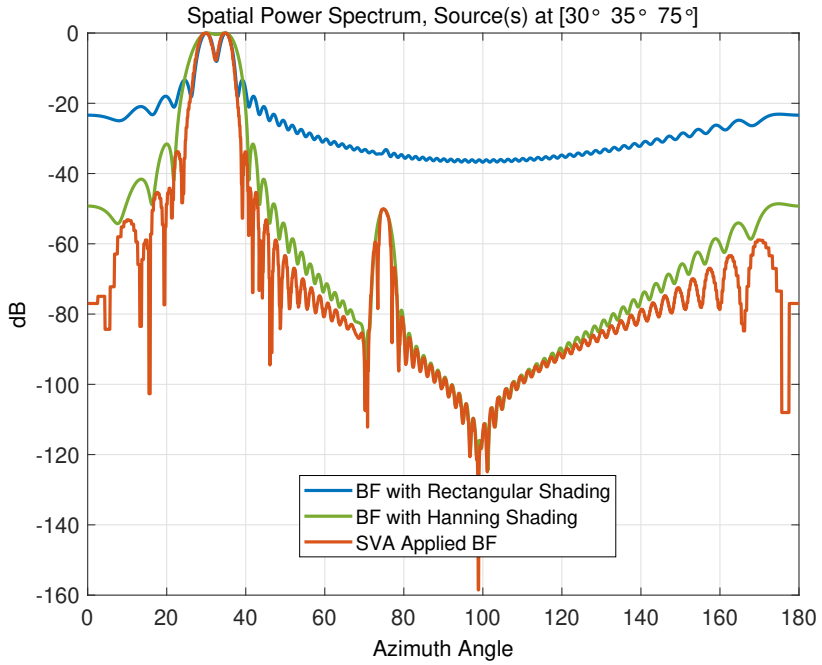

Figure 5.3: SVA Based Beamforming

5.5 Some Practical Issues

Additive noise: The method presented in this chapter inherits the properties of SVA therefore it has no effect on noise, that is the sidelobe level can be reduced at most to the level of the noise. The results of an example with the same parameters of the case given in Figure 5.3 but with additive noise at specified SNRs are provided in Figure 5.4. Figure 5.4 reveals that for the regions where sidelobe level is greater than the noise level, around the mainlobe, the sidelobe has been suppressed to the noise level, however for other regions sidelobe level remains at the noise level.

The low powered target in Figure 5.4 can be observed when the processing gain exceeds the noise level. The results for the same scenario with Figure 5.4 but with different SNR levels for the target at 75° are given in Figure 5.5. The low powered target became clear around -18 dB. Notice that, although 1024 points DFT is used, the effective processing gain is limited by the number of sensors which is 64.

The peak-to-peak variation around the target peaks: The number of sensors affects the resolving capability, there may be cases where rectangular shading has better resolu-

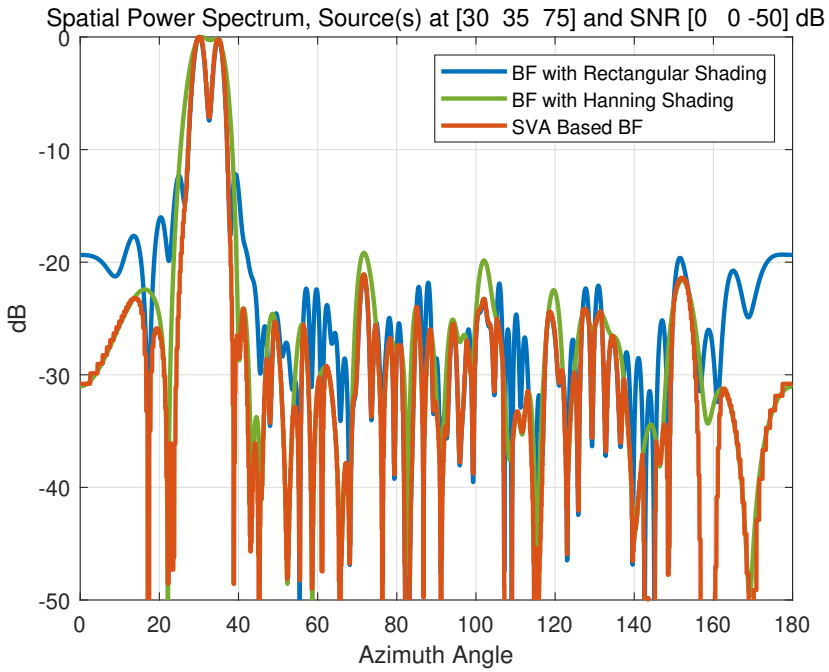

Figure 5.4: SVA Based Beamforming with noise

tion compared to that of SVA based beamforming. The results for two close targets, with the same parameters of the case given in Figure 5.3 but with 32 sensors, are provided in Figure 5.6. As it is seen from Figure 5.6 there is about $2\,dB$ loss compared to rectangular shading. The reason for this is the decrease in mainlobe energy [86, 87]. When Figure 5.6 is analyzed it is seen that around the mainlobe the optimal weights are close to $1/2$ instead of 0. To have the same resolution with rectangular shading, the number of sensors has to be increased or modified SVA (MSVA) method described in [86, 87] can be applied. In MSVA, the filter length is increased from 3-taps to 5-taps and the constraints are adjusted accordingly. The result of MSVA based beamforming is given in Figure 5.7. It is seen that MSVA and rectangular shading curves almost coincide around the peaks.

DFT length: The number of DFT points has to be large enough to have an acceptable accuracy and better performance. Increasing the number of DFT points decreases the error in nonlinear mapping. Moreover, having the number of DFT points as an integer multiple of the number of sensors has a positive effect on the performance. Choosing the number of DFT points as an integer multiple of the number of sensors makes the

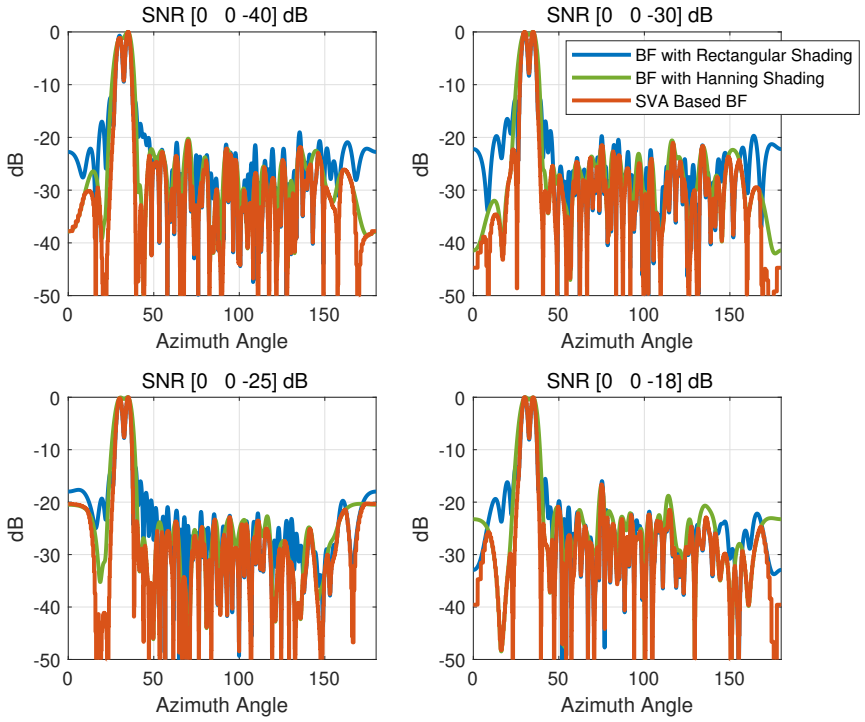

Figure 5.5: SVA Based Beamforming with noise and different SNR levels for the low powered target

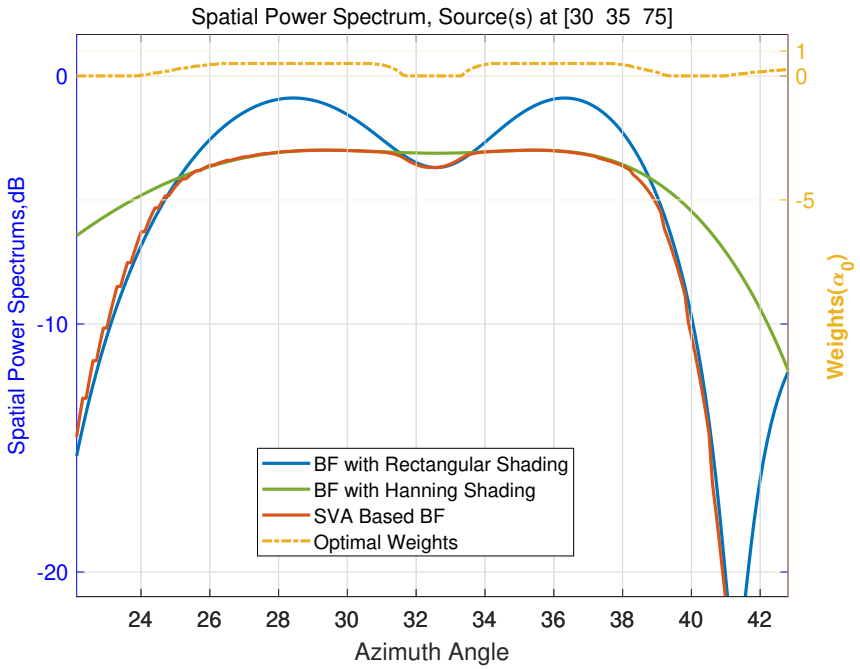

Figure 5.6: SVA Based Beamforming with 32 sensors

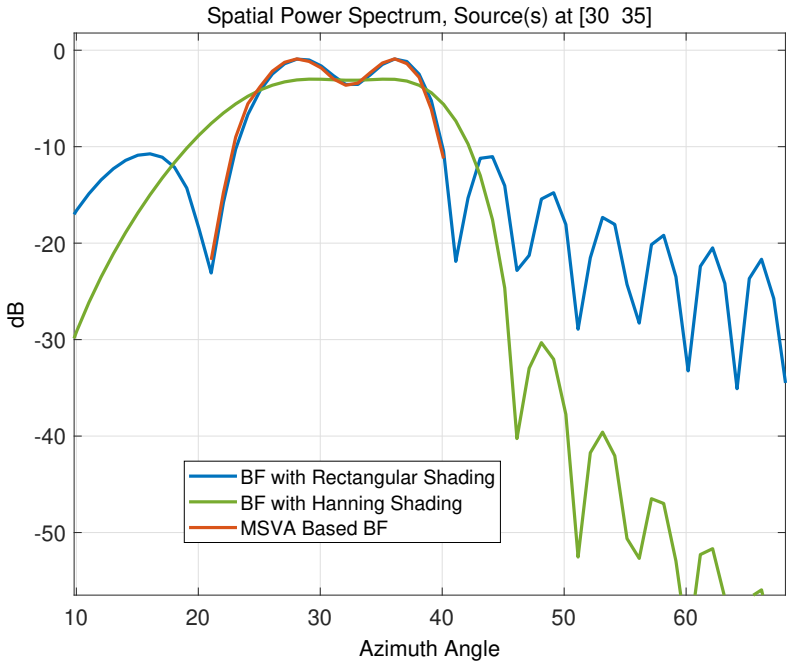

Figure 5.7: MSVA Based Beamforming with 32 sensors

zero padding factor an integer and this decreases the mapping loss.

5.6 Conclusion

As a specific multi-apodization approach, SVA is a computationally convenient method that brings together the advantages of different window functions in spectral analysis. In this chapter, SVA has been adapted to beamforming by a uniform linear array. The main idea is to use the similarity of beamforming and DTFT operations and the fact that optimization in SVA is done in frequency domain. SVA based beamforming achieves the resolving capability of rectangular shading with much lower sidelobe level. SVA based beamforming naturally inherits the properties of SVA; A possible drawback, its poorer resolution (relative to that of rectangular shading) when the number of sensors is reduced can be overcome by a modified SVA method. Choosing the number of DFT points as an integer multiple of the number of sensors reduces possible deviation in array output pattern to a negligible level. That this is a frequency domain method can be considered as a practical advantage due to the availability of custom FFT routines for many processors.

CHAPTER 6

A HYBRID NONLINEAR THINNED ARRAY DESIGN METHOD

A nonlinear method for array thinning is proposed. The method is based on hybrid usage of genetic algorithm and nonlinear apodization. The method proposes a special layout which consists of two sub-arrays. Layout and weights for the sub-array having larger aperture are designed by genetic algorithm. Layout and weights for the second sub-array are determined according to results of the aforementioned design. Dual-apodization is applied to the outputs of the sub-arrays to obtain the output. Results show that there is an improvement in peak side lobe level, beam-width and current taper ratio for some particular test problems in the literature.

6.1 Introduction

A sparse array is an array which contains neighboring elements with a spacing larger than the Nyquist spatial limit ($\lambda/2$ for linear arrays, where λ is the wavelength). As a special case of sparse arrays, if the element spacings are quantized to multiples of $\lambda/2$ then they are called thinned arrays. Quantizing element spacings has the advantages of Nyquist spatial sampling rate validity at all frequencies below the design frequency and of having no limit on scan angle [88]. On the other hand, the degree of freedom in the array design is decreased by quantizing element spacings.

The advantages of sparse arrays are reduced cost, complexity and computational burden of the system and to have a spatial resolution similar to that of the full array which obeys Nyquist spatial limit. However, sparse arrays cause spatial aliasing which may yield high sidelobes in the array pattern [6]. High sidelobes are undesired, and there are many studies to suppress them. In these studies, layout and weights are opti-

mized to improve the performance in terms of the peak sidelobe level (PSLL), the beam width (BW) and the current taper ratio (CTR). High sidelobe level may result in ambiguities in signal processing operations therefore low sidelobe level is always desired. BW determines the angular resolution of the array, the smaller the BW, the better close targets can be resolved. CTR is the ratio of the largest weight to the smallest weight. High CTR means high complexity in hardware design. Moreover, the best SNR gain is obtained when an equal weighting, CTR value of 1, is used.

In [42, 46] and [47] both layout and weight optimizations are done by Simulated Annealing (SA). The same study is conducted in [49] by Genetic Algorithm (GA). In [40, 50] solely layout optimization is done with GA. In [89], in addition to optimization of the layout and the weights, solely weights optimization for fixed locations is done with linear programming. In [90–92] the problem is handled in a different way and a beam-pattern that is similar to a desired/reference beam-pattern is searched to find the layout and the weights. In [48], a hybrid approach combining GA and a local optimizer has been utilized to solve the problem. In [88], a version of iterative FFT has been proposed for the solution of the problem. [93] and [94] have used deterministic approaches for designing linear sparse arrays. In [93], the solution is based on simple analytical expressions which jointly optimize sensor positions and dimensions with pre-assigned power levels. The method in [94] exploits an analytical formulation of the problem and convex programming routines and generates shaped beams by changing the location and the phase of the uniform amplitude sensors. Recently, compressive-sensing (CS) based methods have been proposed in the design of sparse arrays, [52–55, 57–59]. [58] uses a famous greedy algorithm known as orthogonal matching pursuit (OMP) together with spherical wave expansion for the problem. In the design process of that study, both element field patterns and mutual coupling between elements are considered. In [57], the extension of CS to wideband arrays has been provided. Inspiring the idea used in robust beamforming methods, a robust CS method has been presented in [54] by adding an extra constraint. Extension of Bayesian Compressive Sensing (BCS) to sparse arrays has been successfully used in [55] and [52].

In this chapter, a nonlinear method for the design of sparse linear arrays is proposed. The method is based on nonlinear apodization and GA. The motivation of the work

is to combine two array structures to make use of their desirable characteristics while eliminating their weaknesses. The objective in this combination and in the work presented is to obtain a new structure that has a "good" pattern over the whole spatial region. The innovative part of this work in terms of methodology is to combine two different algorithms for sparse array design. The combined usage of those algorithms has not been encountered previously and yields improved PSLL, BW, and CTR compared to those in the literature. The proposed method can be used for the receiving operation only.

In the study, the aperture size and the maximum number of sensors are determined a priori. The objective is to obtain the best performance given these values. Unlike the settings of the existing methods, in this method thinned array is divided into two subarrays called SA1 and SA2. The motivation to use two sub-arrays is due to the inherent property of dual apodization. Dual-apodization needs two sub-arrays (windows in spectral context) in order to apply the nonlinear "minimum" operation. Another contribution of this study is to optimize the sensor locations of the sub-arrays so as to get the best performance of dual apodization. The method successfully combines the patterns of sub-arrays which are complementary in their "good" spatial regions.

The number of sensors in sub-arrays is not determined a priori but their sum is limited and subarrays may have common elements. Subarray SA1 has a nonuniform structure and extends over the whole, predetermined aperture. It is designed by GA. For optimization of SA1, however, any appropriate optimization algorithm capable of handling the constraints of the problem can also be used. SA2 obeys Nyquist spatial criterion and is designed according to the design of SA1.

In the proposed method, there are mainly two steps; optimization and nonlinear apodization. In optimization step, SA1 is designed such that its maximum side-lobe level within the mainlobe of SA2 is minimized. Remaining side-lobes are disregarded in this step since they will be suppressed in the second step. The layout and weights of SA2 are also determined in this step. After determining layout and weights of the sub-arrays, dual-apodization is applied to the output of the sub-arrays in the second step. The method is adapted for two cases. In the first case, merely the layout of SA1 is designed and in the second case, both the layout and the weights of SA1 are

designed. In both cases, both the layout and the weights of SA2 are designed. The method has been studied for two test problems in the literature.

The study as mentioned above is inspired by the idea of nonlinear apodization and uses two sub-arrays, dual-apodization and related designs. However, for an "optimal" result many sub-arrays, multi-apodization and related designs should be used. At least one of those sub-arrays should have a mainlobe width satisfying required resolution. Moreover, when steered to any particular direction, all the remaining interfering directions should be in a notch of the design. The idea actually converges to the Capon method; roughly stated, placing a notch to every interfering point. However, a practical solution is not feasible due to the high computational load. Therefore, in this study practical concerns and optimum computation for necessary performance is considered and the method given in the following sections has been presented. It has much less computational demand compared to Capon and free from its finite numerical problems since it does not require the inversion of the covariance matrix of the input.

Section 6.2 gives the description of beam-pattern function and dual apodization. Details of constructing sub-arrays and of the proposed method are provided in Section 6.3. Section 6.4 presents results obtained by this method and compares them to those from the literature. Section 6.5 concludes up the work.

6.2 Preliminaries

6.2.1 Beam Pattern (BP) Formulation

Beam pattern $(BP(\theta))$ of a linear array, made of N omnidirectional sensors, and located along x-axis is

$$BP(\theta) = \left| \sum_{n=0}^{N-1} w_n e^{j\frac{2\pi}{\lambda} d_n (cos(\theta_0) - \cos(\theta))} \right|, \tag{6.1}$$

where d_n and w_n are the position and the weight of the n^{th} sensor, respectively. θ and θ_0 are the scan angle and the steered direction of the array which are measured

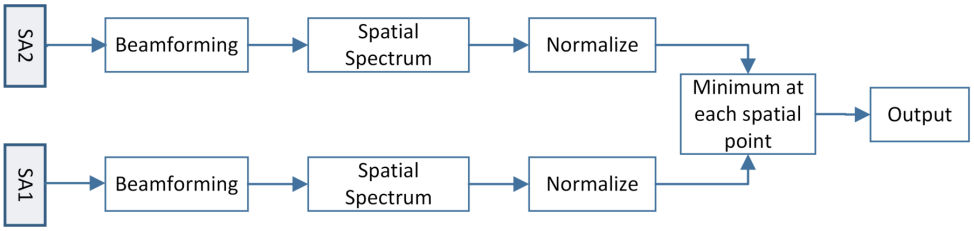

Figure 6.1: Architecture for obtaining dual apodization in the array context

with respect to the x axis. In this chapter, it is accepted that $\theta_0 = 90°$. It is known that $(BP(\theta))$ is an even function. Moreover, when the sensor locations are quantized with $\lambda/2$, the domain to be examined can be restricted to $90° \leq \theta \leq 180°$ and the mainlobe is centered at $\theta = 90°$ [91].

6.2.2 Dual Apodization

Dual-apodization has been introduced in Chapter 4. It has been adapted for beam-patterns and used for the spatial domain in the proposed method. The counterpart of the temporal frequency in the spatial domain is the scanning angle. The windows and the DFTs of the windows have been replaced by the sub-arrays and the beam patterns of the sub-arrays respectively. Moreover, beamforming for a linear array in the array context and DFT of a windowed time signal in the spectral context are dual. In practice, the spatial spectra for both arrays will be obtained by beamforming methods. In beamforming, the sensor locations and the weights determined by this study will be used. Then dual apodization will be applied to spatial spectra of two arrays. Architecture of the operations explained above is given in Figure 6.1.

6.3 Description of the Algorithm

As in the existing studies, the main goal of this study is to obtain the narrowest BW and to keep PSLL and CTR as low as possible. To this end, a special array layout is proposed. The whole array is considered as the combination of two subarrays, named as SA1 and SA2, and SA2 is located approximately around the center of the aperture of SA1. SA1 covers a predefined/desired aperture and the spacing between

any two neighboring elements is $\lambda/2$ or a multiple of $\lambda/2$. SA2 is a uniform array with a significantly smaller aperture and its element spacings are $\lambda/2$. The optimization process is carried out for either only locations or both locations and weights of sensors in SA1. The target of the optimization at this step is to minimize the PSLL of SA1 within the mainlobe of SA2. Since it is a uniform array, mainlobe of SA2 is limited by the size of its aperture. The fitness function is defined accordingly. The weights of the elements of SA2 are determined according to the result of the design of SA1. Then dual apodization, [78], is applied to beam-patterns of these two sub-arrays. SA2 obeys Nyquist limit but it has a small aperture, therefore, its beam-pattern has a good sidelobe level behavior whereas its mainlobe is very large. On the other hand, SA1 has a large aperture but violates the Nyquist limit, therefore, its beam-pattern has a narrow mainlobe, however, with possible strong sidelobes. Dual-apodization of these two sub-arrays results effectively in a narrow mainlobe and low sidelobe levels. Before we give a step-by-step description of the design algorithm below in Section 6.3.3, we provide preliminary information in Section 6.3.1 and 6.3.2 about the formation of subarrays to expose the underlying motivation.

6.3.1 Formation of Subarrays

Let, the desired aperture in wavelengths, the maximum number of all sensors in the complete array, the number of sensors of the subarray SA1 and the number of sensors of the subarray SA2 be L, N, N_1 and N_2, respectively. In general, $N \leq N_1 + N_2$, and the equality is satisfied when there is no common element of SA1 and SA2. As an example, layout configuration and beam-patterns BP_{SA1} and BP_{SA2} for SA1 and SA2 are shown in Figure 6.2. Uniform weighting has been applied to both sub-arrays in Figure 6.2. In Figure 6.2(b) it is seen that the mainlobe of BP_{SA2} covers the first few sidelobes of BP_{SA1}. Therefore, if dual-apodization is applied to the example given in Figure 6.2, PSLL will be around $-8\ dB$ which is not satisfactory practically. However, if SA1 is designed such that its side-lobes within the mainlobe of SA2 (i.e. the region between the edges of the mainlobes of SA1 and SA2, this region is denoted by u_{stop} in Figure 6.2(b)) are suppressed, dual apodization will result in a beam-pattern with a narrow mainlobe and well-suppressed sidelobes.

6.3.2 Suppression region by GA (u_{stop})

The first null beam-width (FNBW) of a linear array is defined as [95]

$$FNBW = \lambda / D_{eff} \tag{6.2}$$

where D_{eff} is the effective aperture of the array. Effective aperture is related to the physical aperture D by $D_{eff} = \rho D$ where ρ depends on steering direction. D_{eff} takes the maximum value at the broadside and the minimum value at the end-fire. u_{stop} is the spatial interval over which the response of SA1 will be suppressed. Its length, $|u_{stop}|$, can be defined as,

$$\begin{aligned} u_{stop} &= \{u | u > B_1 \text{ and } u <= B_2\}, \\ |u_{stop}| &= (B_2 - B_1), \end{aligned} \tag{6.3}$$

where

$$B_1 = FNBW_{SA1}, \;\; B_2 = FNBW_{SA2}. \tag{6.4}$$

This region is shown in Figure 6.2(b).

6.3.3 Layout Optimization

In this part, GA will optimize solely the layout of SA1. The design variables of the GA for this part will be the locations of sensors in SA1 at multiples of $\lambda/2$. SA1 will be stimulated with uniform weighting. The fitness function of the GA is defined as,

$$f(\mathbf{d}) = 1 / \max_{u \in u_{stop}} (\text{abs}(BP_{SA1}(\mathbf{d}, u))), \text{ subject to } |BP_{SA1}(\theta_0)| = 1, \tag{6.5}$$

where $\mathbf{d}$ is the elements' position vector. GA finds the element positions of SA1 such that, the PSLL of BP_{SA1} in u_{stop} region, see Figure 6.2(b), will be minimized. The remaining regions will be disregarded by GA, since those regions will be suppressed by dual-apodization. During GA optimization, each chromosome in the population consists of N_1 genes, each of which represents the location of a sensor. The details of the algorithm are given below:

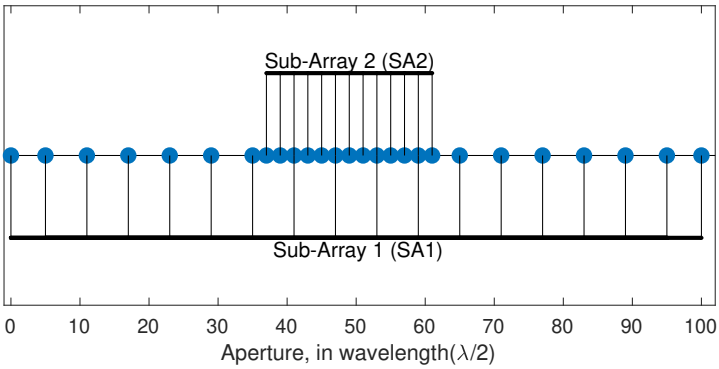

(a)

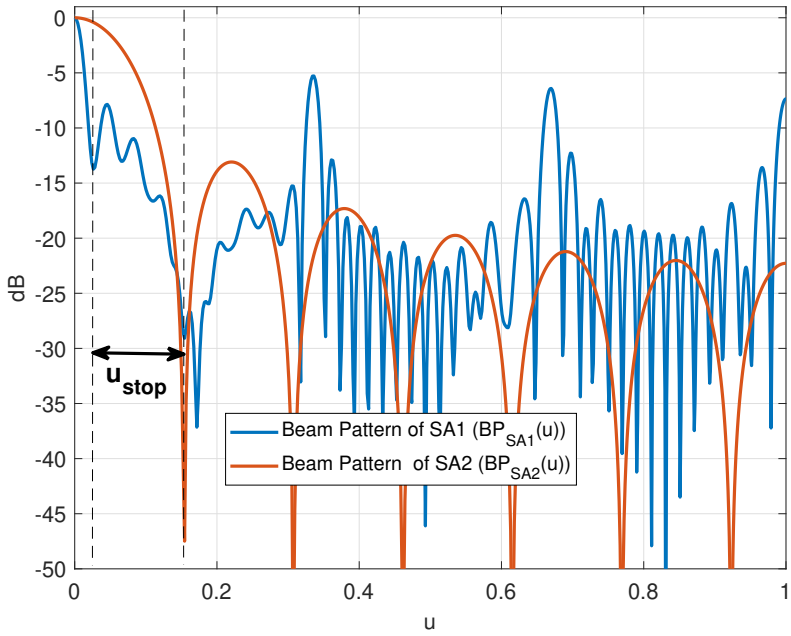

(b)

Figure 6.2: (a)An example layout configuration for $L = 50, N = 27, N_1 = 18, N_2 = 13$, (b) beam-patterns for SA1 and SA2 and regions of BP_{SA1} to be suppressed by GA, $u = cos(\theta_0) - \cos(\theta)$.

1. The algorithm starts with a sought aperture, L, and an allowed maximum number of sensors N.

2. Initially $N_1 = N$, $N_2 = floor(N/2)$.

3. First null beamwidths are found using L, N_1 and N_2. Initial region for u_{stop}, is

determined.

4. A random population is generated for locations of SA1, the first and the last sensors are located at extreme points of the aperture ($0(\lambda/2)$ and $(2L)(\lambda/2)$). Remaining sensor positions are chosen randomly between the extreme points.

5. $N_1 - 2$ optimum sensor locations are found according to fitness function provided in (6.5) by GA. Temporal counterpart of this step can be assumed as the selection of an optimum window such that BP of SA1 in u_{stop} region has lowest PSLL possible.

6. If there are any repeating sensor locations, they are excluded. N_1 is set to the number of remaining sensors. Although fitness function is defined according to u_{stop}, the suppression region after design may be larger. u_{stop} is updated.

7. Sensors of SA2 are positioned such that SA1 and SA2 have a maximum number of common elements. This is the location where a group of sensors are positioned firmly in SA1 and generally occurs around the center of the aperture. The maximum coincidence is desired in order to reduce the total number of sensors. The details of this step is given below as Algorithm-A.

8. If the total number of the sensors exceeds N, decrease N_1 by 1 and proceed to step 3, otherwise, proceed to step 9

9. A weighting function is applied to elements of SA2 such that after dual-apodization the best sidelobe behavior is obtained. The details of this step is given below as Algorithm-B.

10. If the mainlobe of SA2 fits u_{stop}, proceed to dual-apodization step. If the mainlobe is smaller/larger than the u_{stop}, increase/decrease N_2 by 1 and proceed to step 7.

Algorithm-A: The details of the step-7 of the design algorithm.

A1) Initially, locate uniformly the sensors of SA2 between 0 and$(N_2 - 1)\lambda/2$.

A2) Find the number of SA1 sensors coinciding with the sensors of SA2. Set this value as the score of this region. Ultimately, SA2 will be positioned using these scores.

A3) If all aperture has been browsed, proceed to step A4, otherwise shift SA2 to the right by $1(\lambda/2)$ and go to step A2.

A4) Place SA2 to the region with the highest score.

Algorithm-B: The details of the step-9 of the design algorithm.

B1) The weighting function for SA2 is in the form of $(1 - \alpha\cos(2\pi n/N_2))$, where $n = 0, 1, ...N_2 - 1$, $0 \leq \alpha \leq 1$. Set $\alpha = 0$ initially.

B2) Set the upper edge of u_{stop} as u_e.

B3) Find B_2 ($FNBW_{SA2}$) for the current α value. Neglect the α values satisfying $B_2 < u_e$, otherwise find the scalar difference $B_2 - u_e$

B4) If $\alpha = 1$, proceed to step B5 otherwise increase α by 0.01 and go to step B3.

B5) Select the α value that yields the minimum difference $|B_2 - u_e|$.

6.3.4 Layout and Weight Optimization

In this part, both the layout the and weights of SA1 will be optimized. The design variables of GA for this case will be the locations and the weights of the sensors in SA1. The fitness function will be as:

$$f(\mathbf{w}, \mathbf{d}) = 1/\max_{u \in u_{stop}} (\text{abs}(BP_{SA1}(\mathbf{w}, \mathbf{d}, u))), \text{ subject to } |BP_{SA1}(\theta_0)| = 1, \quad (6.6)$$

where **w** is the weight vector. Each chromosome in the population will consist of $2N_1$ genes. First N_1 genes represent the sensor locations whereas the last N_1 genes represent the weights. Crossover and mutation operations for the weights and the sensor locations are done separately. The steps of the algorithm for this case are the same with steps in Part 6.3.3 except the steps 4, 5 and 6 are modified as:

4. A population for sensor locations and weights is generated. Each chromosome in the population consists of N_1 genes representing sensor locations and N_1

genes representing the sensor weights. The first and the last sensors are located at extreme points of the aperture ($0(\lambda/2)$ and $(2L)(\lambda/2)$). Remaining sensor positions are chosen randomly between extreme points. Genes representing sensor locations are integer numbers which are decoded as multiples of half-wavelength. Generated weights are real and uniformly distributed between [0, 1] with resolution of 0.0001.

5. $N_1 - 2$ optimum sensor locations and N_1 optimum real weights are found according to fitness function provided in (6.6).

6. If there are any repeating sensor locations, they are eliminated and the weight for that location is chosen as the sum of the weights of the repeated sensors. In that case, the weight of a sensor in SA1 can be larger than 1. N_1 is set to the number of remaining sensors.

6.4 Results and Discussion

Two test problems will be handled to compare the results of the proposed method with the existing methods. The first problem is a widely studied problem and considers an aperture of $50\lambda,\ 101$ locations with 25 sensors. Some results in the literature for this problem are provided in Table 6.1, taken from [88]. The second problem considers an aperture of $31.5\lambda, 64$ locations with 48 sensors. Although in existing solutions, symmetric placement is required for this problem, in our solution we will not enforce symmetric placement. The existing results for this problem are provided in Table 6.2, taken from [88].

6.4.1 Layout Optimization

The population in GA is produced randomly, therefore different solutions may be observed in different simulation runs. The best solutions obtained by layout optimization for 25-element, 50-wavelength problem are provided in Table 6.3.

Results in Table 6.3 show that the PSLL of the proposed method, compared to existing solutions that can scan all angles, is better by at least $3\ dB$ and has much better CTR

Table 6.1: Existing solutions for 25-sensors, 50-wavelength problem

Solution	Source	PSLL (dB)	BW (u_{3dB})	CTR	Length (λ)
L1	[42]	-13.51	0.0143	4.1	50
L2	[91]	-14.45	0.0192	6.5	50
L3	[49]	-14.67	0.0190	7.3	50
L4	[48]	-14.67	0.0190	3.1	50
L5	[48]	-14.77	0.0204	7.1	50
L6	[88]	-14.00	0.0160	2	50
L7	[88]	-14.83	0.0206	5.98	50
L8	[96][1]	-17.01	0.0166	3.33	26.013
L9	[96][1]	-20.1	0.0185	2.63	26.013

[1]The pattern cannot be scanned. The design is done for a particular steering angle, if steering angle is changed grating lobes show up.

Table 6.2: Existing solutions for $31.5\lambda, 64$ locations with 48 sensors problem

Solution	Source	PSLL (dB)	BW(3dB) (degrees)	CTR	Length (λ)
L10	[89]	-18.76	1.812	2.76	31.5
L11	[88]	-19.72	1.839	1.91	31.5

Table 6.3: Solutions by the proposed method for layout optimization for 25-sensors, 50-wavelength problem

Solution	N,N_1,N_2	PSLL (dB)	BW (u_{3dB})	CTR	Length (λ)
S1	25,18,11	-18.25	0.0192	1.86	50
S2	25,18,11	-18.31	0.0188	1.86	50
S3	25,18,11	-19.02	0.0188	1.86	50
S4	24,17,10	-17.9	0.0192	1.86	50
S5	23,17,9	-17.55	0.0192	1.66	50

Table 6.4: Solutions by the proposed method for layout optimization for $31.5\lambda, 64$ locations with 48-sensors problem

Solution	N,N_1,N_2	PSLL (dB)	BW(3dB) (degrees)	CTR	Length (λ)
S6	38,30,22	-21.54	1.78	2.08	31.5
S7	41,30,30	-22.01	1.76	2.12	31.5
S8	47,30,38	-24.85	1.76	2.77	31.5

and comparable BW. Only the solution L9 seems to provide better PSLL and BW but with a cost of disability to scan the pattern. The sensor locations, the weights and the beam-patterns of SA1 and SA2 together with output beam-pattern for solution S3 are provided in Figure 6.3. Furthermore, better results can be obtained even with less sensors, solutions S4 and S5. Results of solution S5 are provided in Figure 6.4.

The reason for some solutions of this method to have the same BW is the fact that SA1 has the same BW in all cases. Thanks to the nonlinear operation of dual-apodization, BW of the output is the same with the one having narrower BW. Mainlobe of SA1 is affected by the lower end of u_{stop} and by keeping lower end of u_{stop} fixed, widening of mainlobe is prevented.

Solutions for the second problem obtained by layout optimization are given in Table 6.4.

Results in Table 6.4 show that the proposed method get better results even with less number of sensors; at least $2dB$ better PSLL, smaller BW and comparable CTR. Results of solution S8 are provided in Figure 6.5.

6.4.2 Layout and Weight Optimization

The best solutions obtained for the first problem by layout and weights optimization are provided in Table 6.5. The PSLLs are even better than previously presented results of Part 6.4.1. However, BW and CTR are increased but still comparable with solutions from the literature. Beam-patterns for solution S10 are provided in Figure

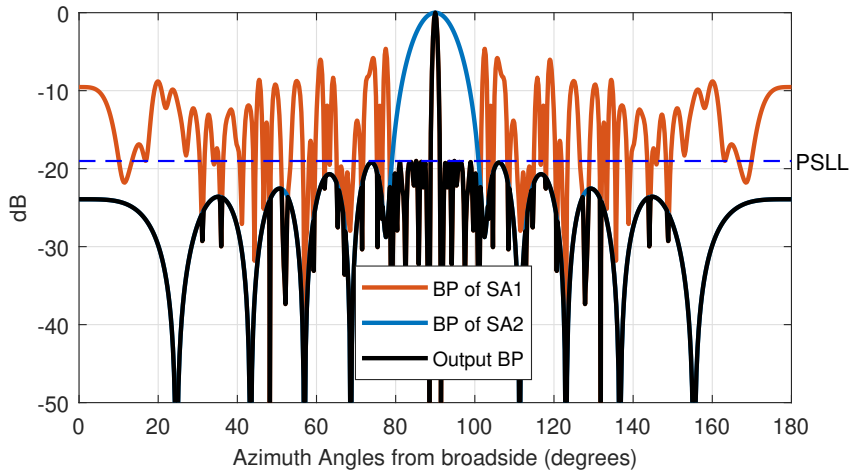

(a)

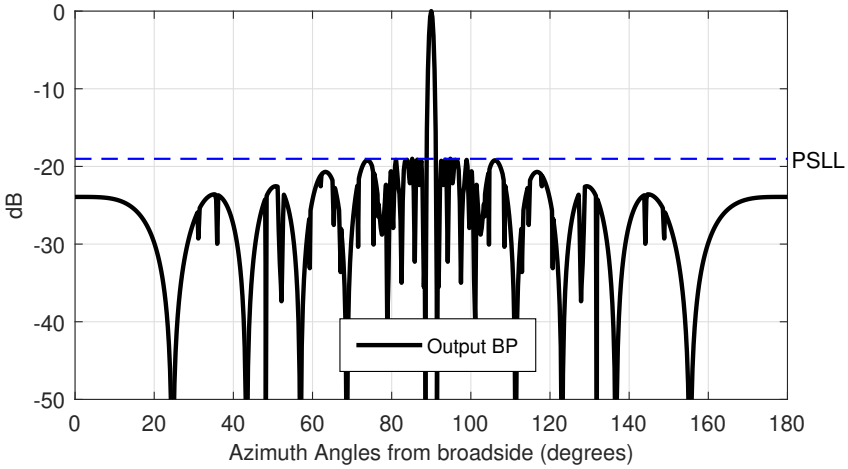

(b)

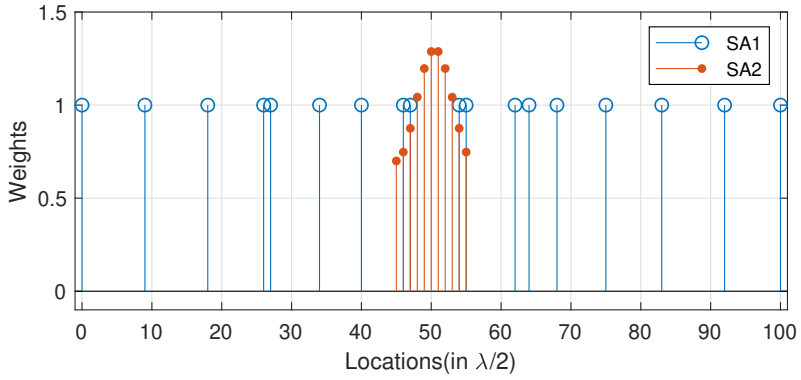

(c)

Figure 6.3: Beam-patterns (a,b), weights and locations (c) for S3

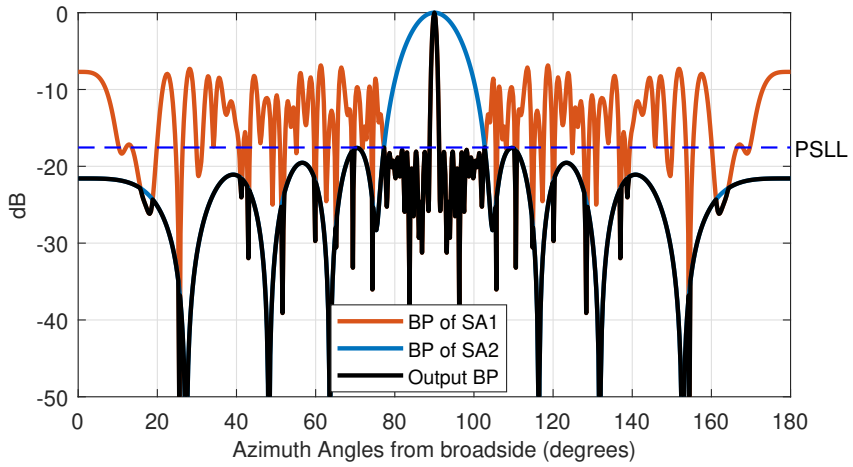

(a)

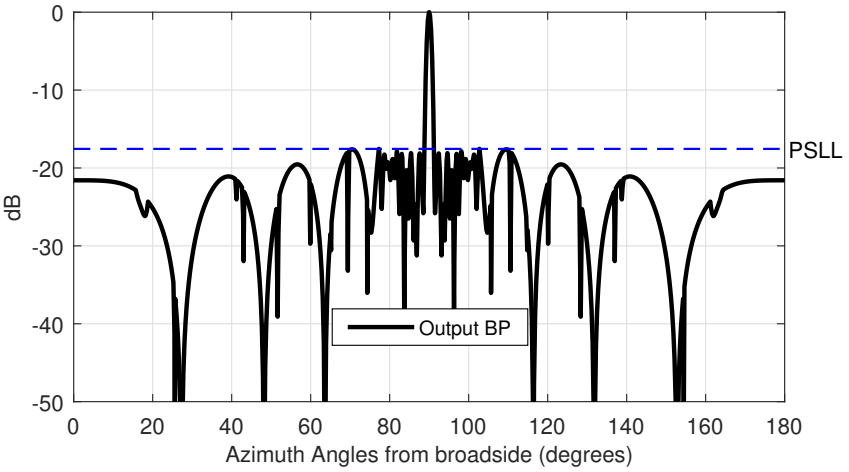

(b)

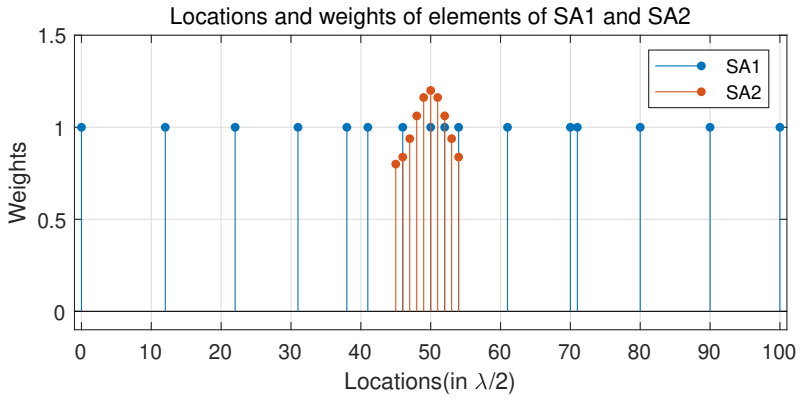

(c)

Figure 6.4: Beam-patterns (a,b), weights and locations (c) for S5

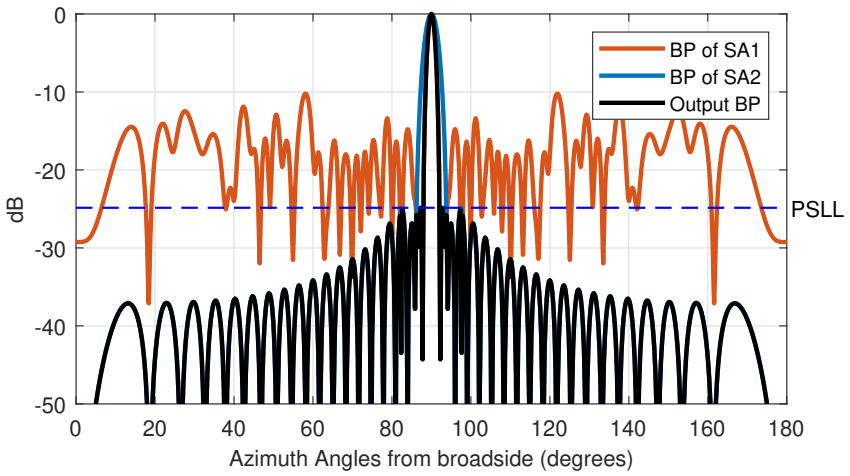

(a)

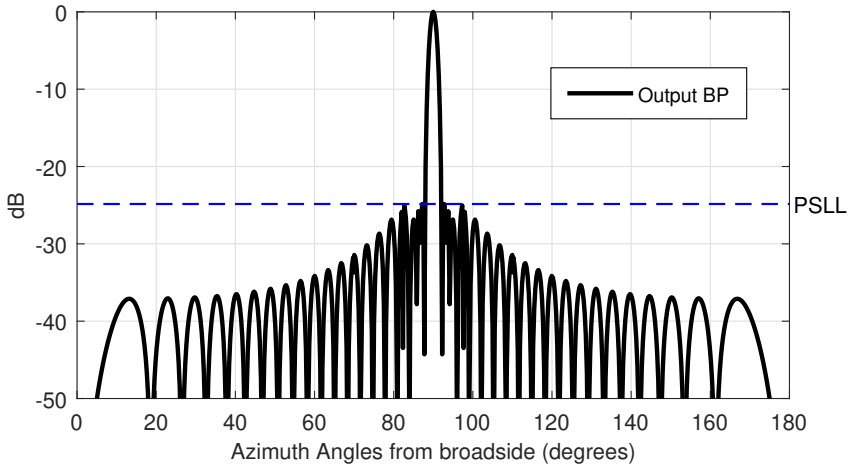

(b)

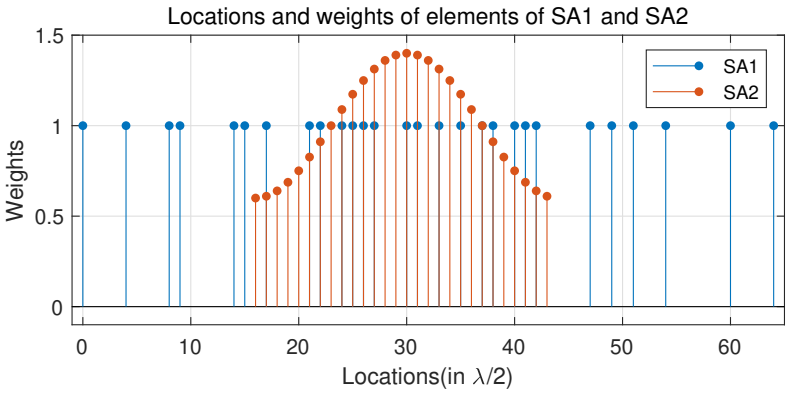

(c)

Figure 6.5: Beam-patterns (a,b), weights and locations (c) for S8

Table 6.5: Solutions by the proposed method for layout and weights optimization for 25-sensors, 50-wavelength problem

Solution	N,N_1,N_2	PSLL (dB)	BW (u_{3dB})	CTR	Length (λ)
S9	25,18,11	-19.72	0.0188	6.16	50
S10	25,18,12	-20.37	0.0192	6.35	50

Table 6.6: Solutions by the proposed method for layout and weights optimization for $31.5\lambda, 64$ locations with 48-sensors problem

Solution	N,N_1,N_2	PSLL (dB)	BW(3dB) (degrees)	CTR	Length (λ)
S11	42,28,33	-25.16	1.64	7.258	31.5
S12	42,29,33	-25.38	1.64	12.22	31.5

6.6, positions and weights are provided in Table 6.7.

Solutions to the second problem by layout and weights optimization are provided in Table 6.6. PSLL and BW values are better than the solutions presented in Part 6.4.1 and in the literature, however, CTR values are worsened. Beam-patterns for solution S12 are provided in Figure 6.7, positions and weights are provided in Table 6.7.

Table 6.7: Positions and weights of sensors for S10 and S12. x is position (in $\lambda/2$) and w is the weight

S10				S12			
SA1		SA2		SA1		SA2	
x	w	x	w	x	w	x	w
0	0,4708	45	0,6500	0	0,9037	16	0,4800
8	0,8035	46	0,6969	1	0,8146	17	0,4894
17	0,9590	47	0,8250	9	0,6590	18	0,5172
26	0,4896	48	1,0000	11	0,8028	19	0,5625

Continued on next page

Table 6.7 – continued from previous page

S10				S12			
SA1		SA2		SA1		SA2	
x	w	x	w	x	w	x	w
28	0,6813	49	1,1750	14	0,2561	20	0,6237
35	0,5242	50	1,3031	15	0,8742	21	0,6984
37	0,5653	51	1,3500	18	0,1843	22	0,7840
46	0,8161	52	1,3031	21	0,8130	23	0,8774
48	0,2293	53	1,1750	22	0,5471	24	0,9753
52	0,2134	54	1,0000	23	0,8439	25	1,0740
54	0,6764	55	0,8250	25	0,4566	26	1,1701
56	0,2402	56	0,6969	26	0,5297	27	1,2600
61	0,6587			28	0,9496	28	1,3405
67	0,8858			29	0,1508	29	1,4087
75	0,7212			32	0,5531	30	1,4622
84	0,4488			33	0,1615	31	1,4989
91	0,5570			34	0,7736	32	1,5176
100	0,3039			36	0,4515	33	1,5176
				38	0,2016	34	1,4989
				39	0,6763	35	1,4622
				41	0,6075	36	1,4087
				42	0,4446	37	1,3405
				43	0,9058	38	1,2600
				44	0,2636	39	1,1701
				47	0,6346	40	1,0740
				50	0,7337	41	0,9753
				51	0,5767	42	0,8774
				54	0,5455	43	0,7840
				63	1,8425	44	0,6984
						45	0,6237
						46	0,5625

Continued on next page

Table 6.7 – continued from previous page

S10				S12			
SA1		SA2		SA1		SA2	
x	w	x	w	x	w	x	w
						47	0,5172
						48	0,4894

A drawback of the solutions presented here is the loss in SNR gain since the sensors are apportioned among the two sub-arrays. However, considering the main reasons for using thinned arrays; economy, complexity and computational load, and the fact that the performance in terms of PSLL, CTR and BW of these solutions is better than the cases with larger numbers of sensors, it is meaningful to use these solutions. For example, for the first problem of the first part, SNR gain loss is $10log_{10}(25) - 10log_{10}(18) \approx 1.43\ dB$ however, PSLL is improved at least $3\ dB$. This figure is even better in the other cases. Moreover, when compared to the existing solutions for the first problem, the proposed method yields less SNR loss in layout optimization. The comparisons of SNR losses are provided in Table 6.8. Since in some references the numbers are not provided, they are estimated from figures. Although it seems that the proposed solution yields higher SNR losses for layout and weight optimization case, it leads to better sidelobe suppression. This result also supports that it may be advantageous to use this method.

Another drawback of the proposed method is that in classical designs once the layout

Table 6.8: SNR losses (dB) by the proposed method and those of the indicated references.

Solution	SNR Loss	Solution	SNR Loss
[42]	1.7263	[96]	1.7975
[91]	2.8485	S1-S3	1.4267
[49]	1.7958	S4-S5	1.6749
[48]	1.6067	S9	4.5451
[88]	1.9004	S10	3.1965

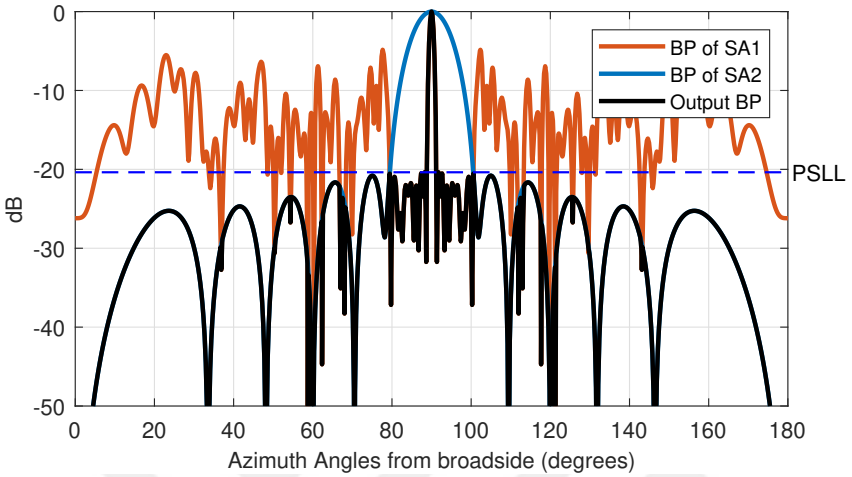

(a)

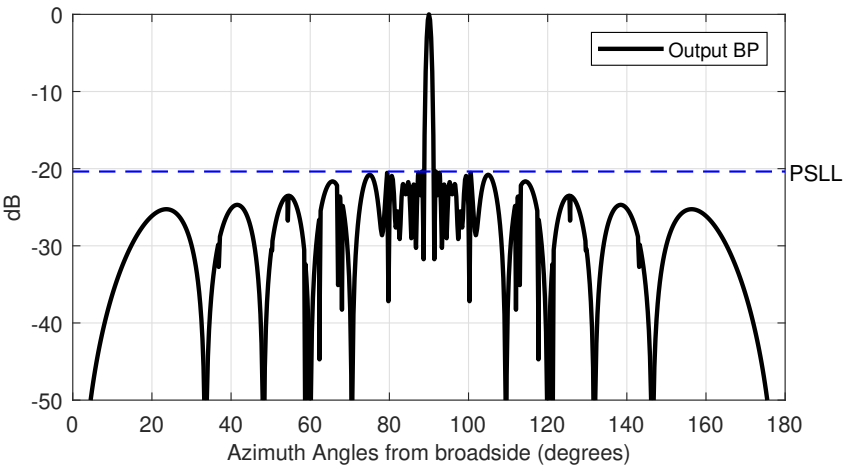

(b)

Figure 6.6: Beam-patterns for S10

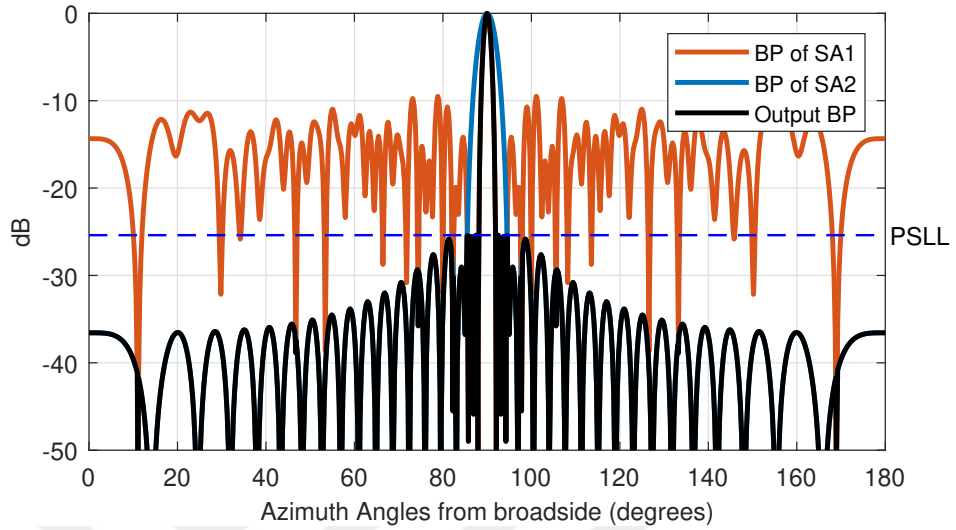

(a)

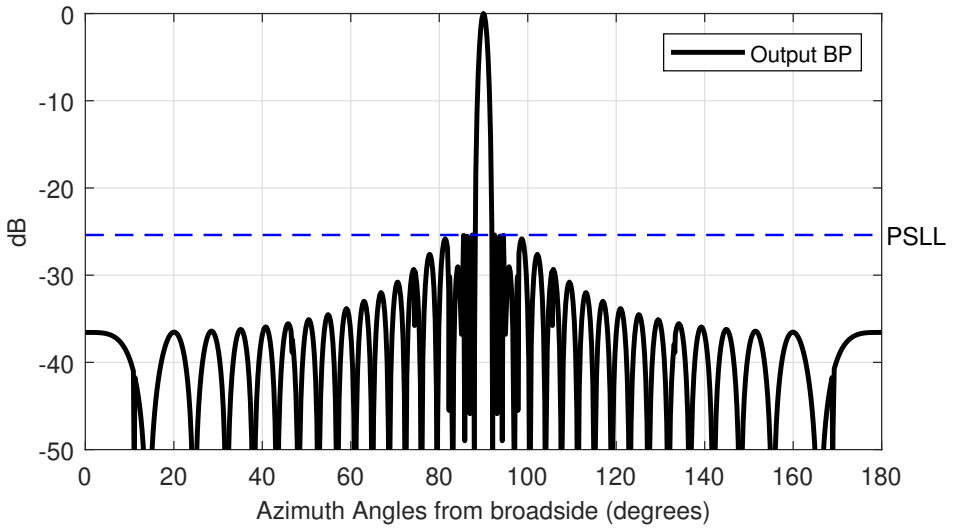

(b)

Figure 6.7: Beam-patterns for S12

Table 6.9: Computational complexity for CBF and Capon with S10 and an array with 25-sensors

	CBF	Capon
25-sensors	$180 * 25$	$180 * (25^3 + 2 * 25)$ $= 180 * 15675$
S10	$180 * (18 + 12)$ $+180 * (2 * 2) + 180$ $= 180 * 35$	$180 * (18^3 + 36) + 180 * (12^3 + 24)$ $+180 * (2 * 2) + 180$ $= 180 * 7625$

and weights of the sensors are determined, nothing is done related to design in real time operation. However, in the proposed method, dual-apodization is done continuously in real time operation. This makes obtained design suitable for receiver arrays only. In addition to that, any beamforming or direction-of-arrival (DOA) estimation algorithm used in the system will be executed for each sub-array. Change of computational complexity in this matter depends on the algorithm used. For example, for the solution S10 the complexity comparison should be done between an array with 25-sensors and two subarrays with 18-sensors and 12-sensors. Therefore, in the case where computational burden becomes prohibitive with the increasing number of sensors, it will be advantageous. In the case where computational complexity increases slightly with increasing number of sensors, it will be disadvantageous. The extra computations due to dual apodization are finding the maximum of the both spatial spectra, dividing each value by the corresponding maximum and finding the minimum of the two values at each spatial point. Therefore, the complexity increase due to dual apodization also depends on the number of scanning angles (N_s). The change of computational complexities for S10 when conventional beamforming (CBF) and Capon are used are given in Table 6.9. In Table 6.9 the number of scanning angles is taken as $N_s = 360$, but due to symmetry in the spatial spectrum of a linear array only half of the spectrum has been considered, and the second lines of S10 are due to nonlinear apodization (normalization and minimum operation).

In CBF, the computational complexity is $O(n)$. On the other hand, in Capon, the biggest part of the complexity is due to inversion operation, $O(n^3)$, and the remaining

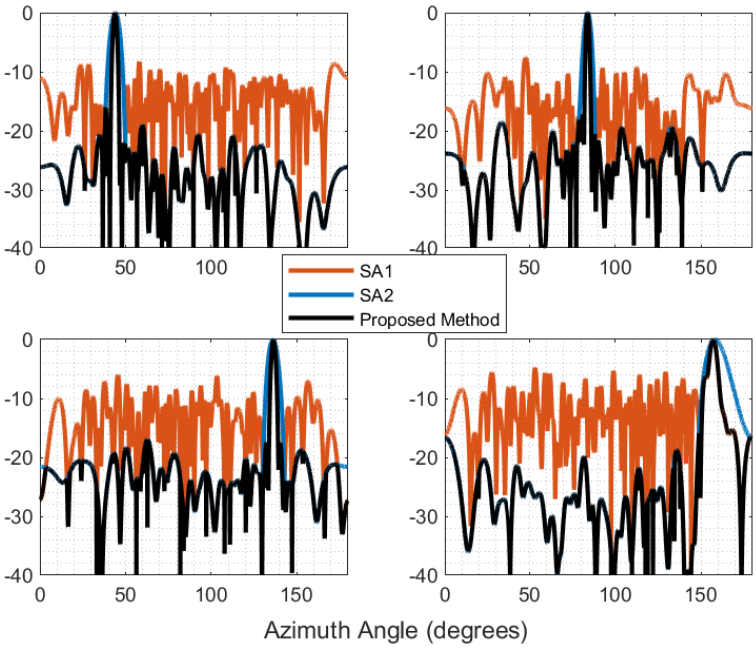

Figure 6.8: Spatial power spectra with S12 for a single target at different azimuth locations

computations are comparatively negligible. Therefore, dividing the whole array in two subarrays will be advantageous in Capon but disadvantageous in CBF. Moreover, the computational complexity increase due to nonlinear apodization is dramatically high when CBF is used, whereas it is negligible when Capon is used.

In order to see the effectiveness and the disadvantages of the proposed method, a DOA search simulation has been conducted using conventional beamforming. Synthetically generated frequency domain data has been used and solutions S10 and S12 have been selected. The simulation results with S12 for a single target are provided in Figure 6.8. In Figure 6.8 the spatial power spectra for a single target with an SNR of 10 dB at different azimuth locations are provided. Figure 6.8 shows that the target has been successfully detected in all locations with high resolution and low sidelobe level.

As mentioned before, for an optimum result many subarrays and designs should be used. However, the method used in this study uses two subarrays one of which is effective around the mainlobe regions and one at the sidelobe regions. Therefore, the

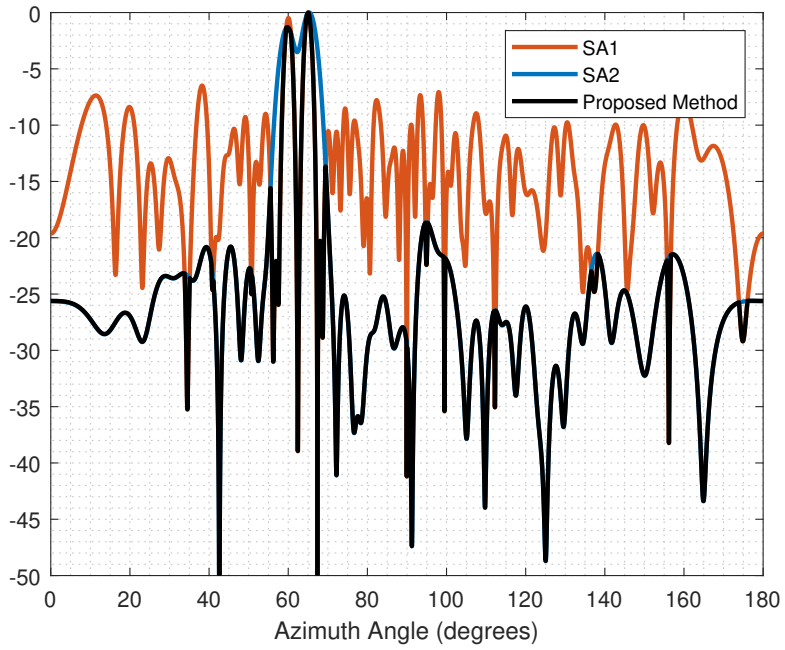

Figure 6.9: Spatial power spectrum with S12 for two close targets, SNR 10 dB

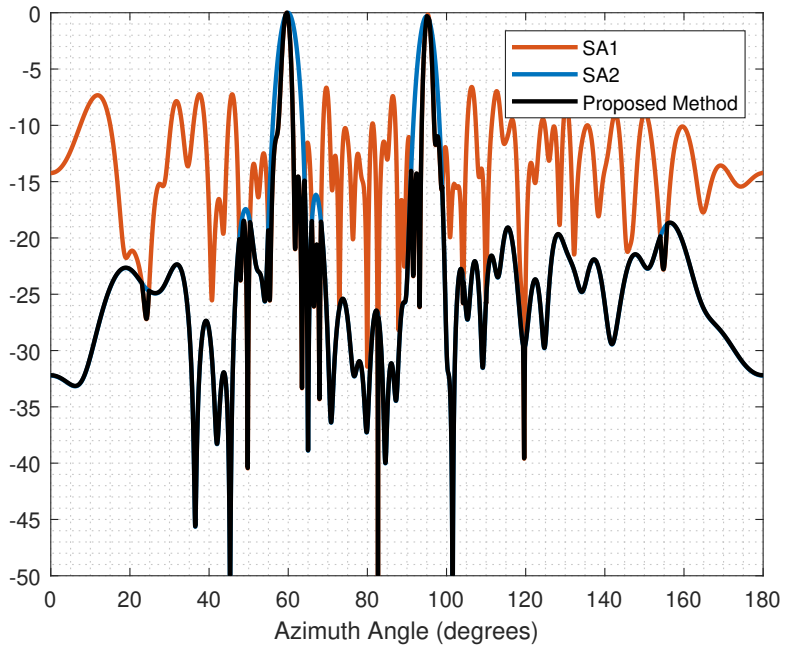

Figure 6.10: Spatial power spectrum with S12 for two separated targets, SNR 10 dB

method has acceptable results for two close targets (Figure 6.9) and two separated targets (Figure 6.10). However, when there are more than two targets with close SNR values, the proposed method is expected to under-perform. The simulation results for three targets located at $[60^\circ\ 65^\circ\ 95^\circ]$ with S10 is given in Figure 6.11. The distant target cannot be located clearly and the sidelobe level is around -5 dB. However, any agent with an expertise in the analyses of such designs, Figure 6.11(b), can conclude that there are at least two targets located around 60° and 90°. This conclusion can also be obtained with the result of SA2. On the other hand, looking at the result of the proposed method it can also be concluded that quite likely there are two close targets around 60°. That makes the proposed method more advantageous compared to SA2.

6.5 Conclusion

In this chapter, a nonlinear method for array thinning has been proposed. The proposed method depends on the hybrid usage of dual-apodization and genetic algorithm. PSLL, BW and CTR parameters have been used for performance comparison. Results show that the proposed method gives better results compared to existing solutions for two test problems in the literature. Moreover, these results can also be obtained with less number of sensors which improves the economy, complexity and computational load performance of the system. Although reducing the number of sensors for the test problems was not one of the initial aims of this study, it comes out to be another advantage of the proposed method. In previous works in the literature, the genetic algorithm is used to suppress PSLL in all side-lobes region. However, in this method, the genetic algorithm considers the side-lobes within the mainlobe of SA2. Therefore, suppression level of genetic algorithm increases. The main drawback of this method is that it requires continuous dual-apodization of two sub-arrays in real time operation and is that it is applicable to receiver arrays only. The design of arrays in this chapter has been done merely considering the beam patterns.

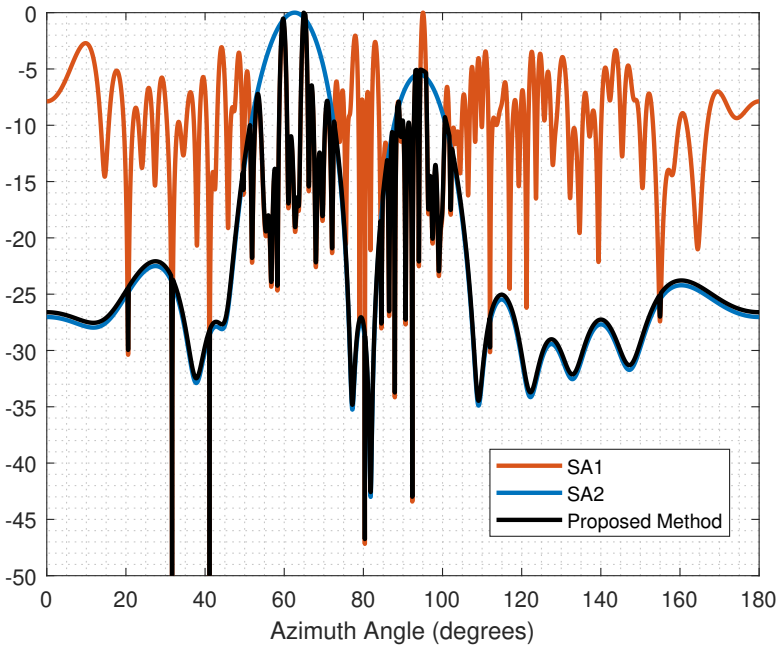

(a)

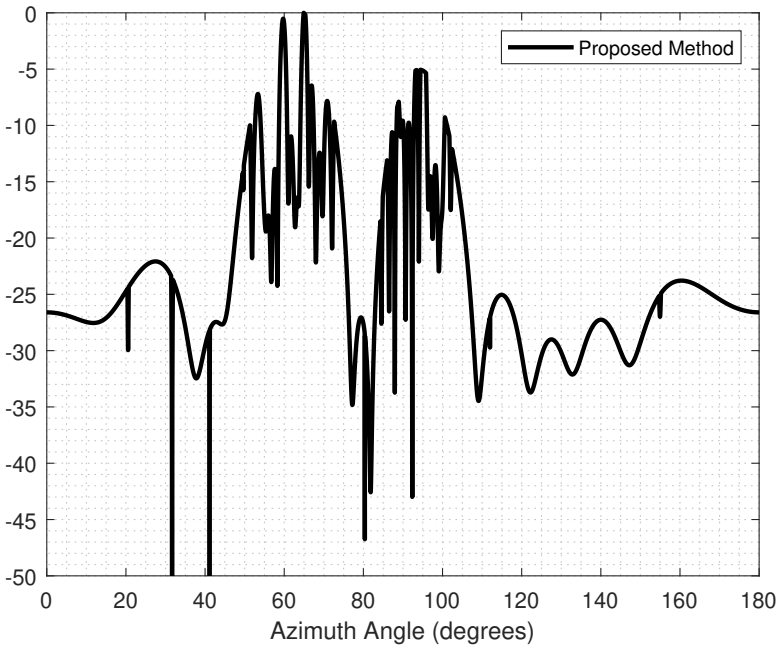

(b)

Figure 6.11: Spatial power spectrum with S10 for three targets, SNR 10 dB

CHAPTER 7

CONCLUSION

In Chapter 3, the historical progress of sparse linear arrays and analysis and comparison of the recently proposed sparse linear arrays have been presented. One of the most recent and popular methods in designing sparse arrays is the "coarray based" method. In this method, no optimization for the placement of array elements is required. A closed-form structure is used, and the aim is to maximize the size of the hole-free segment of the difference coarray. The most known five of these methods have been studied and their performances in terms of DOA estimation accuracy, degrees of freedom, DOA resolution, and mutual coupling have been compared. The aim is to determine their advantages, disadvantages, necessities, and success in case of fixed aperture and a fixed number of sensors scenarios. The arrays used in the comparison are Nested Array (NA), Co-prime Array (CA), Super Nested Array (SNA), Augmented Nested Array (ANA), and Sparse Ruler Array (SRA), which are called the comparison group. The outcomes of the analysis and comparison can be summarized as follows: In the case of the fixed aperture, using a filled array seems to be the best option in terms of performance. Coarray based arrays are not advantageous in this case. In case, the number of sensors is fixed, the array which has the largest physical aperture always has a bigger degrees of freedom (DOF) and resolvability. In simulations, this one comes out to be SRA. Therefore, contrary to the authors of the comparison group, we believe that it is the physical aperture that determines DOF and resolvability. However, using this physical aperture efficiently is the success of the coarray based methods. On the other hand, even if they have the same physical aperture, their performances may differ. Therefore, it can be concluded that the performances of the coarray based arrays depend on their coarray apertures and coarray topologies (distribution of redundancies) together with their physical apertures and

physical topologies.

As a specific multi-apodization approach, SVA is a computationally convenient method that brings together the advantages of different window functions in spectral analysis. In Chapter 5, SVA has been adapted to beamforming by a uniform linear array. The main idea is to use the similarity of beamforming and DTFT operations and the fact that optimization in SVA is done in frequency domain. SVA based beamforming achieves the resolving capability of rectangular shading with much lower sidelobe level. SVA based beamforming naturally inherits the properties of SVA; a possible drawback, its poorer resolution (relative to that of rectangular shading) when the number of sensors is reduced can be overcome by a modified SVA method. Choosing the number of DFT points as an integer multiple of the number of sensors reduces possible deviation in array output pattern to a negligible level. That this is a frequency domain method can be considered as a practical advantage due to the availability of custom FFT routines for many processors.

In Chapter 6, a nonlinear method for array thinning has been proposed. The proposed method depends on the hybrid usage of dual-apodization and genetic algorithm. PSLL, BW, and CTR parameters have been used for performance comparison. Results show that the proposed method gives better results compared to existing solutions for two test problems in the literature. Moreover, these results can also be obtained with less number of sensors which improves the economy, complexity and computational load performance of the system. Although reducing the number of sensors for the test problems was not one of the initial aims of this study, it comes out to be another advantage of the proposed method. In previous works in the literature, the genetic algorithm is used to suppress PSLL in all side-lobes region. However, in this method, the genetic algorithm considers the side-lobes within the mainlobe of SA2. Therefore, suppression level of genetic algorithm increases. The main drawback of this method is that it requires continuous dual-apodization of two sub-arrays in real time operation and is that it is applicable to passive arrays only. The design of arrays in this chapter has been done merely considering the beam patterns.

In the design given in Chapter 6, the constraint on the numbers of array elements, N_1 and N_2, is loose. In future studies, the values of these parameters can be obtained

by an optimization algorithm such that they are kept fixed during the design process, and result in the best mainlobe width and sidelobe level. Moreover, the results of the design in practice can be best evaluated by an agent with an expertise. The role of this agent can be fulfilled by machine learning methods. Firstly, the machine learning methods can be used for the estimation of number of sources by using the spatial spectra of SA1, SA2, and their dual apodization. Then, given the number of sources, the DOA of sources can be estimated with machine learning methods. A combined machine learning model which estimates both the number of sources and their DOAs can be used. However, this will require a dynamic output length and increase the complexity of the machine learning model.

REFERENCES

[1] A. Moffet, "Minimum-redundancy linear arrays," *IEEE Transactions on antennas and propagation*, vol. 16, no. 2, pp. 172–175, 1968.

[2] M. Ishiguro, "Minimum redundancy linear arrays for a large number of antennas," *Radio Science*, vol. 15, no. 6, pp. 1163–1170, 1980.

[3] W.-K. Ma, T.-H. Hsieh, and C.-Y. Chi, "Doa estimation of quasi-stationary signals via khatri-rao subspace," in *Acoustics, Speech and Signal Processing, 2009. ICASSP 2009. IEEE International Conference on*, pp. 2165–2168, IEEE, 2009.

[4] V. K. I. D. G. Manolakis and S. M. Kogo, *Statistical and Adaptive Signal Processing*. 685 Canton Street Norwood, MA 02062: Artech House, Inc., 2005.

[5] S. Visuri, *Array and Multichannel Signal Processing Using Nonparametric Statistics*. PhD thesis, Helsinki University of Technology Signal Processing Laboratory, 2001.

[6] D. H. Johnson and D. E. Dudgeon., *Array Signal Processing, Concept and Techniques*. Englewood Cliffs, NJ: Prentice-Hall, 1993.

[7] M. V. H. Krim, "Two decades of array signal processing research: the parametric approach," *IEEE Signal Processing Magazine*, vol. 13(4), pp. 67–94, July 1996.

[8] J. Capon, "High-resolution frequency-wavenumber spectrum analysis," *IEEE Proc*, vol. 57(8), pp. 1408–1418, Aug. 1969.

[9] Y. Y. Z. Chen, G. Gokeda, *Introduction to Direction-of-Arrival Estimation*. 685 Canton Street Norwood, MA 02062: Artech House, Inc., 2010.

[10] J. Li and P. Stoica, *Robust adaptive beamforming*. Wiley Online Library, 2006.

[11] P. Stoica, Z. Wang, and J. Li, "Robust capon beamforming," in *Conference Record of the Thirty-Sixth Asilomar Conference on Signals, Systems and Computers, 2002.*, vol. 1, pp. 876–880, IEEE, 2002.

[12] R. Willey, “Space tapaering of linear and planar arrays,” *IRE Transactions on Antennas and Propagation*, vol. 10, no. 4, pp. 369–377, 1962.

[13] M. Skolnik, G. Nemhauser, and J. Sherman, “Dynamic programming applied to unequally spaced arrays,” *IEEE Transactions on Antennas and Propagation*, vol. 12, no. 1, pp. 35–43, 1964.

[14] A. Ishimaru, “Theory of unequally-spaced arrays,” *IRE Transactions on Antennas and Propagation*, vol. 10, no. 6, pp. 691–702, 1962.

[15] A. Ishimaru and Y.-S. Chen, “Thinning and broadbanding antenna arrays by unequal spacings,” *IEEE Transactions on antennas and propagation*, vol. 13, no. 1, pp. 34–42, 1965.

[16] Y. Lo, “A mathematical theory of antenna arrays with randomly spaced elements,” *IEEE Transactions on Antennas and Propagation*, vol. 12, no. 3, pp. 257–268, 1964.

[17] L. Lasdon, D. Suchman, and A. Waren, “Nonlinear programming applied to linear-array design,” *The Journal of the Acoustical Society of America*, vol. 40, no. 5, pp. 1197–1200, 1966.

[18] P. Bricout, “Pattern synthesis using weighted functions,” *IRE Transactions on Antennas and Propagation*, vol. 8, no. 4, pp. 441–444, 1960.

[19] M. Andreasen, “Linear arrays with variable interelement spacings,” *IRE Transactions on Antennas and Propagation*, vol. 10, no. 2, pp. 137–143, 1962.

[20] Y. Lo and S. Lee, “A study of space-tapered arrays,” *IEEE Transactions on Antennas and Propagation*, vol. 14, no. 1, pp. 22–30, 1966.

[21] M. Skolnik, J. Sherman, and F. Ogg, “Statistically designed density-tapered arrays,” *IEEE Transactions on Antennas and Propagation*, vol. 12, no. 4, pp. 408–417, 1964.

[22] T. T. Taylor, “Design of line-source antennas for narrow beamwidth and low side lobes,” *Transactions of the IRE Professional Group on Antennas and Propagation*, vol. 3, no. 1, pp. 16–28, 1955.

[23] P. Woodward, "A method of calculating the field over a plane aperture required to produce a given polar diagram," *Journal of the Institution of Electrical Engineers-Part IIIA: Radiolocation*, vol. 93, no. 10, pp. 1554–1558, 1946.

[24] C. L. Dolph, "A current distribution for broadside arrays which optimizes the relationship between beam width and side-lobe level," *Proceedings of the IRE*, vol. 34, no. 6, pp. 335–348, 1946.

[25] J. Arsac and A. DANJON, "Nouveau reseau pour lobservation radioastronomique de la brillance sur le soleil mcs," *Comptes Rendus Hebdomadaires Des Seances De L Academie Des Sciences*, vol. 240, no. 9, pp. 942–945, 1955.

[26] R. A. Haubrich, "Array design," *Bulletin of the Seismological Society of America*, vol. 58, no. 3, pp. 977–991, 1968.

[27] R. T. Hoctor and S. A. Kassam, "The unifying role of the coarray in aperture synthesis for coherent and incoherent imaging," *Proceedings of the IEEE*, vol. 78, no. 4, pp. 735–752, 1990.

[28] R. Bracewell, "Interferometry and the spectral sensitivity island diagram," *IRE Transactions on Antennas and Propagation*, vol. 9, no. 1, pp. 59–67, 1961.

[29] J. Picken and G. Swarup, "The stanford compound-grating interferometer," *The Astronomical Journal*, vol. 69, p. 353, 1964.

[30] R. N. Bracewell and J. A. Roberts, "Aerial smoothing in radio astronomy," *Australian Journal of Physics*, vol. 7, no. 4, pp. 615–640, 1954.

[31] P. Pal and P. Vaidyanathan, "Nested arrays: a novel approach to array processing with enhanced degrees of freedom," *Signal Processing, IEEE Transactions on*, vol. 58, no. 8, pp. 4167–4181, 2010.

[32] R. Bracewell, "Optimum spacings for radio telescopes with unfilled apertures," *Natl. Acad. Sci. Natl. Res. Council. Publ*, vol. 1408, pp. 243–244, 1966.

[33] W. Stutzman, "Shaped-beam synthesis of nonuniformly spaced linear arrays," *IEEE Transactions on Antennas and Propagation*, vol. 20, no. 4, pp. 499–501, 1972.

[34] R. Streit, "Sufficient conditions for the existence of optimum beam patterns for unequally spaced linear arrays with an example," *IEEE Transactions on Antennas and Propagation*, vol. 23, no. 1, pp. 112–115, 1975.

[35] P. Murthy and A. Kumar, "Synthesis of linear antenna arrays," *IEEE Transactions on Antennas and Propagation*, vol. 24, no. 6, pp. 865–870, 1976.

[36] A. Kumar and P. Murthy, "Synthesis of equally excited linear arrays," *IEEE Transactions on Antennas and Propagation*, vol. 25, no. 3, pp. 425–428, 1977.

[37] F. Hodjat and S. Hovanessian, "Nonuniformly spaced linear and planar array antennas for sidelobe reduction," *IEEE Transactions on Antennas and Propagation*, vol. 26, no. 2, pp. 198–204, 1978.

[38] S. DeGraaf and D. Johnson, "Optimal linear arrays for narrow-band beamforming," in *Acoustics, Speech, and Signal Processing, IEEE International Conference on ICASSP'84.*, vol. 9, pp. 214–217, IEEE, 1984.

[39] P. Jarske, T. Saramaki, S. K. Mitra, and Y. Neuvo, "On properties and design of nonuniformly spaced linear arrays (antennas)," *IEEE Transactions on Acoustics, Speech, and Signal Processing*, vol. 36, no. 3, pp. 372–380, 1988.

[40] R. L. Haupt, "Thinned array using genetic algorithms," *IEEE Trans. Antennas Propagat*, vol. 42, pp. 993–999, July 1994.

[41] K.-K. Yan and Y. Lu, "Sidelobe reduction in array-pattern synthesis using genetic algorithm," *IEEE Transactions on Antennas and Propagation*, vol. 45, no. 7, pp. 1117–1122, 1997.

[42] A. T. V. Murino and C. S. Regazzoni, "Synthesis of unequally spaced arrays by simulated annealing," *IEEE Trans. Signal Processing*, vol. 44, pp. 119–123, Jan. 1996.

[43] D. Marcano and F. Durán, "Synthesis of antenna arrays using genetic algorithms," *IEEE Antennas and Propagation Magazine*, vol. 42, no. 3, pp. 12–20, 2000.

[44] L. Cen, Z. L. Yu, W. Ser, and W. Cen, "Linear aperiodic array synthesis using an

improved genetic algorithm," *IEEE Transactions on Antennas and Propagation*, vol. 60, no. 2, p. 895, 2012.

[45] C. A. Meijer, "Simulated annealing in the design of thinned arrays having low sidelobe levels," in *Communications and Signal Processing, 1998. COMSIG'98. Proceedings of the 1998 South African Symposium on*, pp. 361–366, IEEE, 1998.

[46] A. Trucco, "Synthesizing wide-band sparse arrays by simulated annealing," *Proc. Oceans 2001, MTS/IEEE Conference and Exhibitions*, vol. 2, pp. 989–994, Nov. 2001.

[47] A. Trucco, "Thinning and weighting of large planar arrays by simulated annealing," *IEEE Trans. Ultrasonics, Ferroelectrics, and Frequency Control*, vol. 46, pp. 347–355, Mar. 1999.

[48] M. Donelli, S. Caorsi, F. DeNatale, M. Pastorino, and A. Massa, "Linear antenna synthesis with a hybrid genetic algorithm," *Progress In Electromagnetics Research*, vol. 49, pp. 1–22, 2004.

[49] E. S. A. Lommi, A. Massa and A. Trucco, "Sidelobe reduction in sparse linear arrays by genetic algorithms," *Microwave and Opt. Technol. Lett.*, vol. 32(3), pp. 194–196, Feb. 2002.

[50] D. J. O'Neill, "Element placement in thinned arrays using genetic algorithms," *in Proc. IEEE Int. Conf. Oceans'94 Osates, Brest, France*, vol. II, pp. 301–306, Sept. 1994.

[51] S. Kirkpatrick, C. D. Gelatt, and M. P. Vecchi, "Optimization by simulated annealing," *science*, vol. 220, no. 4598, pp. 671–680, 1983.

[52] G. Oliveri and A. Massa, "Bayesian compressive sampling for pattern synthesis with maximally sparse non-uniform linear arrays," *IEEE Transactions on Antennas and Propagation*, vol. 59, no. 2, pp. 467–481, 2011.

[53] F. Viani, G. Oliveri, and A. Massa, "Compressive sensing pattern matching techniques for synthesizing planar sparse arrays," *IEEE Transactions on Antennas and Propagation*, vol. 61, no. 9, pp. 4577–4587, 2013.

[54] M. B. Hawes and W. Liu, "Robust sparse antenna array design via compressive sensing," in *Digital Signal Processing (DSP), 2013 18th International Conference on*, pp. 1–5, IEEE, 2013.

[55] G. Oliveri, M. Carlin, and A. Massa, "Complex-weight sparse linear array synthesis by bayesian compressive sampling," *IEEE Transactions on Antennas and Propagation*, vol. 60, no. 5, pp. 2309–2326, 2012.

[56] G. Oliveri, F. Robol, M. Carlin, and A. Massa, "Synthesis of large sparse linear arrays by bayesian compressive sensing," in *Antennas and Propagation (EUCAP), Proceedings of the 5th European Conference on*, pp. 2078–2081, IEEE, 2011.

[57] M. B. Hawes and W. Liu, "Sparse array design for wideband beamforming with reduced complexity in tapped delay-lines," *IEEE/ACM Transactions on Audio, Speech and Language Processing (TASLP)*, vol. 22, no. 8, pp. 1236–1247, 2014.

[58] J. Rubio, J. Córcoles, J. F. Izquierdo, and R. Gómez-Alcalá, "Array thinning of coupled antennas based on the orthogonal matching pursuit method and a spherical-wave expansion for far-field synthesis," *IEEE Transactions on Antennas and Propagation*, vol. 63, no. 12, pp. 5425–5432, 2015.

[59] B. Zhang, W. Liu, and X. Gou, "Sparse antenna array design for directional modulation," in *Sensor Array and Multichannel Signal Processing Workshop (SAM), 2016 IEEE*, pp. 1–5, IEEE, 2016.

[60] E. J. Candès, J. Romberg, and T. Tao, "Robust uncertainty principles: Exact signal reconstruction from highly incomplete frequency information," *IEEE Transactions on information theory*, vol. 52, no. 2, pp. 489–509, 2006.

[61] P. P. Vaidyanathan and P. Pal, "Sparse sensing with co-prime samplers and arrays," *Signal Processing, IEEE Transactions on*, vol. 59, no. 2, pp. 573–586, 2011.

[62] S. Shakeri, D. D. Ariananda, and G. Leus, "Direction of arrival estimation using sparse ruler array design.," in *SPAWC*, pp. 525–529, 2012.

[63] J. Liu, Y. Zhang, Y. Lu, S. Ren, and S. Cao, "Augmented nested arrays with enhanced dof and reduced mutual coupling," *IEEE Transactions on Signal Processing*, vol. 65, no. 21, pp. 5549–5563, 2017.

[64] C.-L. Liu and P. Vaidyanathan, "Super nested arrays: Linear sparse arrays with reduced mutual coupling part i: Fundamentals," *IEEE Transactions on Signal Processing*, vol. 64, no. 15, pp. 3997–4012, 2016.

[65] S. U. Pillai, Y. Bar-Ness, and F. Haber, "A new approach to array geometry for improved spatial spectrum estimation," *Proceedings of the IEEE*, vol. 73, no. 10, pp. 1522–1524, 1985.

[66] Z. Ye, J. Dai, X. Xu, and X. Wu, "Doa estimation for uniform linear array with mutual coupling," *IEEE Transactions on Aerospace and Electronic Systems*, vol. 45, no. 1, pp. 280–288, 2009.

[67] B. Friedlander and A. J. Weiss, "Direction finding in the presence of mutual coupling," *IEEE transactions on antennas and propagation*, vol. 39, no. 3, pp. 273–284, 1991.

[68] C.-L. Liu and P. Vaidyanathan, "Super nested arrays: Linear sparse arrays with reduced mutual coupling part ii: High-order extensions," *IEEE Transactions on Signal Processing*, vol. 64, no. 16, pp. 4203–4217, 2016.

[69] J. Leech, "On the representation of 1, 2, ... , n by differences," *Journal of the London Mathematical Society*, vol. 1, no. 2, pp. 160–169, 1956.

[70] C.-L. Liu and P. Vaidyanathan, "Remarks on the spatial smoothing step in coarray music," *IEEE Signal Processing Letters*, vol. 22, no. 9, pp. 1438–1442, 2015.

[71] M. Wang and A. Nehorai, "Coarrays, music, and the cramér–rao bound," *IEEE Transactions on Signal Processing*, vol. 65, no. 4, pp. 933–946, 2017.

[72] P. Stoica and A. Nehorai, "Music, maximum likelihood, and cramer-rao bound," *IEEE Transactions on Acoustics, Speech, and Signal Processing*, vol. 37, no. 5, pp. 720–741, 1989.

[73] P. Stoica and A. Nehorai, "Music, maximum likelihood and cramer rao bound: further results and comparisons," *IEEE Trans. Acoust. Speech Signal Process*, vol. 38(12), pp. 2140–2150, Dec. 1990.

[74] C.-L. Liu and P. Vaidyanathan, "Cramér–rao bounds for coprime and other sparse arrays, which find more sources than sensors," *Digital Signal Processing*, vol. 61, pp. 43–61, 2017.

[75] A. Koochakzadeh and P. Pal, "Cramér–rao bounds for underdetermined source localization," *IEEE Signal Processing Letters*, vol. 23, no. 7, pp. 919–923, 2016.

[76] Y. I. Abramovich, D. A. Gray, A. Y. Gorokhov, and N. K. Spencer, "Positive-definite toeplitz completion in doa estimation for nonuniform linear antenna arrays. i. fully augmentable arrays," *Signal Processing, IEEE Transactions on*, vol. 46, no. 9, pp. 2458–2471, 1998.

[77] F. J. Harris, "On the use of windows for harmonic analysis with the discrete fourier transform," *Proceedings of IEEE*, vol. 66, pp. 51–83, Jan. 1978.

[78] H. C. Stankwitz, R. Dallaire, and J. Fienup, "Nonlinear apodization for sidelobe control in sar imagery," *IEEE Trans. Aerosp. Electron.Syst*, vol. 31, pp. 23–52, Jan. 1995.

[79] J. A. C. Lee and D. C. Munson(Jr), "Spatially variant apodization for image reconstruction from partial fourier data," *Image Processing, IEEE Transactions on*, vol. 9, pp. 1914–1925, Nov. 2000.

[80] J. A. C. Lee and D. C. Munson(Jr), "Effectiveness of spatially-variant apodization," *Image Processing, 1995. Proceedings., International Conference*, vol. 1, pp. 147–150, Oct. 1995.

[81] V. Kumar *et al.*, "Design of effective window function for fir filters," in *Advances in Engineering and Technology Research (ICAETR), 2014 International Conference on*, (Unnao, India), pp. 1–5, Aug. 2014.

[82] H. Rakshit and M. A. Ullah, "A comparative study on window functions for designing efficient fir filter," in *Strategic Technology (IFOST), 2014 9th International Forum on*, (Cox's Bazar), pp. 91–96, Oct. 2014.

[83] B. H. Smith, "Generalization of spatially variant apodization to noninteger nyquist sampling rates," *IEEE Transaction on Image Processing*, vol. 9, no. 6, pp. 1088–1093, 2000.

[84] C. Castillo-Rubio, S. Llorente-Romano, and M. Burgos-Garcia, "Robust sva method for every sampling rate condition," *IEEE Transactions on Aerospace and Electronic Systems Vol. 43, No. 2 April 2007*, vol. 43, no. 2, pp. 571–580, 2007.

[85] Y. Z. W. Zhai, "Apply spatially variant apodization to sar/insar image processing," in *Strategic Technology (IFOST), 2014 9th International Forum on*, (Cox's Bazar), pp. 91–96, Oct. 2014.

[86] N. Chong *et al.*, "A sar sidelobe suppression algorithm based on modified spatially variant apodization," *Sci China Tech Sci*, vol. 53, pp. 2542–2551, March 2010.

[87] N. Chong *et al.*, "A super-resolution algorithm for synthetic aperture radar based on modified spatially variant apodization," *Science China Physics, Mechanics, Astronomy*, vol. 54, pp. 355–364, Feb. 2010.

[88] W. P. Du Plessis, "Weighted thinned linear array design with the iterative fft technique," *Antennas and Propagation, IEEE Transactions on*, vol. 59, no. 9, pp. 3473–3477, 2011.

[89] B. E. S. Holm and G. Dahl, "Properties of the beampattern of weight- and layout-optimized sparse arrays," *IEEE Trans. Ultrason., Ferroelect., Freq. Contr.*, vol. 44, pp. 983–991, Sept. 1997.

[90] R. M. Leahy and B. D. Jeffs, "On the design of maximally sparse beamforming arrays," *IEEE Trans. Antennas Propagat*, vol. 39, pp. 1178–1187, Aug. 1991.

[91] A. Trucco and V. Murino, "Stochastic optimization of linear sparse arrays," *IEEE J. Ocean. Engrg.*, vol. 24(3), pp. 291–299, Sept. 1999.

[92] A. Trucco and F. Repetto, "A stochastic approach to optimizing the aperture and the number of elements of an aperiodic array," *in Proc. Int. Conf. Oceans'96 MTS/IEEE, Fort Lauderdale, FL*, pp. 1510–1516, Sept. 1996.

[93] P. Angeletti and G. Toso, "Array antennas with jointly optimized elements positions and dimensions part i: Linear arrays," *IEEE Transactions on Antennas and Propagation*, vol. 62, no. 4, pp. 1619–1626, 2014.

[94] O. M. Bucci, T. Isernia, and A. F. Morabito, "An effective deterministic procedure for the synthesis of shaped beams by means of uniform-amplitude linear sparse arrays," *IEEE Transactions on Antennas and Propagation*, vol. 61, no. 1, pp. 169–175, 2013.

[95] H. L. Van Trees, *Optimum array processing: Part IV of detection, estimation, and modulation theory*. John Wiley & Sons, 2004.

[96] T. Isernia, F. Ares, O. M. Bucci, M. D'Urso, J. F. Gomez, and J. Rodriguez, "A hybrid approach for the optimal synthesis of pencil beams through array antennas," in *Antennas and Propagation Society International Symposium, 2004. IEEE*, vol. 3, pp. 2301–2304, 2004.

[97] L. Wang, *Array Signal Processing Algorithms for Beamforming and Direction Finding*. PhD thesis, Communications Research Group, Department of Electronics, University of York, 2009.

[98] P. Tsakalides, *Array Signal Processing with Alpha-Stable Distributions*. PhD thesis, University of Southern California, Dec. 1995.

APPENDIX A

DOA ESTIMATION METHODS

A.1 ESPRIT:

ESPRIT (Estimation of Signal Parameters via Rotation Invariant Techniques) method, in contrast to the MUSIC method, is a signal subspace method. ESPRIT does not involve a search algorithm and decreases computational load and storage requirement dramatically compared to the MUSIC method [5, 9]. Moreover, ESPRIT does not need to know the array steering vector, $\mathbf{A}(\boldsymbol{\theta})$, exactly. However, this method can only be used for certain array configurations which consist of two sub-arrays with fixed separation, Δ, between doublets each from one sub-array [5,9]. The doublets in each sub-array should be identical.

Consider the signal model given in (2.1), the array steering vector $\mathbf{A}$ now is the combination of two sub-matrices. Assume $\mathbf{A}_1$ is steering matrix of the first sub-array and $\mathbf{A}_2$ of the second sub-array. $\mathbf{A}$ is given as follows:

$$\mathbf{A} = \begin{bmatrix} \mathbf{A}_1 \\ \mathbf{A}_2 \end{bmatrix} \tag{A.1}$$

where $\mathbf{A}_1$ and $\mathbf{A}_2$ are related by

$$\mathbf{A}_2 = \mathbf{A}_1\mathbf{D} \tag{A.2}$$

and $\mathbf{D}$ is a diagonal matrix and is given by

$$\mathbf{D} = diag(e^{-j\omega\Delta\cos\theta_1/c}, e^{-j\omega\Delta\cos\theta_2/c}, ..., e^{-j\omega\Delta\cos\theta_K/c}) \tag{A.3}$$

where $\theta_k, k = 1, 2, ..., K$ are DOA angles. Therefore, DOA angles can be estimated

from the eigenvalues $\lambda_k, k = 1, 2, ..., K$ of $\mathbf{D}$ by

$$arg(\lambda_k) = j\omega\Delta \cos\theta_k / c \rightarrow \theta_k = acos(\frac{-jarg(\lambda_k)}{2\pi\Delta}) \tag{A.4}$$

Therefore, the problem of DOA estimation is reduced to finding the $\mathbf{D}$ matrix [7]. As stated before in Chapter 2, $\mathbf{A}$ and $\mathbf{U}_s$ span the same column space, therefore there should be a unique and non-singular matrix $\mathbf{C}$ such that

$$\mathbf{U}_s = \begin{bmatrix} \mathbf{U}_{s1} \\ \mathbf{U}_{s2} \end{bmatrix} = \begin{bmatrix} \mathbf{A}_1 \\ \mathbf{A}_2 \end{bmatrix} \mathbf{C} \tag{A.5}$$

combining (A.2) and (A.5) yields $\mathbf{U}_{s2} = \mathbf{U}_{s1}\mathbf{C}^{-1}\mathbf{D}\mathbf{C}$. Let $\mathbf{\Phi} = \mathbf{C}^{-1}\mathbf{D}\mathbf{C}$, then $\mathbf{\Phi}$ and $\mathbf{D}$ are related by similarity transformation, therefore they have the same eigenvalues [5, 7, 9]. Therefore, DOA estimation can be completed by finding such a $\mathbf{\Phi}$ that satisfies $\mathbf{U}_{s2} = \mathbf{U}_{s1}\mathbf{\Phi}$ relation. Applying (A.4) to the eigenvalues of $\mathbf{\Phi}$, DOA estimations can be found.

Even though its performance is similar to MUSIC algorithm, ESPRIT does not require a search algorithm and is simple [7, 97]. Moreover, the sensor positions is not required to be known exactly and array geometry is flexible. In contrast to these advantages, ESPRIT requires identical doublets and the separation between doublets Δ should satisfy $\Delta < \lambda/2$. Furthermore, there exists an 180° of ambiguity in the estimation of ESPRIT.

Algorithm steps of ESPRIT for K sources is as follows:

1. Collect output data samples $\mathbf{y}(1)$, $\mathbf{y}(2)$, ..., $\mathbf{y}(N)$
2. Evaluate the estimate of covariance matrix from (2.16)
3. Eigen-decompose $\hat{\mathbf{R}}_y$ and determine signal subspace $\mathbf{U}_s$ and $\mathbf{U}_{s1}$, $\mathbf{U}_{s2}$, note that number of signals can be found by extracting number of repeating smallest eigenvalues from the number of sensors
4. Find $\mathbf{\Phi}$ such that $\mathbf{U}_{s2} = \mathbf{U}_{s1}\mathbf{\Phi}$ is satisfied, in this step to find a solution for $\mathbf{\Phi}$

either a Least Squares (LS-ESPRIT) or a Total Least Squares approach (TLS-ESPRIT) can be used

5. Apply (A.4) to the eigenvalues of Φ for DOAs.

A.2 Maximum Likelihood Methods

The DOA estimation methods provided previously do not result in sufficient performance specifically in low SNR and in the existence of coherent signals. Maximum likelihood (ML) methods, on the other hand, have optimum performance. That is, the covariance of the estimates asymptotically reaches the stochastic Cramer Rao Bound (CRB) [98], even in low SNR and in the existence of coherent signals. However, this success comes with the cost of an increase in computational load mainly due to multidimensional search requirements [7]. ML methods are parametric methods and make use of a data set and a statistical model.

In DOA estimation two techniques of the ML method are used depending on the signal model, these techniques are the Stochastic and the Deterministic ML methods. In the Stochastic Maximum Likelihood(SML) technique the incoming signals are modeled as zero-mean, temporally white Gaussian processes whereas in the Deterministic Maximum Likelihood (DML) technique the incoming signals are modeled as unknown deterministic quantities. In both cases, the noise is modeled as a zero-mean, spatially, and temporally white Gaussian process [5]. In the following parts, a brief overview of these two techniques will be provided.

A.2.1 Deterministic Maximum Likelihood:

As mentioned before in this case the signal is assumed to be unknown constant and the noise is white Gaussian process with zero mean. Therefore from (2.1) the output $\mathbf{y}(t)$ will be a Gaussian process with mean $\mathbf{A}(\boldsymbol{\theta})\mathbf{s}(t)$ and covariance matrix $\mathbf{R}_y = \sigma_v^2\mathbf{I}$. Therefore the probability density function of each measurement will be given as

follows:

$$f(\mathbf{y}(t)) = \frac{1}{(\pi\sigma_v^2)^M} e^{-||\mathbf{y}(t)-\mathbf{A}(\boldsymbol{\theta})\mathbf{s}(t)||^2/\sigma_v^2} \tag{A.6}$$

Note that (A.6) is M variate complex Gaussian distribution and $||.||$ is Euclidean norm. In (A.6) the unknowns are $\boldsymbol{\theta}, \mathbf{s}(t)$ and σ_v^2. The measurements in each snapshot are independent, therefore the likelihood function for N snapshots becomes as follows:

$$L_{DML}(\boldsymbol{\theta}, \mathbf{s}(t), \sigma_v^2) = \prod_{t=1}^{N} (\pi\sigma_v^2)^{-M} e^{-||\mathbf{y}(t)-\mathbf{A}(\boldsymbol{\theta})\mathbf{s}(t)||^2/\sigma_v^2} \tag{A.7}$$

The ML estimates of the unknown parameters $\hat{\boldsymbol{\theta}},\ \hat{\mathbf{s}}(t)$ and $\hat{\sigma}_v^2$ are the ones which maximizes (A.7). Alternatively for simplicity, ML estimates of the unknown parameters can also be found as the ones which minimizes the negative log-likelihood function [7]:

$$l_{DML}(\boldsymbol{\theta}, \mathbf{s}(t), \sigma_v^2) = -\log(L_{DML}(\boldsymbol{\theta}, \mathbf{s}(t), \sigma_v^2)) \tag{A.8}$$

Inserting (A.7) in (A.8), neglecting the constant terms and normalizing by N yields:

$$l_{DML}(\boldsymbol{\theta}, \mathbf{s}(t), \sigma_v^2) = M\log(\sigma_v^2) + \frac{1}{N\sigma_v^2}\sum_{t=1}^{N} ||\mathbf{y}(t) - \mathbf{A}\mathbf{s}(t)||^2 \tag{A.9}$$

Then the ML estimates $\hat{\mathbf{s}}(t)$ and $\hat{\sigma}_v^2$ are obtained as follows [7]:

$$\hat{\sigma}_v^2 = \frac{1}{M} Tr\Big\{(I - \Pi_{\mathbf{A}})\mathbf{R}_y\Big\} \tag{A.10}$$

$$\hat{\mathbf{s}}(t) = \mathbf{A}^{\dagger}\mathbf{y}(t) \tag{A.11}$$

where $\mathbf{A}^{\dagger} = (\mathbf{A}^H\mathbf{A})^{-1}\mathbf{A}^H$ is pseudo inverse of $\mathbf{A}$ and $\Pi_{\mathbf{A}} = \mathbf{A}\mathbf{A}^{\dagger}$ is orthogonal projection on the range space of $\mathbf{A}^H$. Inserting (A.10) and (A.11) in (A.9) the ML estimate

$\hat{\boldsymbol{\theta}}$ is found as the solution of the following optimization problem:

$$\hat{\boldsymbol{\theta}}_{DML} = arg\Big\{ \min_{\boldsymbol{\theta}} Tr\big\{\Pi_A^{\perp}\mathbf{R}_y\big\}\Big\} \tag{A.12}$$

Where $\Pi_A^{\perp} = \mathbf{I} - \Pi_A$. Analytical solutions for this problem are not available generally, therefore numerical methods should be implemented [5, 7].

A.2.2 Stochastic Maximum Likelihood:

In this method the signal is modeled as a zero-mean temporarily white Gaussian random process [5, 7] with covariance matrix $\mathbf{R}_s = E\{\mathbf{s}(t)\mathbf{s}^H(t)\}$. The output $\mathbf{y}(t)$ is therefore a zero-mean Gaussian random process with covariance matrix $\mathbf{R}_y = \mathbf{A}\mathbf{R}_s\mathbf{A}^H + \sigma_v^2\mathbf{I}$. Similarly, as in *DML* case, measurements are independent and identically distributed, however the unknown parameters are now $\boldsymbol{\theta}$, $\mathbf{R}_s$ and σ_v^2. The likelihood function for N snapshot is obtained as follows:

$$L_{SML}(\boldsymbol{\theta}, \mathbf{R}_s, \sigma_v^2) = \prod_{t=1}^{N} \frac{1}{\pi^M |\mathbf{R}_y|} e^{(-\mathbf{y}^H(t)\mathbf{R}_y^{-1}\mathbf{y}(t))} \tag{A.13}$$

Normalizing by N and neglecting the constant terms, the negative log-likelihood function is found to be proportional to [5, 7]:

$$\frac{1}{N}\sum_{t=1}^{N} ||\Pi_A^{\perp}\mathbf{y}(t)||^2 = Tr\{\Pi_A^{\perp}\mathbf{R}_y\} \tag{A.14}$$

For fixed $\boldsymbol{\theta}$, the minimum with respect to $\mathbf{R}_s$ and σ_v^2 are found to be [7]:

$$\hat{\sigma}_v^2 = \frac{1}{M-K} Tr\{\Pi_A^{\perp}\mathbf{R}_y\} \tag{A.15}$$

$$\hat{\mathbf{R}}_s = \mathbf{A}^{\dagger}(\mathbf{R}_y - \hat{\sigma}_v^2\mathbf{I})\mathbf{A}^{\dagger H} \tag{A.16}$$

Using the estimates (A.15) and (A.16), the estimation for $\boldsymbol{\theta}$ is obtained as follows:

$$\hat{\boldsymbol{\theta}}_{SML} = arg\Big\{ \min_{\boldsymbol{\theta}} log|\mathbf{A}\hat{\mathbf{R}}_s\mathbf{A}^H + \hat{\sigma}_v^2\mathbf{I}| \Big\} \tag{A.17}$$